UNIVERSITY OF OKLAHOMA

GRADUATE COLLEGE

MAGNETOSTRATIGRAPHIC CONSTRAINTS OF THE PRE COLORADO-

RIVER INTEGRATION BOUSE FORMATION, BLYTHE BASIN, ARIZONA

A THESIS

SUBMITTED TO THE GRADUATE FACULTY

In partial fulfillment of the requirements for the

Degree of

MASTER OF SCIENCE

By

David Sanger

Norman, Oklahoma

2023

MAGNETOSTRATIGRAPHIC CONSTRAINTS OF THE PRE COLORADO-

RIVER INTEGRATION BOUSE FORMATION, BLYTHE BASIN, ARIZONA

A THESIS APPROVED FOR THE SCHOOL OF GEOSCIENCES

BY THE COMMITTEE CONSISTING OF

Dr. Shannon Dulin, Chair

Dr. Caitlin Hodges

Dr. Michael Soreghan

ACKNOWLEDGEMENTS

TABLE OF CONTENTS

LIST OF TABLES

LIST OF FIGURES

ABSTRACT

Magnetostratigraphic studies offer unique insights into the orientation of Earth's ancient magnetic field and provide an opportunity to determine the chronology of depositional events, particularly when combined with other dating methods. A successive series of basins trending south from Needles, California to Cibola, Arizona, records the evolution of the lower Colorado River through the preservation of sediments within the Bouse Formation. The Bouse Formation is characterized by basal marl, tufa, alternating silts and muds and Colorado River sands. It was deposited between ~5.24 and ~4.6Mya and represents pre-Colorado River integration deposits. Magnetic polarities are recorded in sediments during deposition and are revealed through the stepwise, destructive process known as alternating field (AF) demagnetization. The magneto-stratigraphic record near the end of the deposition of the Bouse Formation is poorly constrained trained and can be improved through the identification of a transition between the normal polarity Sidjufall (4.81-4.89Mya) and Nunivak (4.49-4.63Mya) subchrons. This study is anchored by dates acquired through tephrachronology of $^{40}Ar/^{39}Ar$ in detrital sanidine grains in the middle of the Sidjufall and Thvera subchrons. Sanidine grain analysis within Hart Mine Wash revealed an age of ~4.72Mya, corresponding to the age of the Lawlor Tuff, within the Bouse formation. Additional tephrachronology of the Bouse Formation revealed an age of 5.24Mya for the Wolverine Creek Tuff, just below the base of the Bouse Formation in the Lost Cabin Beds in Cottonwood Valley. The

magnetic inclinations of the samples were anchored by the absolute ash dates and compared to the geomagnetic polarity timescale (GPTS) to determine the timing of deposition of the Bouse, and therefore the timing of arrival of the Colorado River to Blythe Basin. Surrounding the Hart Mine Wash ash lie sections of both normal and reversed polarity. Additional normal polarity intervals were captured in sediments surrounding Parker, AZ (Riversides) and further North near Lake Havasu City, within Mohave Valley (See Figure 2). The study consists of 3 unique locations, 26 individual sites, 40 sediment core specimens and 76 oriented specimens. Rock magnetic tests include hysteresis, first-order reversal curve (FORC) diagrams and Curie temperature analysis of thermomagnetic curves. These tests yielded low-quality results due to a low abundance of magnetic minerals, although the presence of stable ancient magnetization in specimens has been established through AF demagnetization. The results of this magnetostratigraphic study will improve the understanding of the timing of deposition of the Bouse Formation and date the arrival of the Colorado River within Blythe Basin to ~4.6-4.7Mya.

INTRODUCTION

The methodology and timing of integration of the lower Colorado River has been a topic of debate since the Bouse Formation was initially described around 50 years ago (Howard et al., 2016; Kukla et al., 1976; Malmon et al., 2011). The Bouse Formation within the Colorado River depositional system is modelled as a lacustrine and estuarine environment. Most models agree that the upper Colorado River corridor took form by a series of "filling and spilling" over individual paleo divides, separating the corridor into a series of isolated basins (Bright et al., 2018; Crow et al., 2019; House, Pearthree, and Perkins., 2008; O'Connell., 2016; Pearthree and House., 2014; Roskowski et al., 2010; Spencer and Jonathan Patchett., 1997; Spencer et al., 2021). This was followed by a catastrophic breach of paleo divides, resulting in the subsequent release of pre-Colorado River integration sediments downstream to the next catchment. Bouse sediments would have continued filling and spilling through the basins North to South in the order of: Cottonwood Valley, Mohave Valley, Chemehuevi Valley, Blythe Basin, and finally the Fish-Creek Vallecitos Basin located near the Salton Trough in California (See Figure 3).

The lower portion of the corridor has been modelled as an estuarine environment, where progressively more saline Colorado river water meets an estuary (Gardner and Dorsey., 2021; McDougall and Miranda Martínez., 2014; O'Connell, Dorsey, and Humphreys., 2017). This model is tied to sparse marine fossil assemblages surrounding Blythe Basin and high carbonate content as evidenced by the Bouse Marl.

The Bouse Formation is divided into three basic units, consisting of initial spillover units, a basal carbonate unit (Bouse Marl), associated clastic shoreline deposits and a lacustrine/fluvial unit characterized by alternating sands and muds (Buising., 1990; House, Pearthree, and Perkins., 2008; Pearthree and House., 2014; Spencer, Pearthree, and House., 2008). The Bouse Marl, the most widely preserved deposit within the formation, commonly forms a crust like surface on bedrock exposures, as well as thicker accumulations of calcareous sandstones and tufa's. The majority of preserved Bouse sediments lie on upper piedmonts where they were unaffected by major drainage systems running axially in the valley.

It is important to understand the timing of deposition of the Bouse Formation and associated deposits to further constrain the timing of integration of the lower Colorado River, and the mechanisms which drove it towards the Gulf of California. Recent work conducted by Schwing., (2019) captured a geomagnetic polarity reversal within the Lost Cabin beds, a well-preserved pre-Bouse deposit in the depocenter of Cottonwood Valley found at 350-365m asl (Schwing., 2019; see Fig. 1-3). The age of this reversal correlates to the transition of the C3r to C3n.4n (Thvera) subchron, yielding an age of 5.23Mya for the pre-Bouse Lost Cabin Beds (Figure 4) (Ogg., 2012). Tephrachronology conducted by Crow et al., (2021) constrains the timing of integration further through the discovery of a discrete ash located within the Bouse Marl at Hart Mine Wash, revealing an age of ~4.72Mya, suggesting the Bouse Formation was deposited after 4.72Mya. Additional work by Wojcicki et al., (2011) places the Lawlor Tuff, an ash layer interbedded in the Bouse Marl, at 4.83 Mya, coinciding with the age of the Hart Mine Wash ash. Crow et al., (2021) places the

Bullhead Alluvium, a deposit consistent with a through flowing Colorado River, at 4.6Mya. The Lawlor Tuff was sampled near Palo Verde Valley, within Blythe Basin, while the Bullhead Alluvium DS (detrital sanidine) was sampled in Cottonwood Valley, above the Lost Cabin Beds. The most recent Hart Mine Wash ash was sampled in the southernmost portion of Blythe Basin, near Cibola, AZ (See Figure 2).

To resolve the ambiguity surrounding the age of integration of the Colorado River, this study conducts a magnetostratigraphic analysis of three locations along the LOCO (Lower Colorado River Corridor). The northernmost site is in Mohave Valley, while the other three sites are throughout Blythe Basin (See Figure 2). The furthest south of the sites is in Hart Mine Wash (HMW) near Cibola, AZ, the primary focus of this study. The Bouse Marl within Hart Mine Wash lies above the ash in the Lost Cabin Beds and below the ash in the Bullhead Alluvium, creating an anchoring top and bottom age bound for this study (5.23-4.6Mya). Fine grained, flat lying marl in HMW makes an excellent target for paleomagnetic study since single domain magnetic grains capable of carrying ancient remanent magnetizations are less than one micron in size. Flat lying beds require no bedding correction and are more likely to represent a primary magnetization. This study aims to capture the geomagnetic polarity reversal between the 4.8-4.9Mya C3n.3n Sidufjall subchron and 4.49-4.63Mya C3n.2n Nunivak subchron. The recently dated ~4.72Mya ash within the Bouse Marl at Hart Mine Wash sets the reference point to the GPTS (Geomagnetic Polarity Timescale) for this section. If paleomagnetism reveals that the ~4.72Mya Hart Mine Wash ash lies within a reverse polarity interval, or a transition from normal to reverse polarity is located near the ash, this will constrain the age of

deposition of Bouse sediments until after 4.75Mya (See Figure 4) (Ogg., 2012). Thus, further constraining the arrival of the Colorado River in Blythe Basin to 4.75-4.6Mya.

2 BACKGROUND

2.1 GEOLOGY OF MOHAVE VALLEY AND BLYTHE BASIN

The Colorado River extensional corridor lies between the borders of California, Arizona, and Mexico (See Figures 1-2). The corridor trends North by Northwest in the upper half, before changing course to a Northeast orientation around Chemehuevi and Parker Valley. The Colorado River extensional corridor has experienced several stress regimes and displays numerous fault types and behaviors. Low angle detachment faults associated with the southern Basin and Range are the most influential in accommodating Mid to Late-Miocene crustal extension, responsible for the creation of the corridor (Bennett et al., 2016; Buising et al., 1990; Dorsey et al., 2017; Howard et al., 2007). This Middle to Late Miocene period is responsible for most extension in the corridor and is the most tectonically active period in the creation of the LOCO. Other potential factors in accommodating extension include influence from the Farallon-North American arc system. Stresses change from compressional to extensional following the steepening of the subduction angle and asthenosphere upwelling associated with the impingement of the Farallon-Pacific spreading ridge (Buising., 1990; Cross and Pilger., 1978; Dickinson and Snyder., 1979; Howard et al., 2017). Most of the subsidence within the extensional corridor occurred in conjunction with early extensional sag associated with the opening of the proto gulf of California (Howard et al., 2015). Additional extension was likely cut short upon a major stress regime change from pure extension to

4

modern trans-tensional forces, related to the opening of the modern Gulf of California (Buising., 1990). Dextral shear influences from the San Andreas fault further complicate the stress regime of the corridor (Bennett., 2016) and cause folding and faulting in Southern, AZ, particularly in the Chocolate Mountains (Beard et al., 2016). The Chocolate, Newberry, and Black Mountains form the bedrock units below the Bouse Formation and provide valuable lower age constraints to Colorado River integration. The Bouse Formation is lined by steeply dipping normal faults on the eastern and northeastern sides of the corridor surrounding Cibola, AZ. Many of these faults exhibit strike slip motion, exhibiting changes in dip and offset between hanging wall and footwall blocks. Active fault subsidence along normal faults could have also played a role in creating a preferential path for the Colorado River (Dorsey et al., 2017).

The Bouse Formation lies conformably on top of the Osborne Wash Strata, which consists of coarse terrigenous strata, deposited on modern topography. The Osborne Wash fanglomerate interfingers with the Bouse Formation basal carbonate unit (Bouse Marl) and consists of closely related suites of volcanic rock, sourced from nearby volcanic provinces, the Black and Newberry Mountains (Buising., 1990). Matrix supported rocks hold abundant volcanic detritus. The upper units of the Osborne Wash consist of coarse conglomerates that commonly interfinger with Bouse Marl near Cibola, AZ.

The Bouse basal carbonate unit (Bouse Marl) is the most common and widespread deposit within the Bouse Formation. It consists of micritic carbonates, calcareous sandstones, occasional interbeds of conglomerate lenses, small calcareous

sand bodies, and tufa (Pearthree and House., 2014). Bouse basal carbonates are commonly deposited on alluvial fan surfaces but also form drapes along bedrock surfaces. Bouse carbonate deposits surrounding the Silver Creek section within Mohave Valley is commonly interbedded with local sands and gravels. This correlation between sand, gravel, and carbonates records the interaction of lacustrine and tributary fan sedimentation when the lake was near its maximum water level (Pearthree and House., 2014). The nearby Paloverde mountains provide all input for siliclastic facies, introducing poorly sorted sand, silt, gravel, and volcanics. Marls in the southernmost portion of Blythe Basin contain sparse assemblages of Batillariid gastropods, other micro-mollusks and barnacles. Additional assemblages include root casts and burrows. Various deposits display flaser and wave ripple cross laminations, and thin horizontal bedding. Additional features include sigmoidal cross bedding architecture with 0.4 to 2.5m set thicknesses (Gardner and Dorsey., 2021).

The uppermost Bouse deposits are divided into the basin margin association and basin fill association (Buising., 1990). Basin margin units reflect steeper slopes, displaying dips of 5 to 30° degrees basin ward, while basin fill units are gently dipping basin ward from 0 to 10° degrees. These deposits are associated with lacustrine and fluviolacustrine basin fill (Pearthree and House., 2014). The basin margin association consists of an array of carbonate and terrigenous clastics as well as a tufa, which commonly occurs as a rind on basement exposures, deposited during maximum basin fill of the Bouse lake systems. The basin fill association corresponds with deposits located near the basin center. The basin fill association is divided into informal members, the bottommost of which consists of bleach white bedded

carbonate limestone and coquina, with terrigenous input on the range of 20-50% of the total volume (Buising., 1990). The carbonate rock is commonly interbedded and contains volcanic input as pebble to cobble sized fragments. Volcanic fragments include angular biotite, epidote, and sparse basement rocks. The upper member of the basin fill is all terrigenous rocks, the lower portion of which is dominated by various colored siltstones and muds, commonly interbedded with sands. Mud ranges from green to yellow with pink siltstone interbedded, and thinner white limestones are present. The top section of the basin fill is dominated entirely by siltstones, fine grained marl, and fossiliferous hash, which are alternating and commonly interbed with one another.

2.2 PREVIOUS GEOCHRONOLOGICAL STUDIES

Recent work conducted on the Lost Cabin Beds, which underlie the Bouse Formation in Cottonwood Valley, by Schwing., (2019) revealed a geomagnetic polarity reversal within the Thvera subchron. One ash layer within the Lost Cabin beds correlates to the 5.7Mya Wolverine Creek eruption in the Idaho Hese eruptive center (Figure 4) (Ogg., 2012). The Wolverine Creek tuff ash layer was analyzed for Ar^{40}/Ar^{39} detrital sanidine dating and revealed an age of 5.35Mya. This data suggests that integration occurred during or after the Thvera subchron (C3n.4n, 5.25-5.01) (Schwing., 2019). This information effectively creates the lower age boundary (older) for this study, establishing a depositional age of the pre-Bouse Lost Cabin beds in the northernmost valley of the LOCO

The Lawlor tuff provides an excellent date for basin fill association, revealing an age of 4.83Mya within the Bouse Formation in Blythe Basin. This date produces

the upper age boundary (younger) for the study (Figure 4) (Ogg., 2012). Detrital

sanidine grains found near the base of the Bullhead Alluvium revealed an age of

4.62Mya, while grains found higher in the section yielded an age of 4.30Mya. This

data is consistent with other published data suggesting an age of 4.5Mya for the onset

of the Bullhead Alluvium deposition (Crow., 2021; Howard et al., 2015). A recently

found ash analyzed within Hart Mine Wash in Blythe basin yielded an MDA (Mean

depositional age) of 4.7 +- 0.5Mya (See Figure 4) (Ogg., 2012). This age is

correlative with that of the Lawlor Tuff but is yet to be defined chemically as the

same ash layer. These constraints help place the potential age of integration for a

through-flowing Colorado River from ~4.7-4.62Mya.

2.3 MAGNETO STRATIGRAPHY

Magnetic polarity stratigraphy can provide age information about specific

deposits by correlating them to the geomagnetic polarity timescale (Opdyke and

Channell., 1996) (Figure 4) (Ogg., 2012). Rock units are characterized based off the

directions of their magnetic minerals, either aligning to a modern field, normal

polarity, or a field that is 180° apart from the modern, a reverse polarity. Consistent

spreading rates of ocean basins provide a continuous record of magnetic anomaly

profiles, allowing for the creation of the geomagnetic polarity timescale, or GPTS

(See Figure 4) (Ogg., 2012). The GPTS is particularly accurate in Late Jurassic-

Quaternary timescales. Absolute ages can be applied directly to the GPTS or

correlated indirectly through the fossil record (Opdyke and Channell., 1996).

Magnetic polarities captured within sediments can also be indirectly applied to the

GPTS, if context is available, like an absolute age date acquired from nearby tephra.

Current constraints on the age and correlation of the early Pliocene Bouse

Formation within Blythe basin are suggested by a review of magnetostratigraphic

data by Howard et al., (2016). The review utilizes comparisons from the more

complete magnetostratigraphic record of the Fish Creek Vallecitos Basin of the Anza

Borrego area in the Western Salton Trough. The earliest work conducted in Blythe

Basin corresponds to a pilot USGS study conducted by Daniel Malmon to assess the

possibility of a magnetostratigraphic study of the Bouse Formation. Magnetic polarity

determinations were made by Malmon and Hillhouse using outcrop samples from the

Bouse between Bouse Wash and Quarry Mountain. These samples displayed normal

polarity, but to the Southwest within the Palo Verde site (Figure 1) display

dominantly reversed polarity. These results suggest a polarity transition at an

elevation of 150m asl, from normal to reverse polarity (Howard et al., 2016). These

results require further testing but agree with measurements reported by Kukla and

Updike., (1976). Kukla and Updike tested polarity on drill cores in Blythe Basin and

reported reversed and normal polarities within the Bouse formation and the overlying

Bullhead Alluvium. Deformation of Bouse units' post-deposition makes correlating

the deposits to the Fish Creek Vallecitos section tentative. However, Howard et al.,

(2016) suggests the Palo Verde reversed interval in the Bouse is stratigraphically

below the normal polarity section of Mesquite Mountain. This inference suggests

there is at least one normal interval sandwiched between two reversed intervals.

Therefore, the Bouse Formation contains at least one polarity boundary, and one full

subchron within the Gilbert polarity chron (Figure 4) (Ogg., 2012). Normal polarity

rocks include the 4.83Mya Lawlor Tephra sampled in California by Sarna-Wojcicki

et al., (2011), which corresponds to the normal polarity Sidufjall subchron (C3n.3n). The interbedded portion of the Bouse Formation (basin fill) includes reversed and normal polarity section but the relationship between adjacent Lawlor tephra remains uncertain. McDougall and Martinez., (2014) suggest that fossil assemblages within the Bouse basal carbonate unit correspond to Miocene age, older than the Sidufjall. Since no subchron between 3.6 and 6.9Mya is shorter than 100kyr, the currently sampled portion of the Bouse must represent a period of at least 100 kyr. This length of time is longer than the 30-40 kyr that Spencer et al., (2008; 2013) suggested was required for the filling and spilling model of the Bouse Formation in Blythe Basin. The 30 kyr period for the filling and spilling model of Spencer et al., (2008; 2013) is informed by two major factors; The necessary salinity level within paleo-lake Blythe to accommodate marine organisms and the lack of evaporite minerals within the Basin.

This study examines samples located throughout Blythe Basin to augment previous work conducted in the area and confirm the presence of a geomagnetic polarity reversal within the Bouse Formation. Modern cryogenic paleomagnetic equipment and analytical procedures can discern weaker magnetizations than previous magnetometers, which would benefit the resolution of the potential reversals in this area. More specifically, this study aims to determine if the basal carbonate unit of the Bouse Formation lies within the normal polarity Sidufjall or Nunivak subchrons by capturing a reversal event within this unit. The presence of a reversal between the normal polarity Sidufjall and Nunivak subcrons within the Hart Mine Wash section is suggested by the work of Crow., (2021) and is validated by the

results of this study. Sampling conducted surrounding Mesquite Mountain supports

the notion of Malmon., (2011) that the lower section of Mesquite Mountain is

dominantly normal polarity, while it does not inform the hypothesis that a polarity

transition exists in the upper quarter of the mountain, due to the extremely high

sedimentation rate at these locations (Andy Cohen, personal communication).

Additional sampling taken to the west of Mesquite Mountain near the Riversides

Mountains, also supports the notion that this area of Blythe Basin near Parker, AZ,

lies in a normal polarity section. A final sampling location around Lake Havasu City,

AZ revealed a normal polarity section which is near the post 5.24 Mya Lost Cabin

Beds, which supports the presence of a reversal into the Thvera subchron, as

proposed by Schwing., (2019).

3 METHODS

3.1 FIELD SAMPLING METHODS

Magnetostratigraphic field sampling was conducted in March of 2022,

throughout Blythe Basin and Mohave Valley, including Hart Mine Wash and The

Riversides. The focus of this study was Hart Mine Wash, near Cibola, AZ along a

small washout revealing a ~5-7m outcrop of Bouse deposits (Figures 5-7). Sampling

was performed both laterally and vertically along the section with a vertical sampling

interval of ~6 cm between samples and a horizontal sampling interval which varies

based on accessibility to the outcrop. Horizontal sampling within sites was conducted

in intervals of ~3cm between samples. Sample coring was dependent on the

competence of the units in question, which resulted in the sampling of primarily

Bouse marl. Other competent units included a fossil hash that was too coarse grained

for single domain magnetic grains to be present. Less competent silts and muds were oriented in hand sample before being removed from the outcrop with a demagnetized chisel and pick. Cores were acquired with a modified water-cooled chainsaw equipped with a Pomeroy drill adaptor (Butler., 1992). Drilled cores were oriented in the outcrop using an aluminum core-orienting device. Cores are marked for an up direction before being removed from outcrop and oriented with an arrow pointing out of the drill hole. Bedding orientations were taken with a Brunton transit field compass.

Additional sampling sites at this location were further south from Hart Mine Wash but parallel to the first outcrop. Sampling efforts were conducted in the Riversides, located North of Parker, AZ (Figures 8-9), and Mohave Valley, near Lake Havasu City, AZ. The Riversides site consisted entirely of loosely bedded muds and clays while Mohave valley samples were collected from fine grained marl. All samples from the Riversides and subsequent sampling in Mohave Valley were collected in hand sample, due to the incompetency of the beds in question.

3.2 PALEOMAGNETISM

3.2.1 SAMPLE PREPERATION

Samples collected through a drill were cut into two or more specimens if the core length exceeded 2.5cm. This was accomplished via a small wet saw, which utilizes a demagnetized saw blade to avoid alteration of magnetic fabric. Samples were cut to lengths of 2.5cm to maximize the number of specimens used for analysis

and allow them to be placed within the cryogenic magnetometer sample handler (Butler., 1992).

Samples oriented in blocks were prepared for analysis by cutting specimen into 2.5cm cubes, before placing them in a clear, plastic, 8cm^3 demagnetized box for magnetic analysis. Dry cutting was performed via band saw with a demagnetized saw blade to avoid inducing or altering the specimen's magnetic fabric. The rocks were cut without water to preserve the integrity of the silt and mudstones. Specimens were sanded in the later stages of preparation, if necessary, to fit into 8cm^3 plastic specimen boxes (Butler., 1992). If specimens were especially difficult to cut to size, small pieces of shop rag were used to pack the samples into the box, to avoid reorientation. Specimens are then marked with a north arrow, and an additional arrow on the side to properly orient them for analysis.

3.2.2 DEMAGNETIZATION

All measurements of magnetic fabrics were acquired by a 2G enterprises cryogenic magnetometer with DC squids, which is housed inside a magnetically shielded room to avoid magnetic interference and prevent housed specimen from acquiring the Earth's modern magnetic field direction The cryogenic magnetometer utilizes an Leeman Geophysical, LLC automated sample handler, which houses and measures the specimen in three directions, x, y, and z. The sample handler measures and rotates the specimen by 90°, 180°, and 270° to achieve these measurements.

Demagnetization was accomplished using two different methods. The first few rounds of demagnetization conducted at the University of Oklahoma in Norman,

Oklahoma, were performed via thermal demagnetization, using an ASC Model TD48

Thermal Demagnetizer-ASC Scientific high temperature oven (ASC Scientific, inc.),

and glass sample tray to house a suite of specimens. Specimens were measured

initially for an NRM (Natural Remnant Magnetization) before being baked in

stepwise fashion to 600°C using a specific demagnetization treatment, beginning with

100°C (100-200°C, in 100°C step, 200-240°C, 40°C step, 260-600°, 20°C steps).

Specimens were baked for 60 minutes during each step, after which they would cool

to room temperature before being measured for that interval. All specimens collected

via drill bit were analyzed via thermal demagnetization due to difficulties associated

with thermal measurement of block samples.

Additional demagnetization methods include AF (Alternating Field)

demagnetization, which, like thermal, is a destructive process, and measures the

decay of magnetic grains. All AF demagnetization was performed at New Mexico

Highlands University in Las Vegas, NM. The orthogonal coil AF demagnetizer is in-

line with an Applied Physics 755-4K cryogenic magnetometer, which then

automatically measures the remaining specimen magnetization after each step of the

AF treatment. AF demagnetization was conducted in 22 steps using a modified

demagnetization sequence more suitable for sedimentary analysis (0-30mT, 3mT

Increments, 30-90mT, 5mT Increments). Demagnetization treatment was modified

this way to capture more incremental measurements as sedimentary rocks tend to

decay more rapidly, and due to the weak nature of the NRM in these samples.

The graphic result of these processes is a magnetic decay curve, which decays

towards the graph's origin, providing an inclination and declination of magnetic

grains (Figures 10-14). The format of these graphs are all orthogonal vector projections (Zijderveld., 1967) while all group statistics are visualized in equal area projections (Butler., 1992; Love, Jeffrey., 2007; Fisher., 1953) (Figures 15-20). This information allows paleomagnetists to place the specimen along a magnetic polarity path acquiring a relative age or determine a more absolute age by referencing it to a specific geomagnetic polarity subchron associated with that time and polarity interval. Data produced at New Mexico Highlands University was modified using Remasoft (Chadima, M., Hrouda, F. 2006. Remasoft 3.0 – a user-friendly paleomagnetic data browser and analyzer. Travaux Géophysiques, XXVII, 20–21) which produces principal component analysis (PCA), Module plots and Group Statistics. Additional software includes SUPER IAPD (Torsvik et al., 2016) which was utilized for all thermal demagnetization techniques performed at the University of Oklahoma, to avoid inconsistencies in data processing between labs.

3.2.3 ROCK MAGNETIZATION TESTS

Rock magnetization tests include Curie temperature acquisition via thermomagnetic curve analysis, utilizing an AGICO KLY5 kappa bridge with a CS-4 furnace apparatus attachment (Agico, inc.). The CS4 furnace attachment analyzes responses in magnetic carriers associated with temperature variation from room temperature to 700°C. Measurements are performed under an argon gas environment to prevent oxidation of materials within the specimen. Specimens are powdered and weighed out to 0.500 grams before being placed in a quartz tube, where a thermometer is inserted into the tube to measure temperature changes in the sample. This process results in a temperature curve revealing the approximate Curie

temperature for the magnetic mineral within the specimen (Figures 21-26).

Temperature curves are then analyzed and corrected utilizing Cureval8 (Agico, inc.).

The correction removes the influence of the quartz tube on the measurement of

magnetic remanence, using a known standard value for the remanence of a quartz

tube.

The Lakeshore Cryogenics 8600 Series Vibrating Sample Magnetometer

(VSM) (Lakeshore Cryogenics, inc.) was used to provide both Hysteresis curves, and

first order reversal curve (FORC) diagrams (Figures 27-35). In the case of this study,

a hysteresis curve is the result of an induced magnetic field in two directions upon a

magnetic material. It is first magnetized in the positive direction and forced back to

zero by applying a magnetic field in the opposite direction. The inability of magnetic

materials to trace back on the same curve is dependent on the magnetic domain of the

material. The result is the "memory" of the magnetization induced on the grain

(Ewing., 1930). First order reversal curves (FORCs) are a set of hysteresis curves,

which begin at an arbitrary saturation field, H. Rock samples were partially powdered

into small chips, weighing around 0.250 grams, and placed in a gel capsule which is

attached to a sample rod. A motorized machine head lowers the sample rod into

position. The sample vibrates between two magnetic sensors, which reads the

response of the magnetic minerals when subjected to both increasing and decreasing

intensities of magnetic fields. The resulting FORC's are transformed into FORC

diagram contour plots, which reveals a single, multi, or vortex domain for the sample

3.2.4 ROCK MAGNETISM DETERMINATION

Curie temperatures of magnetic minerals can be determined from strong-field thermomagnetic experiments. The experiment involves subjecting a rock sample to increasing temperature, and a strong magnetic field. The magnetic saturation of the sample (J_s) is monitored through the heating curve of the experiment. When the J_s of the sample decreases dramatically, the Curie temperature of the magnetic mineral within the sample is revealed. Curie temperature experiments can be performed directly on strong magnetic samples, whereas weaker samples require a concentration of magnetic minerals (Butler., 1992)

Specific magnetic minerals display unique relaxation times whose rates vary based on different temperatures. The relaxation time of a magnetic mineral is the time it takes to lose its induced remanent magnetization. Relaxation times are a product of the ratio of blocking energy to thermal energy. To designate a blocking temperature, a critical relaxation time must be chosen. This chosen relaxation time can then be used to determine the temperature at which a magnetic mineral changes domain type. Magnetite, for example, changes behavior from superparamagnetic to a stable single domain at 550°C. The temperature at which this change occurs is known as the blocking temperature. Acceptable ranges of blocking temperatures for certain magnetic minerals aid in the identification of magnetic carriers within samples (Butler., 1992).

3.2.5 ELONGATION/INCLINATION ANALYSIS

Magnetic grains found within rocks have a fixed orientation in the magnetic field in which they were deposited (Detrital Remnant Magnetization, DRM) that aligns with the long axis of the magnetized particle. As sediments are compacted

during deposition, magnetic grain inclinations are artificially shallowed as

gravitational torques cause the long axis of the grain to become closer to horizontal

(Butler., 1992). In this sense, the magnetization process is in some part a post

depositional remanent magnetization (pDRM). In sedimentary rocks, this can be

corrected using an elongation/inclination shallowing module of paleomagnetism.org

and Mark Hounslows PMagTool software (PMag Tools Version 4.2a by Mark

Hounslow, 1997-2006), which corrects shallow characteristic remnant magnetizations

(ChRM). This process is performed via a computing method which runs 5000

nonparametric bootstraps to fit the magnetic data in question to the TK03.GAD field

model (Tauxe, L, Banerjee, S.K., Butler, R.F. and van der Voo R, Essentials of

Paleomagnetism, 5th Web Edition, 2018). The module calculates the elongation

parameter of the orientation matrix. If the elongation is lower than what is expected in

the field model, it is unflattened using a set of unflattening parameters. The program

computes a corrected sample inclination and a 95% confidence interval as to what the

range of inclinations could represent. This operation is performed initially with only

the normal polarity samples in the data set, followed by the reversed polarity samples.

Finally, the reverse polarity samples are flipped to their antipode and run with the

normal polarity samples, to ensure they fit the range of inclinations provided by the

original normal polarity test. If the samples fit within the 95% confidence interval,

they are corrected and ready for analysis via the reversal test.

3.2.6 REVERSAL TEST

The magnetic reversal test examines group statistics produced by

paleomagnetic data sets to determine whether the two datasets are truly antipodal, or

180° apart (opposite polarity) from one another. The test determines this relationship by examining the directional data of a dataset. Directional data is measured with respect to Earth's magnetic field. It includes an inclination, or the angle measured on the vertical plane, a declination, the angle measured on the horizontal plane and associated α95 and k values. α95 values reflect the confidence interval in which the mean direction has been estimated. Low α95 values correspond to low levels of confidence. K values represent within site scatter of directions, and the precision in which mean direction has been estimated. High k values represent a low degree of within site scatter and a high degree of precision. Additional paleomagnetic statistics include a maximum angular deviation or MAD (Butler., 1992). Low MAD values are associated with stable magnetic components.

The range of inclinations produced via elongation/inclination analysis is used to perform a reversal test, which determines if a negative polarity section is a true reversal. The reversal test uses two average inclination values between normal and reverse polarity sections in addition to an associated declination, number of specimens in the dataset used (N), an α95 value and a K value. The program uses this information to compute whether these values would be considered a true reversal using Mark Hounslow's PMAGTOOL program (PMag Tools Version 4.2a by Mark Hounslow, 1997-2006). This test works by considering the critical angle between mean specimen directions. The program determines the most accurate representation of the data set using either a Fisher, Kent, or Eigen distribution type, which is selected by the user. A positive test is classified as 'Ra' if the critical angle is less than 5°, 'Rb' if the angle is between 5° and 10°, 'Rc' if the angle is between 10 and 20° and

'Ro' (indeterminate) if the angle is greater than 20°. The symbol 'R-' is used to indicate a negative reversal test.

3.2.7 FOLD TEST

The Fold Test, or bedding tilt test, analyzes whether a characteristic remanent magnetization (ChRm) was acquired before or after a folding event (Figure 7). The process involves performing a bedding correction on samples acquired on both sides of the fold limb. If the data set becomes more tightly clustered following the bedding correction, the samples pass the fold test, which is indicative of a primary remanent magnetization. Samples fail the fold test if data becomes more scattered following the bedding correction and is indicative of a secondary magnetization (Butler., 1992).

4 RESULTS

4.1 STRATIGRAPHY

The Bouse Formation within Mohave Valley, near Lake Havasu, AZ, displays continuous marl at lower elevations and more alternating layers of marl and mud near the basin's margins (Figure 36). The lower elevation deposits contain thin layers of Bouse marl, on a scale of 2-5cm. These marls contain abundant recessive layers and are capped by quaternary talus and alluvium. Deposits near the basin's margin are found in large steeply sloping mounds of alluvium. Within the mounds are discrete layers of Bouse marl, interbedded with thick successions of muds and clays. These deposits are alternating and display variations in thickness between the layers up and down section. Mud layers are 2-3x thicker than marls in the lower section. In the upper most section, marls begin to dominate and form individual beds up to 10-12cm

thick. Mud occurs exclusively in some layers, where others display thin layers of marl, around 1-2cm thick, within a dominant mud deposit. Marls here are more competent than marls found further south near Cibola, AZ and commonly display hematite staining near the boundary of marl and mud. Sedimentary structures are sparse, displaying planar bedding and mud cracks.

The portion of the Bouse Formation located in the Riversides and Mesquite Mountain, near Parker, AZ, is dominated by various colored claystone's and mudstones, which are commonly interbedded (See Figures 8-9 and 37-38). Mud ranges in color from green to yellow with pink claystone interbedded. These deposits are commonly found as loosely compacted, highly weathered mounds, displaying sections of more competent mudstones/claystone's surrounded by interbeds of loosely compacted mud. Clays and muds occur as thin layers, on the scale of 5 to 15cm in thickness. Layers are planar, with occasional wavy contact between clays and mud. Green mudstones occur in thinner successions than their pink claystone counterparts and commonly terminate with loosely compacted layers of reddish muds. Sedimentary structures are minimal, displaying mud cracks and planar bedding which weathers reminiscent of badlands topography.

In Hart Mine Wash, near Cibola, AZ, the section becomes dominated by conglomerates, fine grained marl, fossiliferous hash, and a thin ash layer (Figures 5 and 40-43). The entirety of the Hart Mine Wash section dips gently to the West. Marl layers are planar, laterally discontinuous and display bleach white to light pink staining. Marl thins toward the eastern side of the section, and eventually onlaps fossil hash, which then dominates the exposed stratigraphy. In the middle portion of

the exposed outcrop marl begins to display sweeping layers, rather than thin, planar

beds. Moving west, the marl layer thickens on the scale of 2-3x and is highly

irregular. Marl and ash layers are thicker at the top of the section, increasing from

~12cm to 20cm thick. Interbedded marl and ash are sandwiched by more competent,

sandy marls, which are 1-4cm thick. The marl and fossil hash both display several

recessive beds which are used as stratigraphic markers throughout the section. Marl is

interrupted by a thin gravel layer on the bottom, which separates the marl from the

Golden Gravel, the lowermost unit in the section. Some of the finer gravel material

makes its way into the Golden Gravel, and into the marl. The Golden Gravel consists

of sub-rounded boulder-sized clasts, which display a golden color, and thin mud

layers (~2.5cm) in between clasts. Contrary to marl, fossil hash layers increase in

thickness towards the west, and thin in the eastward direction. Towards the middle of

the section, fossil hash increases in thickness, and terminates close to the western

portion of the outcrop. Fossil hash displays cross bedding and sweeping lineation's in

the direction of dip. Western stratigraphy consists of excavated mounds of hash on

the uppermost unit as fossil hash interrupts the lateral continuity of sandy marl. Fossil

hash on the west side displays large vugs and recessive erosion layers. Sedimentary

structures are numerous and varied, including ripple cross lamination, shrinking

cracks (mud cracks) soft sediment deformation, load casts and flame structures.

Primary structures found within the section includes ripple cross lamination, current

lineation's, climbing ripples, herringbone trough cross bedding and parallel

laminations. Sedimentary structures are found exclusively in the marl unit. Basin fill

units of the upper and lower member are commonly fossiliferous, particularly

abundant with barnacles attached to the exterior of the rock, as well as local land plant fragments, foraminifera, and ostracods (Buising 1990).

4.2 QUALITY ANALYSIS (GRADING)

Individual sites, samples and specimens across both demagnetization methods are assigned a letter grade which indicates the quality of the data produced (Figures 5, 9-12). An A letter grade corresponds to a specimen that displays a linear decay curve, decays toward the origin, displays minimal point clustering, and shows a clear direction of remanent magnetization (Figure 11). Letter A grades correspond to green polarity circles. The letter B letter grade corresponds to specimen which displays more clustered point behavior, but still displays a linear component, and dominant remanent magnetization direction, which decays towards the origin (Figure 12). A B letter grade also corresponds to a green polarity circle. A C letter grade corresponds to specimens which display clustered data around, but not reaching, the origin (Figure 13). C letter grades correlate with yellow/orange polarity circles. A D grade corresponds to a sample with no clear direction, and an unstable remanence, leading to a scatter plot of data points (Figure 14). D letter grades correspond with red polarity circles. An F letter grade corresponds to data that was too poor to be considered for analysis (Figure 10). When considering site and sample means, letter grades are assigned based on the number of samples used in the determination, and the proximity of these samples to one another. In most cases, low quality data (C-D ranking, MAD>15°) is removed from consideration when calculating mean directions for each site and sample.

4.3 PALEOMAGNETISM

4.3.1 THERMAL DEMAGNETIZATION

Thermal demagnetization yielded 34/40 (N/No) specimens which produced stable magnetic decay curves (Table 1). Thermal specimen data recorded include a declination, inclination, and MAD. Site means are then determined from specimen lying within the same site. Site mean statistics include a mean declination, inclination, α95 and k value (Tables 1-3). Also included in the site means are the number of samples considered for analysis marked N/No, where N is the number of samples considered, and No is the total number of samples taken.

Specimen analyzed for thermal demagnetization consisted entirely of the Hart Mine Wash site due to poor drilling media located in the Riversides and Mohave Valley. Thermal demagnetization revealed a section in HMW that is primarily normal polarity, with low to mid-level inclination values, ranging from 11.5° to 33.9°. A suite of samples directly below and above the Hart Mine Ash interface yielded negative inclination values, ranging from -24.7° to -64.4°. Un flattened positive inclinations associated with thermal demagnetization specimens at Hart Mine Wash returned a site mean inclination of Decl= 120.2° Incl= 41.3°, where α95=13.4 and k=3.85. Un flattened negative inclinations associated with thermal specimens at Hart Mine Wash returned a site mean inclination of -34.5°. Specimen surrounding the fold test at Hart Mine Wash returned all positive inclination values, ranging from 45° to 73°.

4.3.2 ALTERNATING FIELD DEMAGNETIZATION

The dataset produced from alternating field demagnetization is the higher volume and quality dataset between the two demagnetization methods utilized, the same as previous samples from Cottonwood Valley (Schwing, 2019). AF demagnetization yielded 68/76 (N/No) specimens, consisting entirely of oriented hand samples (Table 2). The AF dataset consists of all three locations analyzed in this study, Hart Mine Wash, The Riversides, and Mohave Valley. 24 of the specimens belong to Hart Mine Wash, 36 to the Riversides, and 16 to Mohave Valley.

Hart Mine Wash returned consistently good data receiving an A letter grade. The site contains a dominantly normal polarity interval, contrary to sparse reversed polarity samples recorded in the thermal run (Table 1-2). Inclination values from Hart Mine Wash range from 18° to 70°, for an average of 49.7°. Two lower quality sites (HMW8 and HMW8+9) were removed from consideration when calculating the means to improve overall accuracy and fit (Figure 15). Hart Mine Wash AF specimens returned a site mean direction of Decl= 4.7°, Incl= 49.7°, where α95= 13.1 and k= 50.05.

The 1RS group (Riversides group 1) revealed another normal polarity section, with a mean inclination of 38.8° and a B letter grade (Figures 16 and 37) (Table 2). The mean direction and related statistics improved by removing 1RS4 from consideration but were kept for the sake of data volume. Individual specimens within 1RS4 produced consistent and agreeable data, of which the highest quality samples are within 10° of each other. The 4RS sites produced more variable data, with both a normal and reverse inclination section, although the normal section is close to negative inclination (0.6°) (Figure 17-18 and 38) (Table 2). Due to this conflict, the

4RS sites were considered in two parts, positive inclination sites, negative inclination sites. The negative inclination sites returned a mean direction of –11.2° and is the higher quality dataset between the two. The presence of the normal polarity 4RS site is entirely dependent on the selection of one higher inclination value, due to a lack of data quality surrounding the selection. The normal polarity 4RS sites have a site mean direction of Decl= 18.3°, Incl= 25.2°, α95= N/A and k= N/A.

The Mohave Valley section earned a cumulative grade of B and produced an average inclination of 66.7°, much higher than previously measured sections (Figures 19 and 36) (Table 2). The group statistics improved by removing sites MV2 and MV5 but were kept for the sake of data volume. Individual sites within Mohave Valley display similar inclinations, within 3° of one another, except MV5, which produced a much lower inclination at 36.2 degrees. The site mean direction of MV samples was Decl= 346.9°, Incl= 66.7°, where α95= 12.8 and k= 52.26.

4.3.3 FOLD TEST

A fold test was attempted around a dewatering structure within Hart Mine Wash to identify a primary magnetization within the Bouse marl. The fold test returned insignificant results due to small limb angles respective to the fold axis. In other words, data points were not significantly scattered from one another and became negligibly closer to one another upon performing the bedding correction.

4.4 ROCK MAGNETISM

4.4.1 CURIE TEMPERATURE

Curie Temperature analysis across all groups produced inconclusive data and display little to no inflection in the heating curve, which you would expect in strongly magnetized samples. However, the cooling curve does deviate from the heating curve, confirming, along with thermal and AF demag, that magnetic minerals are present.

Curves produced from the Hart Mine Wash specimen deviate from the heating curve anywhere from 450 to 550°C. The magnetic strength of these samples ranges between 17 and 20 kT[E-6] (kilo Tesla). The shape of these curves are negative trending lines, with little curvature before, at, or after the suspected Curie temperature (Figures 23-24).

The 1RS and 4RS specimens produced slightly stronger magnetic remanence, ranging from 17 to 22 Kt[E-6]. The shapes of the 1RS curves are more regular, negative trending lines, with cooling curve deviations occurring anywhere from 300 to 450°C. 4RS specimen produced similar magnetic strength but displayed curves that are far more irregular, with multiple points of deviation between the heating and cooling curves. Specimens deviate at a much higher temperature in these curves, around 600°C, and much earlier, around 200°C and around 450°C (Figures 21-22).

The specimens analyzed from Mohave Valley were decisively the highest strength remanence materials, resulting in the clearest deviations from the heating curve out of all other specimens. Cooling curves in Mohave Valley produce clear deviation surrounding 350 to 500°C. Magnetic remanence for MV samples ranges from 28 to 60 Kt[E-6]. Despite their high strength and clear responses in the cooling curve, the samples were still not strong enough to observe a response in the heating curve, resulting in a linear negative trending line (Figures 25-26).

27

4.4.2 FORC ANALYSIS

The results of the FORC analysis for all samples are ambiguous. The experiment returned unorthodox hysteresis curves, with especially long "tails" and considerable amounts of noise. The hysteresis curves were converted into FORC contour plots, which revealed no clear domain signal from any of the samples tested. Two specimens from the 4RS sites returned visible domain data, most consistent with a multi domain behavior, but not clear enough to accurately interpret (Figures 27-31).

4.5 MAGNETIC DECAY CHARACTERISTICS

Magnetic module plots were produced using Remasoft on stable specimens from each location that were subjected to AF demagnetization. These plots, in conjunction with the character of magnetic decay curves, can reveal the magnetic characteristics of the specimen in question. Most specimen subjected to demagnetization techniques displayed unstable remanence, reflected in the instability of data points collected during demagnetization (Figure 10). Linear, stable components produce the most accurate and trustworthy paleomagnetic data (Figure 11), while unstable, low coercivity specimens produce scatter plots and unclear magnetic components.

The Hart Mine Wash specimens produced inconsistent magnetic characteristics. The HMW8-1 module plot (Figure 44) is an example of a specimen that displays a high magnetic moment but decays very rapidly. HMW8-1 produced a maximum moment of 476.e-06 Amps per meter (A/m) and a minimum moment of 6.21e-06 A/m. Fifty % of the specimen's original remanence had been depleted by 5.6

mT and 10 % of the remanence remained by 22.9 mT. The specimen was completely depleted by the time it reached 37.6 mT, less than half of the mT of the entire demagnetization process (90mT). HMW14-2 (Figure 45) is an example of an HMW specimen that displays a lower magnetic moment, but its decay curve is much more sustained. HMW14-2 shows a maximum moment of 257.e-06 A/m and a minimum of 39.3e-06 A/m. 50 % of the specimen's magnetization was depleted at 23.6 mT and the 10 % marker was not reached during the entire demagnetization process. HMW14-2 retained 15.3 % of its original remanence post 90mT.

1RS and 4RS specimens produced more robust magnetic moments, and higher coercivity than specimens found in Hart Mine Wash. 1RS1-2 (Figure 46) is an example of a specimen that contains a much higher magnetic moment than what is found in HMW. Despite this increased strength, 1RS1-2 decays more rapidly than lower strength specimens within HMW. 1RS1-2 produced a plot displaying a maximum moment of 1.14e-03 A/m, 3 orders of magnitude stronger than specimen analyzed in HMW, and a minimum moment of 159.e-06 A/m. 50 % of the magnetic moment was gone by 19.4 mT, but the specimen retains 13.9 % of its original remanence post 90mT. 4RS2-1 (Figure 47) is an example of a high strength specimen which decays slower than other high strength samples in the Riversides sites. 4RS2-1 produced a module plot with a maximum moment of 6.52e-03 A/m, even stronger than its 1RS counterpart, and an M (50%) value of 27.2mT. The specimen retained 10 % of its remanence at 66.3mt, and retains 11.4 % of its remanence post 90mT, making this one of the higher coercivity specimens identified in the study.

Specimens analyzed from Mohave Valley resemble specimens captured in Hart Mine Wash, although MV specimen contain higher magnetic moments. MV1-2 (Figure 48) provides an example of an MV specimen that is lower strength but displays a sustained decay curve. MV1-2 displays an Mmax of 197.e-06 A/m and a minimum moment of 20.8e-06 A/m. MV1-2 had lost 50 % of its magnetic moment by 24.4 mT and retains 10.6 % of its moment post 90mT. MV5-2 is an example of the most prolonged magnetic decay curve captured throughout this study. MV5-2 (Figure 49) displayed a higher maximum moment at 583.e-06 A/m and a minimum moment of 122.e-06 A/m, displaying higher coercivity than its MV1 counterpart. 50 % of MV5-2's moment remained by 29.1 mT, yet the specimen retains 20.9 % of its remanence post 90mT.

4.6 ELONGATION/INCLINATION ANALYSIS

The elongation/inclination shallowing module of PMAGTOOLS identified a flattening factor 1.696 for the HMW data set, which indicates a higher inclination value than what is expected in the field model. The inclination shallowing module only performs corrections on lower-than-expected inclination values; thus, no inclination shallowing correction was performed on the HMW sample data set.

The elongation/inclination shallowing module could not identify any cross over point between the riversides data and the field model, thus, no inclination shallowing correction was performed on the 1RS or 4RS data sets.

4.7 REVERSAL TEST

4.7.1 FISHER DISTRIBUTION

Site means for normal and reversed polarity sections from Hart Mine Wash pass the reversal test with a classification of 'Rc' using a Fisher distribution and the McFadden and McElhinney (1990) method. The direction data used for normal polarity site means was Decl= 356°, Incl= 72.24, where N=55, $\alpha95$= 10.2 and k= 4.6. Data used for reversed polarity specimens was Decl= 228°, Incl= -79.8°, where N=18 $\alpha95$= 23.4 and k= 3.15. The classification "Rc" is associated with an observed gamma of 30.59 and a critical gamma of 20.88.

4.7.2 EIGEN DISTRIBUTION

Site means for normal and reverse polarity sections within Hart Mine Wash pass the reversal test with a classification of 'Rc' using an Eigen distribution and the Common K, McFadden, and Lowes (1981) method. Direction data used for the normal polarity dataset was Decl= 358°, Incl= 63.5°, where N=55, $\alpha95$= 10.2 and k= 4.6. Direction data for the reversed polarity dataset was Decl=198°, Incl= -74.6°, where N=18, $\alpha95$= 23.4 and k= 3.15. The 'Rc' classification is associated with an observed gamma of 13.97 and a critical gamma of 22.55.

5 DISCUSSION/INTERPRETATIONS

5.1 STRATIGRAPHY

The Bouse Formation within Mohave Valley displays more alternating behavior than what is observed in Blythe Basin. Deposits within Mohave Valley consist of thin beds (2-5cm thick) of Bouse marl at lower elevations. Deposits near the basin's margins display large steeply sloping mounds of alluvium and mudstone that have been highly weathered. Bouse marl is preserved in thinner successions,

while mudstone and claystone appear 2-3x larger than the marl. Thickness variations throughout the outcrop suggest variation in suspended load and bed load during the fluvial component of the fluviolacustrine system. Mud occurs exclusively in some layers, where others display thin layers of marl, around 1-2cm thick. The marls found here are more sand rich than in Blythe Basin, corresponding to changes in bedload type as the river moves south. Lack of carbonate input into Mohave Valley marl suggests a less saline lacustrine environment than in Blythe Basin (Figure 36).

The portion of the Bouse Formation in the Riversides and Mesquite Mountain preserves the thickest succession of mudstone and claystone found anywhere else in Blythe Basin (Figures 17-18). Mud ranges in color from green to yellow with pink claystone's interbedded, suggesting alternating lake levels, producing periods of oxidation and reduction. Mudstone and claystone occur as thin, planar layers, suggesting a low energy environment near the maximum level of lake fill in Blythe Basin. Contacts between layers are occasionally wavy, suggesting changes in energy associated with water level variation and the influence of the fluvial component of the fluviolacustrine system. Green mudstones occur in thinner layers than pink claystone's, suggesting relatively shorter periods of reduction compared to oxidation. Sedimentary structures are minimal, suggesting a low energy lacustrine fill environment. Lack of carbonate input within this portion of the Bouse corresponds to a low salinity lacustrine system (Figures 8-9). Sedimentation rates in this area were likely rapid, with the Bouse likened to a "firehouse" of sediments rapidly filling the basin (Cohen, personal communication).

Deposits within Hart Mine Wash consist of primarily flat lying marl, punctuated by thick successions of fossil hash on the uppermost portion of the outcrop. Marl is deposited directly on top of the golden gravel and a thin conglomerate interface. Flat lying successions of deposits suggest this represents the basin center, near the maximum level of lake fill. Gravel and conglomerate deposits represent a temporary fluvial component, following the breach of paleo divides, which returns to lacustrine style deposition upon the appearance of the thin, planar Bouse marl. The abundance of marl suggests lacustrine style deposition for most of the time represented. High carbonate input into Bouse marl and upper fossil hash represents periods of arid climate which correspond to falling lake conditions in Blythe Basin. Sparse fossil assemblages like barnacles correlate to an increasingly saline lake system, creating a euryhaline environment. Sedimentary structures include ripple cross lamination, current lineation's, climbing ripples and parallel laminations, which are consistent with a temporarily fluvial but primarily low energy lacustrine style deposition. All sedimentary structures are found exclusively in the marl unit. Lack of tidal and marine influence in sedimentary structures suggests that this portion of the lower Colorado river corridor preserves lacustrine style deposition, rather than an estuary environment in the southernmost basin (Figures 5-7 and 40-43).

5.2 ROCK MAGNETISM

Rock magnetic tests performed in the study returned poor results, due to a low abundance of magnetic minerals, which causes some ambiguity surrounding the magnetic domain and mineralogy. Curie temperature analysis returned a variety of results but are most consistent with a magnetite and titano-magnetite host. Magnetite

has a Curie temperature of 550° C while titano-magnetite has a lower Curie

temperature depending on the proportion of magnetite and ulvospinel. Higher

proportions of ulvospinel result in even lower Curie temperature for the sample. A

few specimens, like 1RS1, deviate from the heating curve as low as 450°C, which

would indicate a higher proportion of ulvospinel. For example, sample 1RS1 (Figure

21) deviates from the heating curve around 450°C. This temperature is consistent

with a titano-magnetite carrier since the unblocking temperature of titano-magnetite is

less than that of magnetite. The specimens analyzed produced no response on the

heating curve of the Curie temperature curve, which is indicative of a low

concentration of magnetic minerals. This is confirmed by looking at the

corresponding NRM of the sample. For example, HMW8 (Figure 24) displays no

deviation in the heating curve surrounding 550°C and displays a maximum moment

of 476.e-06 A/m. This specimen also decays very rapidly, losing 50% of its total

moment by 5.6mT. Deviations in the cooling curve are indicative of a magnetic

mineral being destroyed by the heating process, but it is certainly not ideal for

confidently predicting magnetic mineralogy.

The quality of results returned from Curie temperature analysis is related to

the volume of material allowed for analysis. The kappa bridge thermal attachment

requires a powdered specimen of 0.500g, which works for most igneous and

metamorphic rocks, whose magnetic moments are much higher than that of sediments

(on the order of NRM = 1×10^2 A/m), but not for the lithologies analyzed in this

study, whose NRM/s are $476 \pm 200 \times 10^{-6}$ A/m. Higher volumes of sediment would

likely produce more conclusive results. One way to potentially increase the quality of

results would be to isolate specific magnetic grains and create a more concentrated powder for analysis. This was attempted, but no individual grains could be retrieved from the powder, which could mean that the magnetic grains in the samples are exceedingly small (<1µm), and difficult to pull out of powder over the timescale and sample amount attempted. A larger quantity of rock would need to be crushed and extracted over multiple passes to yield more meaningful rock magnetic data. The ambiguous results of rock magnetic experiments, while disappointing, do not discount the presence of remanent magnetizations, which are clearly present in both AF and thermal demagnetization (Figure 11).

Hysteresis curves and first order reversal tests (FORCS) produced low quality data and would be difficult to interpret with any degree of accuracy. Most specimens analyzed for FORC analysis produced contour plots that were noisy and displayed no clear cluster of data on the y or x axis. Most hysteresis curves produced from the Lake Shore Vibrating Magnetometer displayed unusual curves with lengthy "tails" on the end of the curves not commonly observed in strong magnetic carriers (Figures 33 and 35). There is also a high degree of noise associated with some hysteresis curves, which is a product of loose packing, or grain disassembly during the experiment due to the friable nature of the sediments (Figure 34). One hysteresis curve from the 4RS group produced a wasp wasted hysteresis loop, which is commonly observed in magnetic materials (Figure 32). Wasp wasted hysteresis loops commonly occur when combining two magnetic minerals of vastly different coercivities, or when combining both single domain and superparamagnetic behaviors (Tauxe, Mullender, and Pick., 1996). Two specimens from the 4RS group produced a higher quality contour plot,

most consistent with a multi domain magnetic behavior (Figure 28-29). It is most likely that these samples contain a multidomain magnetic character, which are large, non-remanence carrying magnetic grains. The poor results for these tests are related to the volume of material allowed for analysis. VSM (Vibrating Sample Magnetometer) samples are limited to 0.250g and are typically glued onto a gel mount lowered into the sensor. In the case of lower density sediments, the chip is far too large to fit on the mount and meet the weight requirement, and instead were chipped into even smaller pieces, and placed in a gel capsule for analysis. Due to the friable nature of the samples, samples vibrated within the capsule itself, despite efforts to mitigate this via tight packing of gel capsules. This vibration produced a lot of the noise identified in hysteresis curves and irregular curves not typically seen via FORC (Figure 34). Responses in cooling curves are indicative of a Titano-magnetite and magnetite host, as inflections occur as early as 450°C and as late as 550°C. Hysteresis analysis also supports this interpretation, as wasp wasted hysteresis curves are commonly observed with multiple magnetic carriers of different coercivities.

5.3 DEMAGNETIZATION

Principal Component Analysis (PCA) was performed on all specimens included in this study, where a representative section of the demagnetization curve was selected to determine DRM direction. The median direction data from Hart Mine Wash was Decl=4.7°, Incl=49.7°, α95= 13.1 and k= 50.05 for the AF specimens, and Decl=5.3°, Incl 66.3°, α95=8.6, and k=24 for the thermal specimens. The thermal group also contained several reversed polarity specimens, whose mean direction was Decl= 217°, Incl= -41°, α95= 9.7 and k=39. The 1RS sites returned a median

direction of Decl= 351.8°, Incl= 38.8°, α95= 16.3 and k= 32.92. The 4RS sites

returned a median direction of Decl= 18.3°, Incl= 25.2°, α95= N/A and k= N/A for

the normal polarity section and Decl= 176.3°, Incl= -11.2°, α95= 19.4, and k= 41.41

for the reversed section. The MV sites returned a mean direction of Decl= 346.9°,

Incl= 66.7°, α95= 12.8, and k= 52.26.

The interpretation for all sites is a primary magnetization. A primary

magnetization is supported by the inability of the magnetic grains to acquire a new

magnetic field component. Reacquisition of a secondary magnetization would require

heating beyond the unblocking temperature (I.e., burial processes) or shock

magnetizations from nearby volcanism or a bolide impact event. There is no evidence

for heating post deposition, or of a collision event. The lack of an observable

secondary component in demagnetization also supports all magnetic grains are

detrital, since authigenic minerals would have acquired a new magnetization. Loosely

packed muds and clays observed in the 1RS and 4RS sites revealed shallow negative

inclinations (Table 2), which were left un-flattened since they produced no crossover

with the GAD.TK03 field model. This makes it difficult to evaluate the credibility of

1RS and 4RS data, as these sediments have certainly shifted and fallen more than any

semi competent rock layer due to the nature of the deposits, which are found in large,

steeply sloping weathered mounds of loose muds and clays. Curie temperature

analysis revealed a magnetite and titano-magnetite host across all sites, which

typically displays multidomain behavior and unblocking temperatures on the range of

450-550°C. The inability of Curie temperature analysis to produce a deviation in the

heating curve makes magnetic mineralogy slightly ambiguous, although a

magnetite/titano-magnetite is most likely. Demagnetization results also support the interpretation that a magnetite host is likely based on unblocking temperatures during thermal demagnetization and near total removal of the NRM during AF demagnetization. This is supported by the rapid decay experienced in all sites, but particularly within Hart Mine Wash, as HMW samples commonly lose 50% of their moment by the 10mT mark (Figures 44-49). HMW samples retain less than 15% of their NRM by the 90mT mark, which supports the interpretation of a magnetite host, since the coercivity of magnetite is 120mT. Thermal demagnetization also supports the notion of a magnetite and titano-magnetite host through rapid decay experienced by the 100-200°C mark and the instability of data points following the 450-550°C mark. For example, samples 12-1 and 12-3 lose 60% of their NRM by 100°C, but don't lose their total stable magnetization until 550°C and 450°C.

Despite low quality rock magnetism results, the samples analyzed via both demagnetization methods display remanent magnetizations which are measurable, and in some cases, very stable. Declination values may vary both within and between sites due to the steep inclinations of the samples, but inclination values within and between sites are consistent, which suggests a stable remanent magnetization for the samples. For example, B quality data from HMW1 produced inclinations of 43.3°, 46.7°, 46.3°, and 53.9°.

5.4 MAGNETO STRATIGRAPHY

Sixty-five specimens were used to determine polarity within the Hart Mine Wash section. 40 of these were processed via thermal demagnetization and the other 25 via alternating field demagnetization. AF demagnetization specimens show a

consistent northern hemisphere mean direction, and a normal polarity component.

Thermal data from HMW displays two unique results, a Northern and Southern

hemisphere component, which indicate both positive and negative inclinations

(Figure 20). Site locations in Hart Mine Wash were located above and below the

~4.75Mya Hart Mine Wash ash which sets the younger age boundary for the study.

HMW1-HMW18 display a consistent positive inclination with a mean direction of

Decl=5.3°, Incl= 66.3°, where α95= 8.6 and k= 24 in the thermal demagnetization,

and Decl= 4.7°, Incl= 49.7°, where α95= 13.1 and k= 50.05 in the AF

demagnetization (Table 1-2). HMW1-18 starts ~1m below the Hart Mine Wash Ash

and HMW18 lies just beneath the same ash layer. HMW19-HMW25 display

consistent negative inclination values, with a mean direction of Decl= 217°, Incl= -

41° where α95= 9.7, k= 39 and lie exclusively on top of the ash layer in the section

(Table 1-2). The inclination shallowing module corrected low characteristic remnant

magnetizations to a mean inclination of 40.3° for the normal and reversed section.

However, the negative inclination site was identified as a poor representation of the

GAD field model by Mark Hounslows PMAGTOOLS program, complicating the

accuracy of negative inclinations. Inclinations between the normal and reverse groups

overlap in their 95 % confidence interval of potential inclinations, which indicates the

correction is statistically significant. The reversal test performed on inclination

corrected HMW specimens using a Fisher distribution returned a negative result, but

uncorrected inclinations pass with a ranking of 'Rc'. The reversal test performed on

inclination corrected and uncorrected HMW specimens using an Eigen distribution,

pass the reversal test with a ranking of 'Rc.' There is a consistent negative inclination

section occurring just above the Hart Mine Wash ash, which returns to positive

inclination values around HMW26 or 1.5 meters above the ash layer. This negative

inclination section is interpreted as the location of a transition between the 4.8Mya

Gilbert chron Sidufjall and 4.63 Mya Nunivak subchrons, using the ~4.72 Mya ash as

a reference to the GPTS (Figure 4) (Ogg., 2012).

Thirty-six specimens, all of which were demagnetized via AF

demagnetization were considered when determining polarity for the Riverside's

location (1RS and 4RS sites). The 1RS sites revealed a consistent normal polarity and

northern hemisphere component throughout all specimens (Table 1) (Figures 16-18).

The mean direction for the 1RS sites was Decl= 351.8°, Incl= 38.8°, α95= 16.3 and

k= 32.92. The 4RS location returned three sites which were shallow negative

inclinations, and plotted in the far southern hemisphere, and two sites which were

shallow positive inclinations and plotted on the high northern hemisphere (Table 1)

(Figure 16). No definite evidence exists to place this section within the geomagnetic

polarity timescale and could belong to either the Sidufjall or Nunivak subchrons

within the Gilbert chron (Figure 4) (Ogg., 2012).

Sixteen specimens, all of which were produced via AF demagnetization were

considered when determining polarity for the Mohave Valley location (MV). The

Mohave Valley sites produced consistent high positive inclinations, which is the most

agreeable data across sites from any other location (Table 1). MV specimen displays a

northern hemisphere component (Figure 19). The mean direction for MV sites was

Decl= 346.9°, Incl= 66.7°, where α95= 12.8 and K= 52.26. Previous work conducted

in this area from Schwing., (2019) place the High wall ash site at ~5.35 Mya, which is

validated by the presence of a reversal, capturing the transition from the C3r subchron to C3n.4n (Thvera) subchron of the Gilbert chron. Using the presence of this reversal as reference, the Mohave Valley site is interpreted to belong to the 5.24-5 Thvera subchron of the Gilbert Chron (Figure 4) (Ogg., 2012).

The magneto stratigraphy across all sites is bound by the presence of a reversal near the ~5.35Mya High wall ash within the Lost Cabin Beds and a ~4.7Mya Hart Mine Wash Ash. The results of this study accurately place the presence of a reversal within the Hart Mine Wash section of the Bouse Formation between the Sidufjall and Nunivak subchrons. This study captured negative inclination specimen directly below, and primarily above, the ~4.72Mya Hart Mine Wash ash which supports the notion that this section lies in the reverse polarity transition from the Sidufjall and Nunivak subchrons within the Gilbert chron (Figure 4) (Ogg., 2012).

6 CONCLUSIONS

The magnetostratigraphic relationships discovered throughout Mohave and Blythe basins further support the notion that Bouse deposition began sometime after 5.24Mya and ceased sometime around 4.62Mya, which is the age of the Bullhead alluvium, a deposit associated with a throughgoing Colorado river. Two ash layers (5.35Mya and ~4.72Mya) were used to reference the polarity of these specimens within the geomagnetic polarity timescale. Both the Mohave and Riversides sites returned entirely normal polarity sections (Table 1). The Mohave section is interpreted to belong to the 5.24Mya Thvera subchron, deposited rapidly during this normal polarity interval. The Riversides data are more enigmatic, sites could lie within the Sidufjall or Nunivak subchrons, but more absolute age dates and sampling

are needed to confirm this. Hart Mine Wash contains both a normal polarity section below the ~4.7Mya ash, and a reverse polarity section immediately surrounding the ash, which continues for several meters up section in Bouse Marl. This section is interpreted to represent the reversal period between the Sidufjall and Nunivak subchrons of the Gilbert Chron.

I suggest that future paleomagnetic sampling conducted around Blythe basin focus on a high-density sampling interval surrounding the ~4.72 Mya ash in Hart Mine Wash, to provide a robust data set capable of accurately predicting the presence of a reversal within the section. I predict such an effort would capture the presence of a reversal and effectively date the age of sediments directly below the ash at 4.8 Mya, the age of the transition from Sidufjall to Nunivak subchrons. Additional sampling should be conducted 1-2m up section to explore the possibility of an additional polarity transition. I predict this would reveal a transition into the normal polarity Nunivak subchron of the Gilbert chron. Further data analysis should be conducted to validate these hypotheses and further inform the magnetostratigraphic record of the Bouse Formation.

REFERENCES

"2G Superconducting Rock Magnetometer." Accessed March 29, 2023.

https://www.marum.de/Christian-Hilgenfeldt/2G-Spec2.html.

"AGICO KLY5 Kappabridges - ASC Scientific." Accessed March 6, 2023.
https://www.ascscientific.com/magnetic-susceptibility-systems/agico-kly5-
kappabridges/.

"ASC Model TD48 Thermal Demagnetizer - ASC Scientific." Accessed March 29,
2023. https://www.ascscientific.com/demagnetizers/asc-model-td48-thermal-
demagnetizer/.

Beard, L Sue, Gordon B Haxel, Rebecca J Dorsey, Kristin A McDougall, and Carl E
Jacobson. "Late Neogene Deformation of the Chocolate Mountains Anticlinorium:
Implications for Deposition of the Bouse Formation and Early Evolution of the Lower
Colorado River." . ., 2016, 9.

Bennett, Scott, Michael Darin, Rebecca Dorsey, Lisa Thompson, Paul Umhoefer, and
Michael Oskin. "Animated Tectonic Reconstruction of the Lower Colorado River
Region: Implications for Late Miocene to Present Deformation." *2016 Desert
Symposium*, April 16, 2016.

Bentham, Peter A., Douglas W. Burbank, and C. a. I. Puigdefabregas. "Temporal and
Spatial Controls on the Alluvial Architecture of an Axial Drainage System: Late
Eocene Escanilla Formation, Southern Pyrenean Foreland Basin, Spain." *Basin
Research* 4, no. 3-4 (November 6, 1992): 335–52. https://doi.org/10.1111/j.1365-
2117.1992.tb00052.x.

Bright, Jordon. "Multi-Disciplinary Paleoenvironmental Context for the Integration of
the Lower Colorado River Corridor, Bouse Formation, CA-AZ, USA, and Middle to
Late Pleistocene Human Evolution, the Koora Plain, Southern Kenya." Ph.D., The

University of Arizona. Accessed October 19, 2022.
https://www.proquest.com/docview/1986553343/abstract/B9A915116FD44036PQ/1.

Bright, Jordon, Andrew S. Cohen, David L. Dettman, and Philip A. Pearthree.
"Freshwater Plumes and Brackish Lakes: Integrated Microfossil and O-C-Sr Isotopic
Evidence from the Late Miocene and Early Pliocene Bouse Formation (California-
Arizona) Supports a Lake Overflow Model for the Integration of the Lower Colorado
River Corridor." *Geosphere* 14, no. 4 (June 8, 2018): 1875–1911.
https://doi.org/10.1130/GES01610.1.

Buising, Anna V. "The Bouse Formation and Bracketing Units, Southeastern
California and Western Arizona: Implications for the Evolution of the Proto-Gulf of
California and the Lower Colorado River." *Journal of Geophysical Research: Solid
Earth* 95, no. B12 (1990): 20111–32. https://doi.org/10.1029/JB095iB12p20111.

Cohen, Andrew, Colleen Cassidy, Ryan Crow, Jordon Bright, Laura Crossey,
Rebecca Dorsey, Brian Gootee, et al. "The Bouse Formation, a Controversial
Neogene Archive of the Evolving Colorado River: A Scientific Drilling Workshop
Report (28 February–3 March 2019 – BlueWater Resort & Casino, Parker, AZ,
USA)." *Scientific Drilling* 26 (December 2, 2019): 59–67. https://doi.org/10.5194/sd-
26-59-2019.

Cross, T. A., and R. H. Pilger. "Constraints on Absolute Motion and Plate Interaction
Inferred from Cenozoic Igneous Activity in the Western United States." *American
Journal of Science* 278, no. 7 (September 1, 1978): 865–902.
https://doi.org/10.2475/ajs.278.7.865.

Crow, R.S., J. Schwing, K.E. Karlstrom, M. Heizler, P.A. Pearthree, P.K. House, S.
Dulin, S.U. Jänecke, M. Stelten, and L.J. Crossey. "Redefining the Age of the Lower
Colorado River, Southwestern United States." *Geology* 49, no. 6 (June 1, 2021): 635–
40. https://doi.org/10.1130/G48080.1.

Crow, Ryan S., Keith A. Howard, L. Sue Beard, Philip A. Pearthree, P. Kyle House,
Karl E. Karlstrom, Lisa Peters, et al. "Insights into Post-Miocene Uplift of the
Western Margin of the Colorado Plateau from the Stratigraphic Record of the Lower

Colorado River." *Geosphere* 15, no. 6 (October 16, 2019): 1826–45.
https://doi.org/10.1130/GES02020.1.

"Crustal Extension along a Rooted System of Imbricate Low-Angle Faults: Colorado
River Extensional Corridor, California and Arizona." Accessed October 31, 2022.
https://doi.org/10.1144/GSL.SP.1987.028.01.19.

Default. "8600 Series VSM." Accessed March 6, 2023.
https://www.lakeshore.com/products/categories/overview/material-characterization-
products/vsm-systems/8600-series-vsm.

Dickinson, William R., and Walter S. Snyder. "Geometry of Subducted Slabs Related
to San Andreas Transform." *The Journal of Geology* 87, no. 6 (1979): 609–27.

"Distinguishing Brackish Lacustrine from Brackish Marine Deposits in the
Stratigraphic Record_ A Case Study from the Late Miocene and Early Pliocene
Bouse Formation, Arizona and California, USA | Elsevier Enhanced Reader."
Accessed September 22, 2022. https://doi.org/10.1016/j.earscirev.2018.08.011.

Dorsey, Rebecca, Gary Axen, Martin Grove, Bernard Housen, George Jefferson,
Kristin McDougall, Lyndon Murray, et al. "Redefining the Age of the Lower
Colorado River, Southwestern United States: COMMENT." *Geology* 49 (September
1, 2021): e531–e531. https://doi.org/10.1130/G49145C.1.

Dorsey, Rebecca J., Amy Fluette, Kristin McDougall, Bernard A. Housen, Susanne
U. Janecke, Gary J. Axen, and Catherine R. Shirvell. "Chronology of Miocene–
Pliocene Deposits at Split Mountain Gorge, Southern California: A Record of
Regional Tectonics and Colorado River Evolution." *Geology* 35, no. 1 (January 1,
2007): 57–60. https://doi.org/10.1130/G23139A.1.

Dorsey, Rebecca, Brennan O'Connell, Mindy Homan, and Scott Bennett. *Influence of
the Eastern California Shear Zone on Deposition of the Mio-Pliocene Bouse
Formation: Insights from the Cibola Area, Arizona*, 2017.

Dorsey, Rebecca, Brennan O'Connell, Mindy Homan, and K. Howard. *Upper Limestone of the Southern Bouse Formation: Evidence for Unsteady Origins of the Colorado River.*, 2016.

"Essentials of Paleomagnetism: Fifth Web Edition." Accessed October 27, 2022. http://ltauxe.github.io/Essentials-of-Paleomagnetism/WebBook3.html.

Ewing, Alfred. "Ferromagnetism and Hysteresis." *Proceedings of the Physical Society* 42, no. 5 (August 1930): 355. https://doi.org/10.1088/0959-5309/42/5/301.

Gardner, Kevin, and Rebecca J. Dorsey. "Mixed Carbonate–Siliciclastic Sedimentation at the Margin of a Late Miocene Tidal Strait, Lower Colorado River Valley, South-Western USA." *Sedimentology* 68, no. 5 (2021): 1893–1922. https://doi.org/10.1111/sed.12834.

Gardner, Kevin Kortum, and this link will open in a new window Link to external site. "Stratigraphy, Sedimentology, and Tidal Processes of the Late Miocene to Early Pliocene Southern Bouse Formation, Southeast Palo Verde Mountains, California." *ProQuest Dissertations and Theses*. M.S., University of Oregon, 2019. https://www.proquest.com/docview/2308261979/abstract/7D95F40A0D0640C5PQ/1.

Gawthorpe, R. L., and M. R. Leeder. "Tectono-sedimentary Evolution of Active Extensional Basins." *Basin Research* 12, no. 3-4 (July 1, 2000): 195–218. https://doi.org/10.1111/j.1365-2117.2000.00121.x.

Gawthorpe, Robert L., Alastair J. Fraser, and Richard E. Li. Collier. "Sequence Stratigraphy in Active Extensional Basins: Implications for the Interpretation of Ancient Basin-Fills." *Marine and Petroleum Geology* 11, no. 6 (December 1, 1994): 642–58. https://doi.org/10.1016/0264-8172(94)90021-3.

Harvey, Janet C. "Zircon Age and Oxygen Isotopic Correlations between Bouse Formation Tephra and the Lawlor Tuff." *Geosphere* 10, no. 2 (April 1, 2014): 221–32. https://doi.org/10.1130/GES00904.1.

Heslop, D., and A. P. Roberts. "Revisiting the Paleomagnetic Reversal Test: A Bayesian Hypothesis Testing Framework for a Common Mean Direction." *Journal of*

Geophysical Research: Solid Earth 123, no. 9 (September 2018): 7225–36. https://doi.org/10.1029/2018JB016081.

House, P. Kyle, Philip A. Pearthree, and Michael E. Perkins. "Stratigraphic Evidence for the Role of Lake Spillover in the Inception of the Lower Colorado River in Southern Nevada and Western Arizona." In *Special Paper 439: Late Cenozoic Drainage History of the Southwestern Great Basin and Lower Colorado River Region: Geologic and Biotic Perspectives*, 439:335–53. Geological Society of America, 2008. https://doi.org/10.1130/2008.2439(15).

Howard, Keith A, Daniel V Malmon, John W Hillhouse, Rebecca J Dorsey, Ryan S Crow, and P Kyle. "Magnetostratigraphic Constraints on the Bouse Formation in the Blythe Basin— Existing Evidence." . ., 2016, 4.

"Hysteresis in Magnetic Materials." Accessed March 22, 2023. http://hyperphysics.phy-astr.gsu.edu/hbase/Solids/hyst.html.

Ingersoll, Raymond V. "Tectonics of Sedimentary Basins, with Revised Nomenclature." In *Tectonics of Sedimentary Basins*, 1–43. John Wiley & Sons, Ltd, 2011. https://doi.org/10.1002/9781444347166.ch1.

"Interactions between Axial and Transverse Drainage Systems in the Late Cretaceous Cordilleran Foreland Basin: Evidence from Detrital Zircons in the Straight Cliffs Formation, Southern Utah, USA | GSA Bulletin | GeoScienceWorld." Accessed November 10, 2022. https://pubs.geoscienceworld.org/gsa/gsabulletin/article/127/3-4/372/126095/Interactions-between-axial-and-transverse-drainage.

Kappelman, John. "The Attraction of Paleomagnetism." *Evolutionary Anthropology: Issues, News, and Reviews* 2, no. 3 (1993): 89–99. https://doi.org/10.1002/evan.1360020304.

"Karlstrom Deformation Obscures Bouse Interpretation," n.d.

Latrubesse, Edgardo M. "Large Rivers, Megafans and Other Quaternary Avulsive Fluvial Systems: A Potential 'Who's Who' in the Geological Record." *Earth-Science Reviews* 146 (July 1, 2015): 1–30. https://doi.org/10.1016/j.earscirev.2015.03.004.

Love, Jeffrey. "Fisher Statistics," 272–73, 2007. https://doi.org/10.1007/978-1-4020-4423-6_100.

McDougall, Kristin, and Adriana Yanet Miranda Martínez. "Evidence for a Marine Incursion along the Lower Colorado River Corridor." *Geosphere* 10, no. 5 (October 1, 2014): 842–69. https://doi.org/10.1130/GES00975.1.

Miller, David M., Robert E. Reynolds, Jordon E. Bright, and Scott W. Starratt. "Bouse Formation in the Bristol Basin near Amboy, California, USA." *Geosphere* 10, no. 3 (June 1, 2014): 462–75. https://doi.org/10.1130/GES00934.1.

O'Connell, Brennan. "Sedimentology and Depositional History of the Miocene–Pliocene Southern Bouse Formation, Arizona and California." *ProQuest Dissertations and Theses*. M.S., University of Oregon, 2016. https://www.proquest.com/docview/1870783246/abstract/81474E94749041DEPQ/1.

O'Connell, Brennan, Rebecca J. Dorsey, Stephen T. Hasiotis, and Ashleigh V. S. Hood. "Mixed Carbonate–Siliciclastic Tidal Sedimentation in the Miocene to Pliocene Bouse Formation, Palaeo-Gulf of California." *Sedimentology* 68, no. 3 (2021): 1028–68. https://doi.org/10.1111/sed.12817.

O'Connell, Brennan, Rebecca J Dorsey, Mindy Homan, Brian F Gootee, and Kyle House. "Structural Controls on Stratigraphic Architecture of the Southern Bouse Formation near Cibola, Arizona." *B. o*, 2016, 5.

O'Connell, Brennan, Rebecca J. Dorsey, and Eugene D. Humphreys. "Tidal Rhythmites in the Southern Bouse Formation as Evidence for Post-Miocene Uplift of the Lower Colorado River Corridor." *Geology* 45, no. 2 (February 1, 2017): 99–102. https://doi.org/10.1130/G38608.1.

Ogg, J.G., (2012). Geomagnetic Polarity Time Scale. In: Gradstein, F.M., Ogg, J.G., Schmitz, M., Ogg, G. (Eds.), The Geologic Time Scale 2012. Elsevier, Amsterdam, 85-114.

Opdyke, Neil D., and J. Channell. *Magnetic Stratigraphy*. International Geophysics Series, v. 64. San Diego: Academic Press, 1996.

"Palaeomagnetic, Paleomagnetic, Mineral Magnetic, Rock Magnetic, Environmental Magnetic Software, Programs, Geomagnetism, Geophysics Software and Programs." Accessed March 29, 2023. https://www.lancaster.ac.uk/staff/hounslow/resources/software.htm.

"Paleogeographic Implications of Late Miocene Lacustrine and Nonmarine Evaporite Deposits in the Lake Mead Region: Immediate Precursors to the Colorado River | Geosphere | GeoScienceWorld." Accessed March 23, 2023. https://pubs.geoscienceworld.org/gsa/geosphere/article/12/3/721/132347/Paleogeographic-implications-of-late-Miocene.

"Paleomagnetism: Magnetic Domains to Geologic Terranes." *Choice Reviews Online* 29, no. 10 (1992): 29.

Pearthree, P. A., and P. K. House. "Paleogeomorphology and Evolution of the Early Colorado River Inferred from Relationships in Mohave and Cottonwood Valleys, Arizona, California, and Nevada." *Geosphere* 10, no. 6 (December 1, 2014): 1139–60. https://doi.org/10.1130/GES00988.1.

Pearthree, Philip A., and P. Kyle House. "Paleogeomorphology and Evolution of the Early Colorado River Inferred from Relationships in Mohave and Cottonwood Valleys, Arizona, California, and Nevada." *Geosphere* 10, no. 6 (December 1, 2014): 1139–60. https://doi.org/10.1130/GES00988.1.

"PMAGTOOL." Accessed March 29, 2023. https://www.lancaster.ac.uk/staff/hounslow/resources/software/pmagtool.htm.

Poulson, Simon R., and Barbara E. John. "Stable Isotope and Trace Element Geochemistry of the Basal Bouse Formation Carbonate, Southwestern United States: Implications for the Pliocene Uplift History of the Colorado Plateau." *GSA Bulletin* 115, no. 4 (April 1, 2003): 434–44. https://doi.org/10.1130/0016-7606(2003)115<0434:SIATEG>2.0.CO;2.

"Professional Paper." Professional Paper. Professional Paper, 1973.

Reheis, Marith C., Robert Hershler, and David M. Miller. *Late Cenozoic Drainage History of the Southwestern Great Basin and Lower Colorado River Region: Geologic and Biotic Perspectives*. Geological Society of America, 2008.

"Remasoft." Accessed March 29, 2023. https://www.agico.com/text/software/remasoft/remasoft.php.

ResearchGate. "Figure 1. Tectonic Map of the Lake Mead Area and Colorado Plateau–Basin..." Accessed November 30, 2022. https://www.researchgate.net/figure/Tectonic-map-of-the-Lake-Mead-area-and-Colorado-Plateau-Basin-and-Range-transition-zone_fig1_245025308.

Roskowski, Jennifer A., P. Jonathan Patchett, Jon E. Spencer, Philip A. Pearthree, David L. Dettman, James E. Faulds, and Amanda C. Reynolds. "A Late Miocene–Early Pliocene Chain of Lakes Fed by the Colorado River: Evidence from Sr, C, and O Isotopes of the Bouse Formation and Related Units between Grand Canyon and the Gulf of California." *GSA Bulletin* 122, no. 9–10 (September 1, 2010): 1625–36. https://doi.org/10.1130/B30186.1.

Sarna-Wojcicki, Andrei M., Alan L. Deino, Robert J. Fleck, Robert J. McLaughlin, David Wagner, Elmira Wan, David Wahl, John W. Hillhouse, and Michael Perkins. "Age, Composition, and Areal Distribution of the Pliocene Lawlor Tuff, and Three Younger Pliocene Tuffs, California and Nevada." *Geosphere* 7, no. 3 (June 1, 2011): 599–628. https://doi.org/10.1130/GES00609.1.

Schlische, Roy W., and Mark H. Anders. "Stratigraphic Effects and Tectonic Implications of the Growth of Normal Faults and Extensional Basins." In *Reconstructing the History of Basin and Range Extension Using Sedimentology and Stratigraphy*, by Kathi K. Beratan. Geological Society of America, 1996. https://doi.org/10.1130/0-8137-2303-5.183.

———. "Stratigraphic Effects and Tectonic Implications of the Growth of Normal Faults and Extensional Basins." In *Reconstructing the History of Basin and Range Extension Using Sedimentology and Stratigraphy*, by Kathi K. Beratan. Geological Society of America, 1996. https://doi.org/10.1130/0-8137-2303-5.183.

Software Informer. "Super-IAPD. Get the Software Safely and Easily.," July 11, 2020. https://super-iapd.software.informer.com/1.0/.

Spencer, Jon E., Kurt N. Constenius, David L. Dettman, and Kenneth J. Domanik. "Identification of Seasonal Varves in the Lower Pliocene Bouse Formation, Lower Colorado River Valley, and Implications for Colorado Plateau Uplift." *Geosphere* 17, no. 6 (November 1, 2021): 1745–61. https://doi.org/10.1130/GES02419.1.

Spencer, Jon E., and P. Jonathan Patchett. "Sr Isotope Evidence for a Lacustrine Origin for the Upper Miocene to Pliocene Bouse Formation, Lower Colorado River Trough, and Implications for Timing of Colorado Plateau Uplift." *GSA Bulletin* 109, no. 6 (June 1, 1997): 767–78. https://doi.org/10.1130/0016-7606(1997)109<0767:SIEFAL>2.3.CO;2.

Spencer, Jon E., P. Jonathan Patchett, Philip A. Pearthree, P. Kyle House, Andrei M. Sarna-Wojcicki, Elmira Wan, Jennifer A. Roskowski, and James E. Faulds. "Review and Analysis of the Age and Origin of the Pliocene Bouse Formation, Lower Colorado River Valley, Southwestern USA." *Geosphere* 9, no. 3 (June 1, 2013): 444–59. https://doi.org/10.1130/GES00896.1.

Spencer, Jon E., Philip A. Pearthree, and P. Kyle House. "An Evaluation of the Evolution of the Latest Miocene to Earliest Pliocene Bouse Lake System in the Lower Colorado River Valley, Southwestern USA." In *Special Paper 439: Late Cenozoic Drainage History of the Southwestern Great Basin and Lower Colorado River Region: Geologic and Biotic Perspectives*, 439:375–90. Geological Society of America, 2008. https://doi.org/10.1130/2008.2439(17).

"Stratigraphy and Depositional Environments of the Upper Pleistocene Chemehuevi Formation Along the Lower Colorado River." Accessed March 31, 2023. https://pubs.usgs.gov/pp/1786/.

Tauxe, Lisa, T. Mullender, and T. Pick. "Potbellies, Wasp-Waists, and Superparamagnetism in Magnetic Hysteresis." *Journal of Geophysical Research* 101 (January 10, 1996): 571–84. https://doi.org/10.1029/95JB03041.

Thacker, Jacob, Karl Karlstrom, Laura Crossey, Ryan Crow, L. Beard, and Rebecca Dorsey. *Hypothesis for Post-Bouse Distributed Deformation of the Lower Colorado River Corridor*, 2017.

Thacker, Jacob O., Karl E. Karlstrom, Laura J. Crossey, Ryan S. Crow, Colleen E. Cassidy, L. Sue Beard, John S. Singleton, Evan D. Strickland, Nikki M. Seymour, and Michael R. Wyatt. "Post–12 Ma Deformation in the Lower Colorado River Corridor, Southwestern USA: Implications for Diffuse Transtension and the Bouse Formation." *Geosphere* 16, no. 1 (December 20, 2019): 111–35. https://doi.org/10.1130/GES02104.1.

"UCD FORC Group - What Is a FORC Diagram?" Accessed March 6, 2023. http://forc.ucdavis.edu/forc.html.

Walter, Robert C. "Potassium-Argon/Argon-Argon Dating Methods." In *Chronometric Dating in Archaeology*, edited by R. E. Taylor and Martin J. Aitken, 97–126. Advances in Archaeological and Museum Science. Boston, MA: Springer US, 1997. https://doi.org/10.1007/978-1-4757-9694-0_4.

Wasilewski, Peter J. "Magnetic Hysteresis in Natural Materials." *Earth and Planetary Science Letters* 20, no. 1 (September 1, 1973): 67–72. https://doi.org/10.1016/0012-821X(73)90140-4.

Whittaker, Alexander C., Mikaël Attal, and Philip A. Allen. "Characterising the Origin, Nature and Fate of Sediment Exported from Catchments Perturbed by Active Tectonics." *Basin Research* 22, no. 6 (October 26, 2010): 809–28. https://doi.org/10.1111/j.1365-2117.2009.00447.x

Tables

Table 1

Sample Name	Demag	Polarity	Declination	Inclination	MAD	Rank	Alpha 95(Site)	K (Site)	N/No
1-1	TH	N	261.4	52.6	6.7	B			
1-2	TH	N	117.8	70.8	9.7	B			
1-3	TH	N	105.9	77.9	9.7	B			
1-4	TH	N	96.8	84.7	9.4	B			
1-5	TH	N	108.7	74.4	9.6	C			
2-1a	TH	N	47	54.1	8.7	C			
2-1b	TH	N	39.9	57.3	9.9	C			
2-2	TH	N	97.2	63.5	9.2	B			
2-4	TH	N	2.6	66.5	6.4	B			
2-5	TH	N	186.4	33.1	7.8	C			
2-6	TH	N	150.3	69.3	9.3	B			
3-3	TH	N	296.6	67.2	9.6	A			
Site	TH	N	99.8	83.4	16.4	B		7	14
4-1	TH	N	159.7	34.9	9.6	B			
4-2	TH	N	119.4	78.1	5.6	B			
4-3	TH	N	149.9	58.9	10	D			
4-4	TH	N	187.6	62.7	9.4	D			
Site	TH	N	159.5	60.1	24.5	B		14.99	4/4
5-1	TH	N	292.2	73.4	7.9	C			
5-2	TH	R	300.6	-50.5	7.3	B			
5-3	TH	R	65.5	-42.1	9.5	C			
Site	TH	R	349.5	-32.8	180	D		0.95	3/3
6-1	TH	R	188.5	-79.2	8.3	B			
6-2	TH	N	181.4	53.8	6	B			
7-1	TH	N	169.5	83.8	9.8	B			
7-2	TH	N	78.3	29.9	10	D			
7-3	TH	R	281.1	-23.8	9.8	C			
Site	TH	N	187.6	60.2	180	D		1.01	5/5
8-2	TH	N	216.4	67.5	9.9	B			
8-3	TH	N	181	59.7	9.3	C			
9-2	TH	R	345.4	-50.7	4.9	C			
9-3	TH	R	311.4	-5.7	9.6	B			
9-4	TH	N	172.5	52.6	7.4	B			

Site	TH	N	238.8	64	84.3	C		1.59	5/5
10-1	TH	N	243.3	47.7	8.3	A			
11-1	TH	N	280	49.6	8.3	D			
11-2	TH	N	313.4	26.9	13.3	C			
11-3	TH	R	56.4	-41.5	17.4	A			
Site	TH	N	303.6	40.4	136.7	A		1.49	4/4
12-1	TH	N	19	30.2	12.3	A			
12-2	TH	N	237.2	36.4	17.2	B			
12-3	TH	N	144	80.7	28.5	A			
13-3	TH	N	125.6	18	5.4	A			
Site	TH	N	122.7	76.8	94.4	C		1.94	4/4
16-3	TH	N	359.1	55.3	9.4	C			
17-1	TH	N	198.4	46.4	9.7	B			
17-2	TH	N	61.8	48.2	9.8	B			
17-3	TH	N	82.5	53.6	9.6	B			
17-4	TH	N	80.1	30.1	75	C			
Site	TH	N	75.8	62.7	42.4	C		4.21	5/5
19-1	TH	R	26.2	-40.5	8.7	B			
19-3	TH	R	40.5	-55	9.3	B			
Site	TH	R	32.3	-48	38.7	C		43.83	2/2
22-2	TH	R	39.8	-59.9	8.7	B			
24-1	TH	R	119.5	-40.6	9	B			
Site	TH	R	89.3	-57.1	180	D		5.16	2/2
25-3	TH	R	37.1	-55.3	5.4	A			
25-5	TH	R	28.9	-57.5	7.4	B			
25-6	TH	R	23.3	-50.8	4.8	A			
25-7	TH	R	35	-64.4	6.2	A			
Site	TH	R	30.6	-57.1	7.6	B		148	4/4
26-1	TH	N	306.3	27.6	6.8	A			
26-2	TH	N	314	21.7	9.8	B			
Site	TH	N	310.2	24.7	20.1	C		156	2/2
Normal	TH	N	120.2	84.3	13.4	B		3.85	40
Reverse	TH	R	26.2	-63.3	14.2	B		5.32	24

Table 2

Sample Name	Demag	Polarity	Decl	Incl	MAD	Rank	Alpha 95(Site)	K (Site)	N/No
HMW0-1	AF	N	15.4	57.3	10.1	B			
HMW0-2	AF	N	149.1	9.1	27.7	D			
HMW0-3	AF	N	4.9	29.4	13.3	B			
HMW0-4	AF	N	344.8	20	18.5	D			
Site	AF	N	359.3	36.2	36.1	C	36.1	12.71	3/4
HMW1-1	AF	N	338.1	43.3	7.2	B			
HMW1-2	AF	N	0.6	46.7	7.6	B			
HMW1-3	AF	N	4.8	46.3	9.7	B			
HMW1-4	AF	N	2.3	53.9	7.4	B			
Site	AF	N	356	48.1	11/6.9	A	11/6.9	71.04	4/4
HMW5-1	AF	N	29.4	49.1	9.1	B			
HMW5-2	AF	N	335.1	68	8.6	B			
HMW5-3	AF	N	245.6	80	18.9	D			
HMW5-4	AF	N	15.1	45.9	12.7	C			
Site	AF	N	12.3	56	28.9/22.3	B	28.9/22.3	19.26	3/4
HMW8-1	AF	N	208.2	78.8	5	A			
HMW8-2	AF	N	299.7	57.8	35.5	D			
HMW8-3	AF	N	140.1	82.4	21.8	C			
HMW8-4	AF	N	157.9	66.1	32	D			
Site	AF	N	181.5	82.1	24	C	24	110	2/4
HMW9-1	AF	N	335	40.6	25.6	D			
HMW9-2	AF	R	317	-17.2	7	B			
HMW9-3	AF	N	227	11.7	29.5	C			
HMW9-4	AF	N	24.8	45.5	13.1	B			
Site	AF	N	345	16.8	N/A	C	N/A	N/A	2/4
HMW14	AF	N	5.9	53.5	5.7	A			
HMW14	AF	N	16.8	49	3.2	A			
HMW14	AF	N	30.1	68.9	11	B			
HMW14	AF	N	N/A	N/A	N/A	F			
Site	AF	N	15.7	57.4	18.5	B	18.5	45.5	3/4
1RS1-1	AF	N	340	33.7	5.9	A			
1RS1-2	AF	N	358	32.9	4.1	A			
1RS1-3	AF	N	344	31.5	5.4	A			
1RS1-4	AF	N	329	51.4	5.8	A			
Site	AF	N	343.8	37.8	15/12	A	15/12	38.42	4/4
1RS2-1	AF	N	323.3	51.8	7.4	A			

1RS2-2	AF	N	314.5	65.3	18.8	C			
1RS2-3	AF	N	354.5	30.5	10.9	B			
1RS2-4	AF	N	339.3	26.5	14	B			
Site	AF	N	336.8	44.4	25.6	C	25.6	13.88	4/4
1RS3-1	AF	N	355.9	51.7	6.3	B			
1RS3-2	AF	N	352.5	51.8	9.2	A			
1RS3-3	AF	N	350.8	34.3	8	A			
1RS3-4	AF	N	12.1	43.6	7.6	A			
Site	AF	N	357.8	45.7	12.4	A	12.4	55.97	4/4
1RS4-1	AF	N	338.2	4.4	10.9	B			
1RS4-2	AF	N	41.2	0.3	12.1	C			
1RS4-3	AF	N	8.8	25.9	9	B			
1RS4-4	AF	N	3.1	23.7	4.7	B			
Site	AF	N	5.9	24.8	12.3	A	12.3	415	2/4
4RS1-1	AF	R	167.5	-0.3	1.8	A			
4RS1-2	AF	R	166.1	-8.3	3.4	A			
4RS1-3	AF	R	161	-6.9	4.7	A			
4RS1-4	AF	R	N/A	N/A	N/A	F			
Site	AF	R	164.9	-5.2	8.3	A	8.3	220	3/4
4RS2-1	AF	R	186.1	-13.4	1.1	A			
4RS2-2	AF	R	150.7	-2.3	9.2	A			
4RS2-3	AF	R	191.8	-14.5	3.8	B			
4RS2-4	AF	R	187.4	-14.7	9.4	B			
Site	AF	R	188.4	-14.2	4.5	A	4.5	739	3/4
4RS3-1	AF	R	356.4	-0.4	9.1	D			
4RS3-2	AF	R	11.7	-2.7	9	B			
4RS3-3	AF	N	12.8	4.8	43.5	D			
4RS3-4	AF	N	174.8	2.1	10.1	D			
Site	AF	N	7	0.6	15.2	C	15.2	66.63	3/4
4RS4-1	AF	R	181.9	-11.8	2.2	A			
4RS4-2	AF	R	168.3	-13.2	1.8	A			
4RS4-3	AF	R	176.3	-19.6	4.1	A			
4RS4-4	AF	R	177.5	-10.3	5	A			
Site	AF	R	176	-13.8	7.8	A	7.8	139	4/4
4RS5-1	AF	N/A	N/A	N/A	N/A	F			
4RS5-2	AF	R	17.7	-19.1	12.6	C			
4RS5-3	AF	N	35.1	50.5	6.3	B			
4RS5-4	AF	R	168.5	-60.3	17.4	D			
Site	AF	R	39.7	-22.1	0	D	0	1.19	3/4
MV1-1	AF	N	350.3	71.5	6.4	B			
MV1-2	AF	N	312	70.3	5.8	B			
MV1-3	AF	N	1	65.8	4.9	B			

MV1-4	AF	N	354.4	55	3.9	B			
Site	AF	N	346.9	66.7	12.8	B	12.8	52.26	4/4
MV2-1	AF	N	156	57.9	8.8	C			
MV2-2	AF	N	27.5	60.6	5	B			
MV2-3	AF	N	306.6	59.7	10.3	C			
MV2-4	AF	N	8.7	64.9	10.2	B			
Site	AF	N	354.4	66.3	30.6	C	30.6	17.28	3/4
MV4-1	AF	N	48.7	31.7	26	D			
MV4-2	AF	N	285.6	71.4	23	D			
MV4-3	AF	N	196	55.6	20.6	F			
MV4-4	AF	N	175.2	2.8	19.2	F			
Site	AF	N	225.4	69.8	97	D	97	8.97	2/4
MV5-1	AF	N	4.5	50.8	5.2	B			
MV5-2	AF	N	7.7	37.2	2.5	A			
MV5-3	AF	N	8.3	16.6	4.2	B			
MV5-4	AF	N	360	39.7	2	A			
Site	AF	N	5.4	36.2	16.7	B	16.7	31.06	4/4
HMW	AF	N	4.7	49.7	13.1	A	13.1	50.05	4/6
1RS	AF	N	351.8	38.8	16.3	B	16.3	32.92	4/4
4RS	AF	N	18.3	25.2	0	C	0	4.63	2/5
4RS	AF	R	176.3	-11.2	19.4	B	19.4	41.41	3/5
MV	AF	N	346.9	66.7	12.8	B	12.8	52.26	4/4

Table 3

Sample Name	Demag	Polarity	Declination	Inclination	MAD	Rank	Alpha 95(Site)	K (Site)	N/No
MM5-1	AF	Normal	8.7	56.2	8.5	B			
MM5-2	AF	Normal	39.1	56.8	6.5	A			
MM5-3	AF	Normal	357.9	59.4	7.9	B			
Site	AF	Normal	9.4	45.1		B	17.6	50.32	3/3
MM7-1	AF	Normal	10.3	33.5	3.9	A			
MM7-2	AF	Normal	22	37.5	7	A			
MM7-3	AF	Normal	305.5	19.8	3.5	A			
Site	AF	Normal	351.6	35.2		A	24.1	109.77	2/3
MM9-2	AF	Normal	301	62	8	B			
Site	AF	Normal	301.4	62	8	B	0	0	1/1
MM12-1	AF	Normal	12.6	42.1	7.1	A			
MM12-2	AF	Normal	12.5	53.2	7.1	B			
Site	AF	Normal	12.6	47.7		B	24.4	107.8	2/2
MM14-1	AF	Normal	345	55	8.1	B			
Site	AF	Normal	345.1	55		B	0	0	1/1
MM15-1	AF	Normal	93.2	55.7	13	C			
Site	AF	Normal	93.2	55.7		C	0	0	1/1
MM16-1	AF	Normal	47.8	32.4	7.6	B			
MM16-2	AF	Reversed	214	-15.2	0.4	A			
MM16-3	AF	Normal	105	43	5.5	A			
Site	AF	Normal	118.7	47		A	130.6	6.26	2/3
MM17-1	AF	Normal	358.2	57.3	3.4	A			
Site	AF	Normal	358.2	57.3		A	0	0	1/1
MM18-1	AF	Normal	340	15.8	8.3	B			
MM18-3	AF	Normal	204	86	7.6	B			
Site	AF	Normal	337.5	54.2		B	180	2.3	2/3
MM19-1	AF	Normal	243	48.9	5.9	A			
MM19-2	AF	Normal	24.9	46	5.2	A			
Site	AF	Normal	318	73.3		A	180	2.19	2/2
MM20-1	AF	Normal	346	65.5	3.4	A			
MM20-2	AF	Normal	60.1	61.2	3.4	A			
Site	AF	Normal	26.5	68		A	74.7	13.4	2/2
MM24-1	AF	Normal	355	33.4	8.4	B			
MM24-2	AF	Normal	14.8	48.6	8.3	B			

Site	AF	Normal	3.8	41.4		B	47.8	29.48	2/2
MM25-1	AF	Normal	348.9	62	6.4	A			
MM25-2	AF	Normal	37.9	63.1	8.1	B			
MM25-3	AF	Normal	286	69.2	9.5	C			
Site	AF	Normal	350.6	71.1		B	33.2	14.86	3/3
MM27-1	AF	Normal	354	42.9	2.5	A			
MM27-2	AF	Normal	24	-8	10.5	C			
Site	AF	Normal	11.6	17.6		B	0	0	1/2
MM28-2	AF	Normal	9.2	2.8	5.3	A			
MM28-3	AF	Normal	353	42.5	6.1	A			
Site	AF	Normal	2.7	22.8		A	110.3	7.5	2/2
MM	AF	Normal	5.8	56.4		B	11.3	6.83	28/30
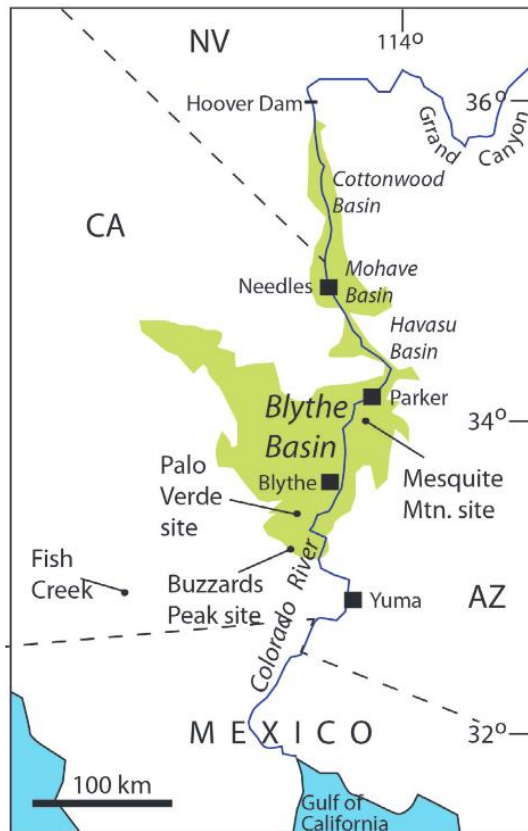
Figure 1) Regional map of the Lower Colorado River Corridor (LOCO). Key locations of Bouse outcrops are labeled, including Cottonwood, Mohave and Blythe Basin, where sampling associated with this study took place. (Howard et al., 2016)
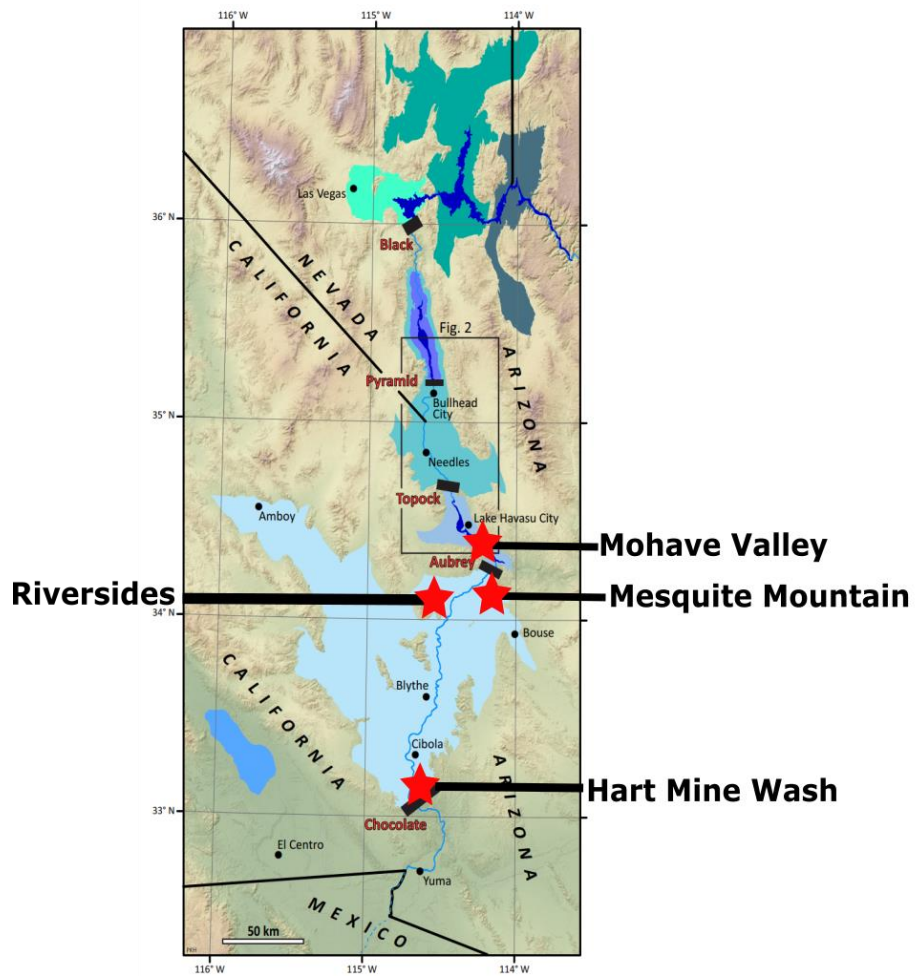
Figure 2) Regional map of LOCO displaying each sampling location conducted in this study. Additional important locations that are discussed in this text include Cibola, AZ and Needles, CA. Modified from Pearthree and House, 2014.
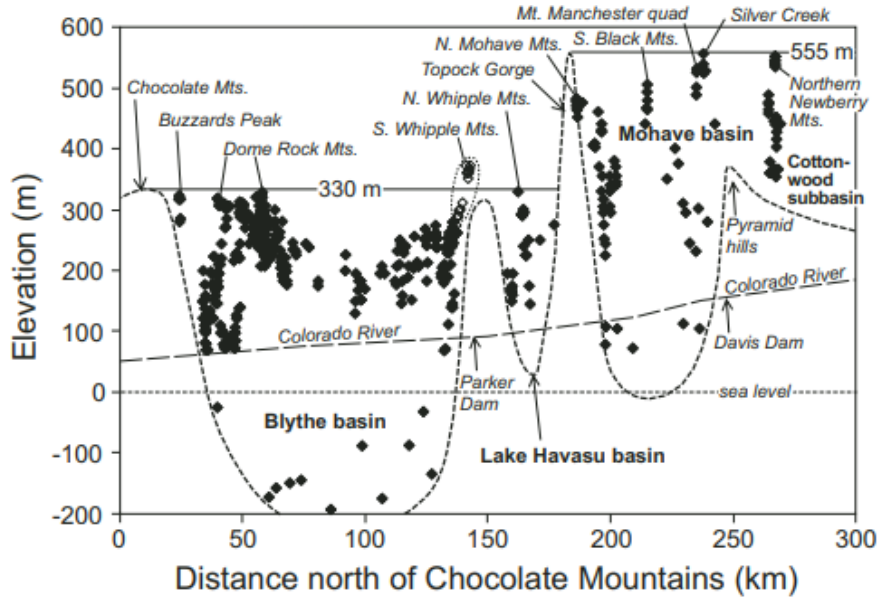
Figure 3. Graph of distance north of the Chocolate Mountains versus maximum elevation of all known Bouse exposures and minimum elevation (greatest depth) of Bouse Formation strata identified in drill cuttings. South Whipple Mountains data points (hollow) represent clastic sediments that are not considered here to be part of the Bouse Formation (see text). Also shown are the modern level of the Colorado River and a schematic representation of bedrock beneath Bouse strata.

Figure 3) Relative elevations of each basin in the Loco, which are separated by paleo dams (lava or mass flows). Black dots are relative locations of Bouse Formation deposits. Relevant mountain ranges shown include the Chocolate Mountains. (from Spencer, Pearthree, and House 2008)
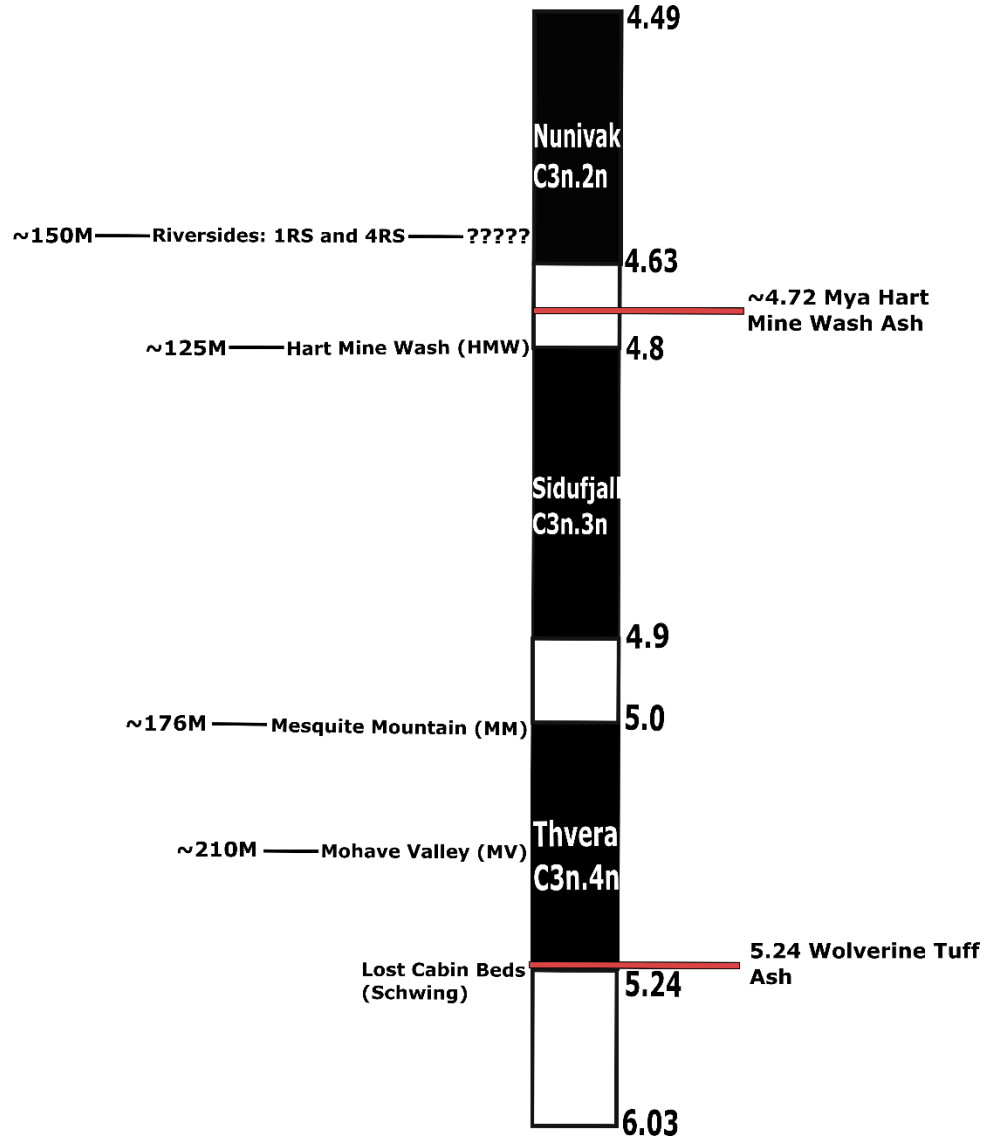
Figure 4) Relative elevations of each site and inferred position on the GPTS. Hart Mine Wash ash and Wolverine Tuff ash provide absolute age boundaries for the study. Lost Cabin Beds inform older age boundary (Schwing, 2018; GPTS from Ogg, 2012)
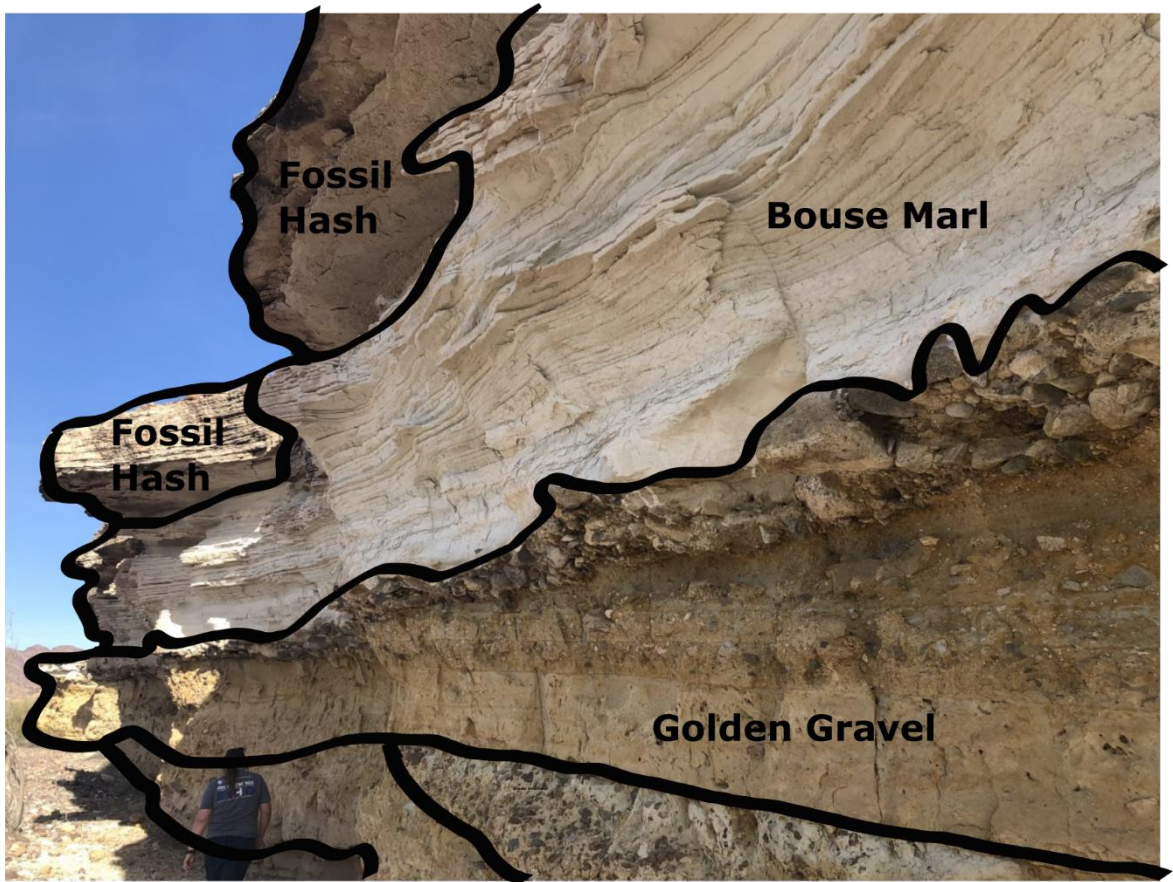
Figure 5) Hart Mine Wash Illustrated, displaying several key units within Hart Mine Wash including Bouse marl, fossil hash, and the golden gravel. Sampling was conducted within the Bouse marl and the fossil hash, although the Bouse marl unit provided most of the usable paleomagnetic data.
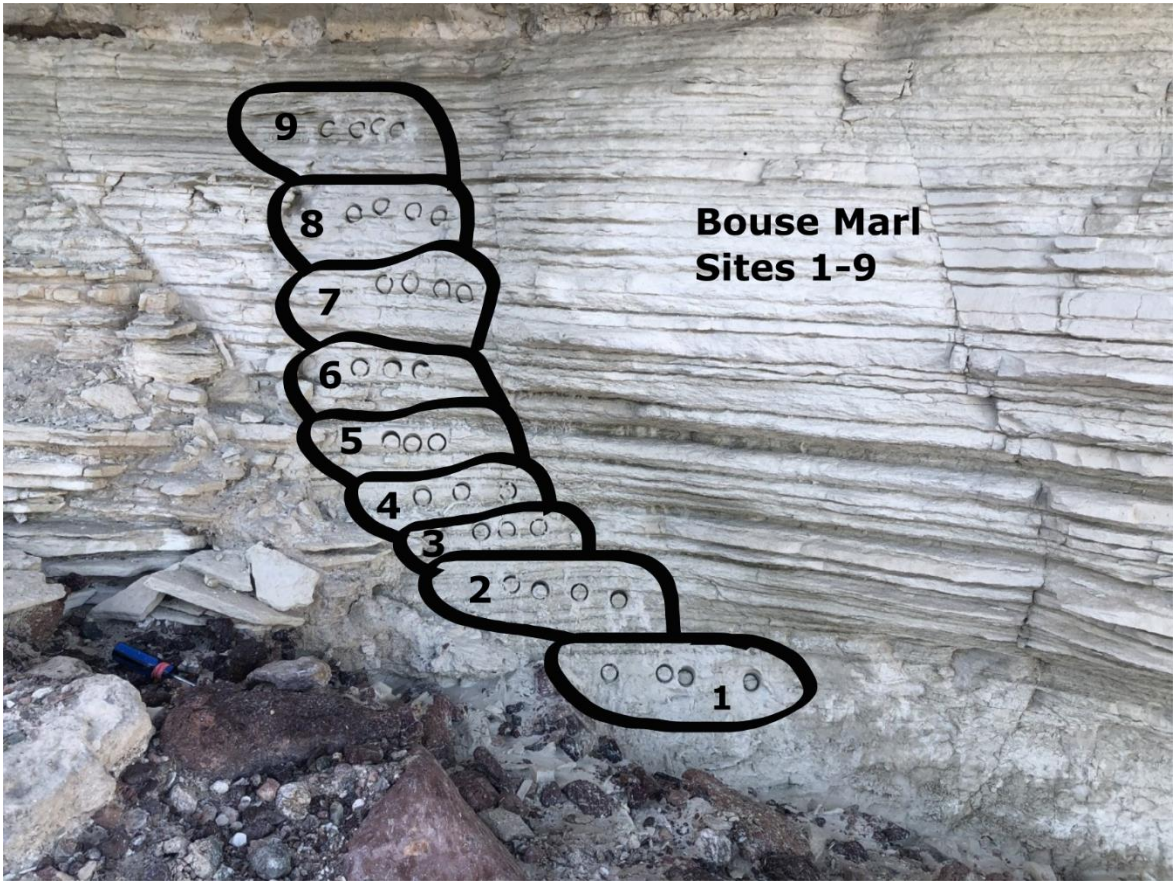
Figure 6) Hart Mine Wash drilling site location example. Each site consists of 3-4 samples. Example: HMW1.
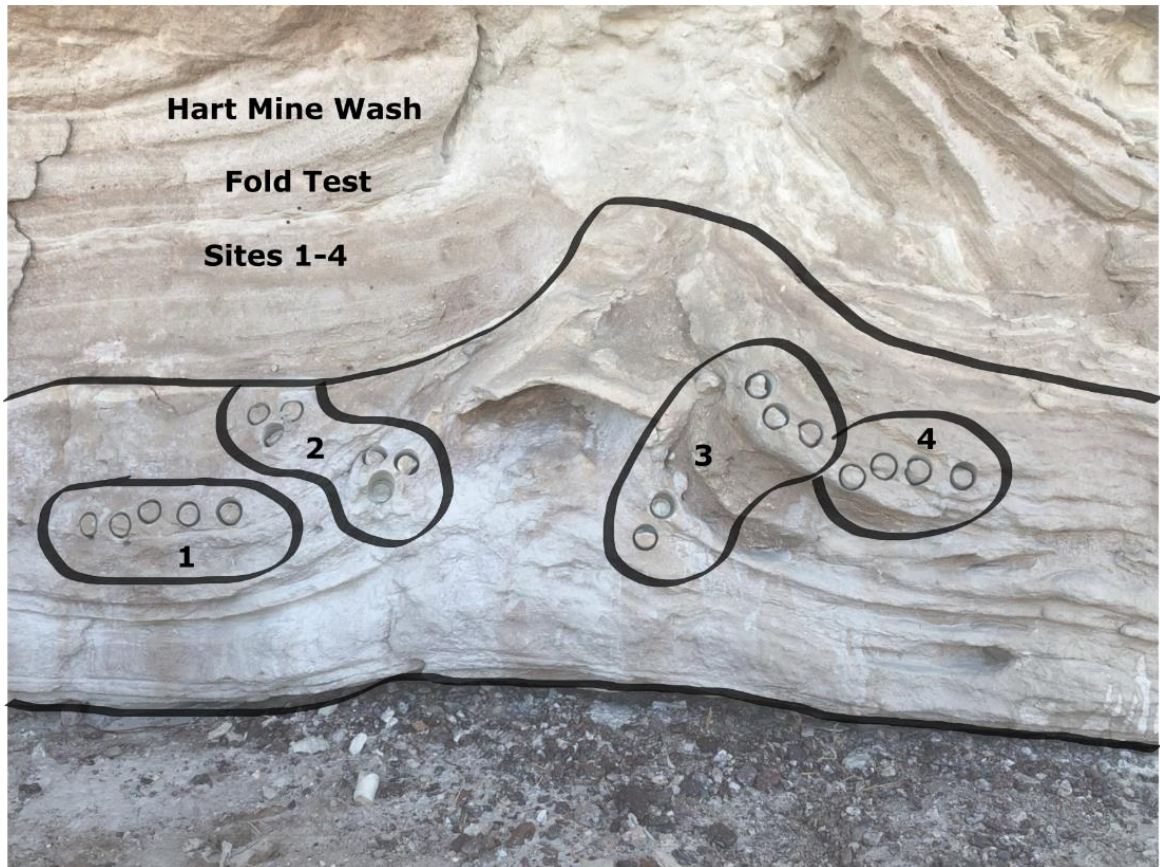
Figure 7) Hart Mine Wash Fold Test illustrated. Performed on a flame structure in an effort to establish evidence for a primary or secondary magnetization. Dip directions within this structure were not different enough to produce significant fold test results.
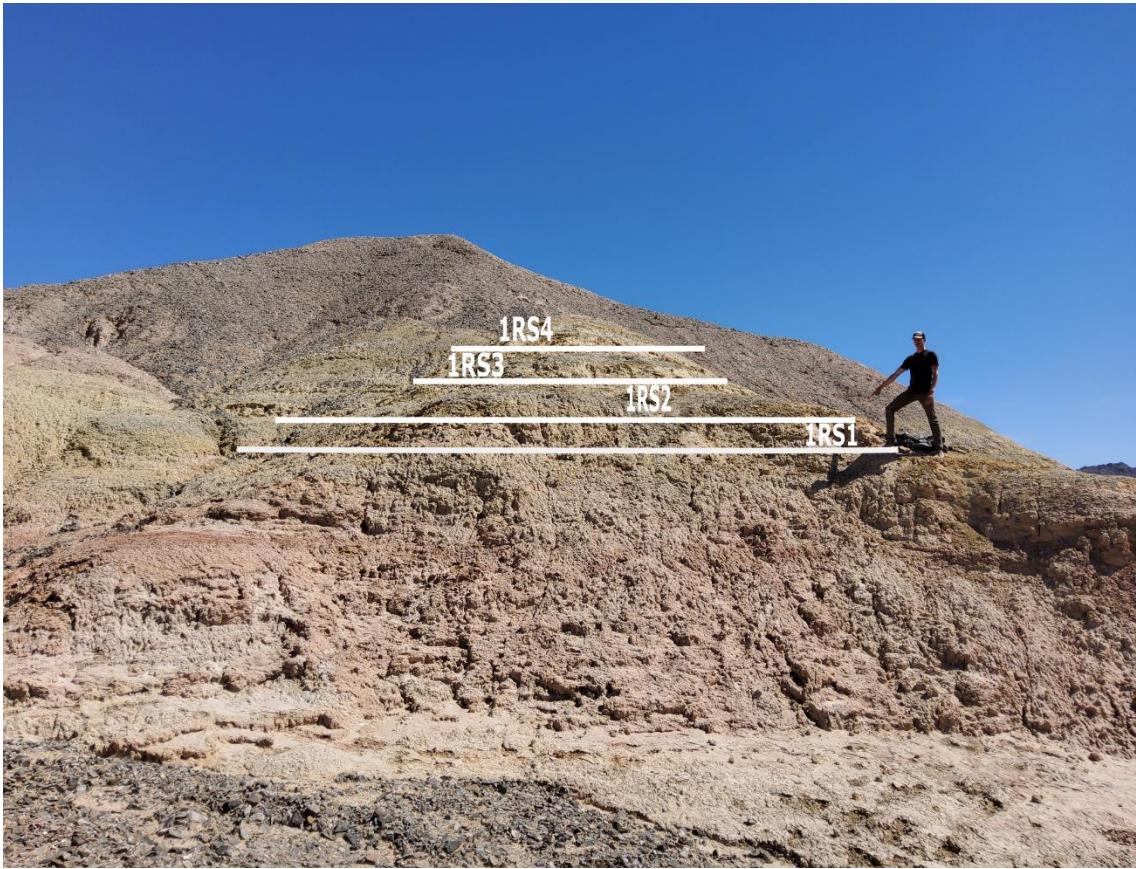
Figure 8) Riversides site location 1 (1RS) illustrated. Representative of claystone and mudstone lacustrine deposits described in stratigraphy.
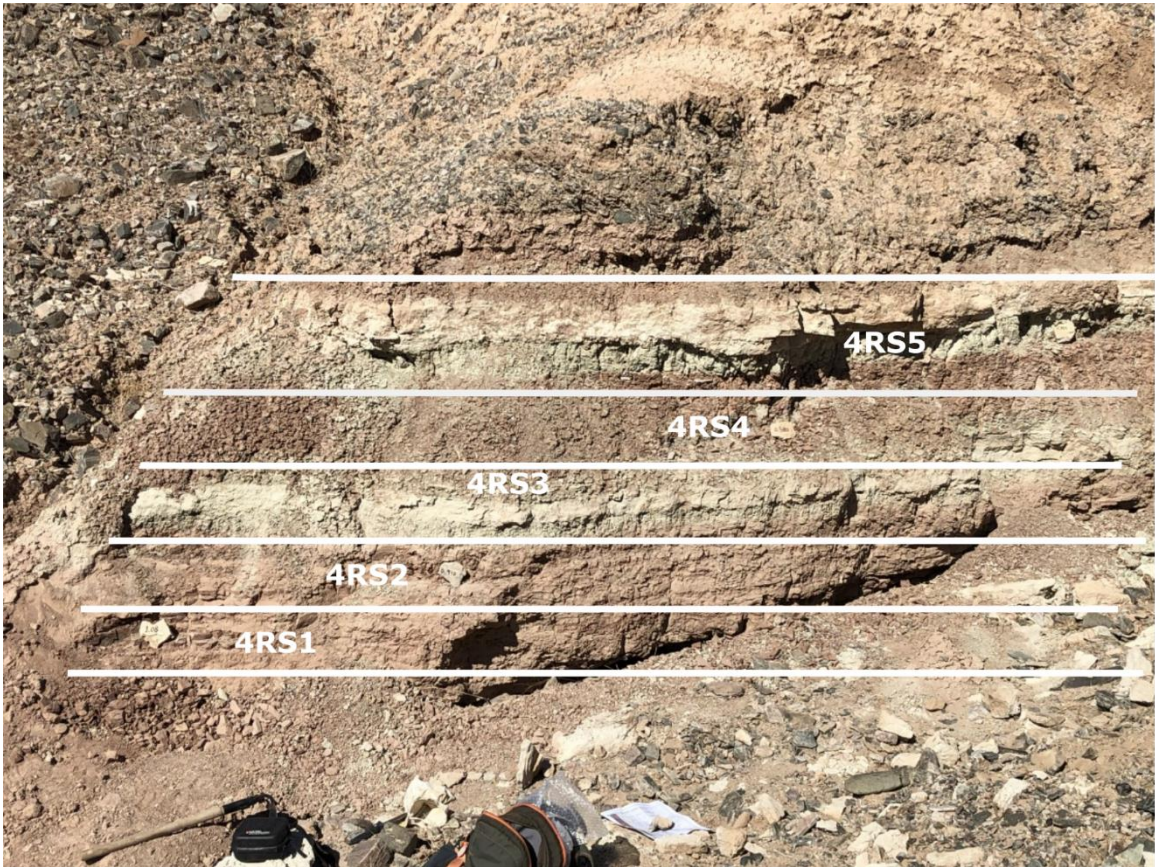
Figure 9) Riversides site location 2 (4RS) illustrated. Representative of green and pink/red mudstones and claystone deposits described in stratigraphy.
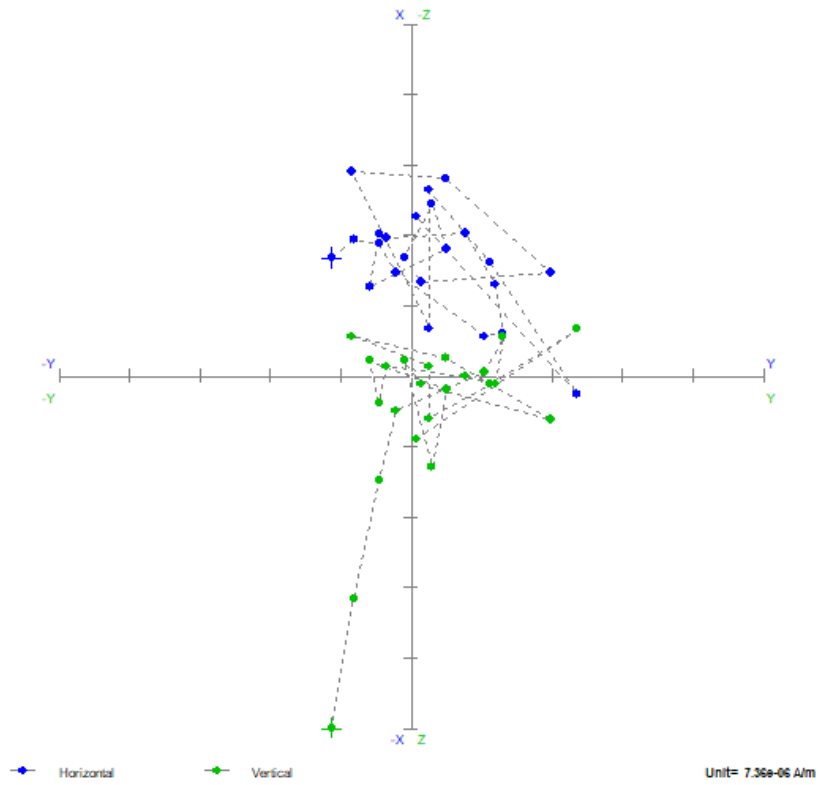
Figure 10) HMW8-2 Zijderveld plot displaying F quality data. Consistent with a multi domain magnetic behavior, and an unstable magnetic remanence. Blue (green) circles represent the declination (inclination).
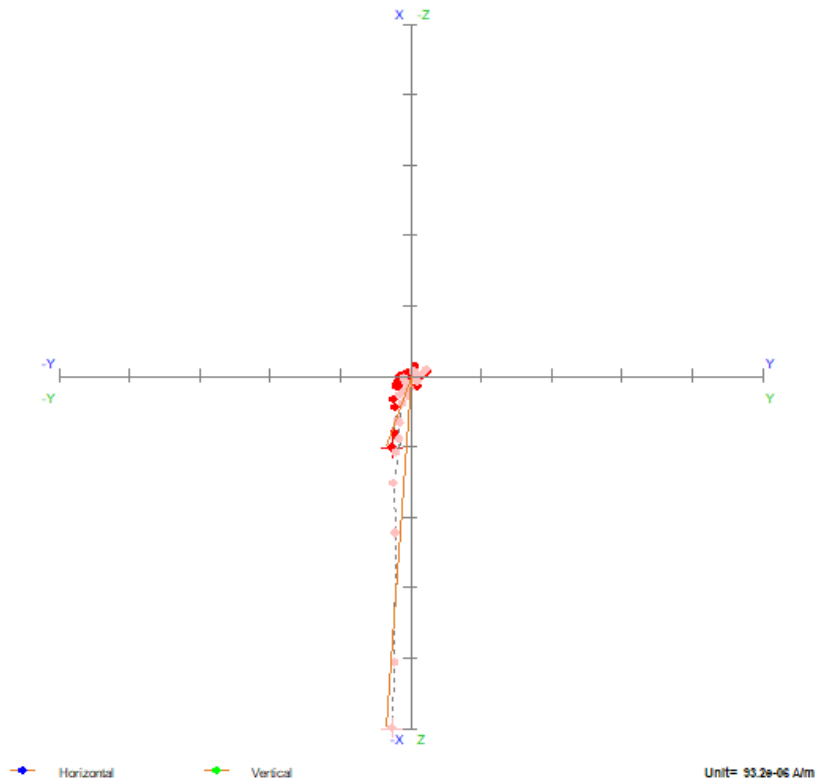
Figure 11) HMW8-1 Zijderveld plot displaying a normal polarity sample, A quality data. Representative of a single domain magnetic behavior and a stable magnetization. Red (pink) circles represent the declination (inclination). The red and pink (declination and inclination, respectively) circles represent the characteristic remanent magnetization identified by the author.
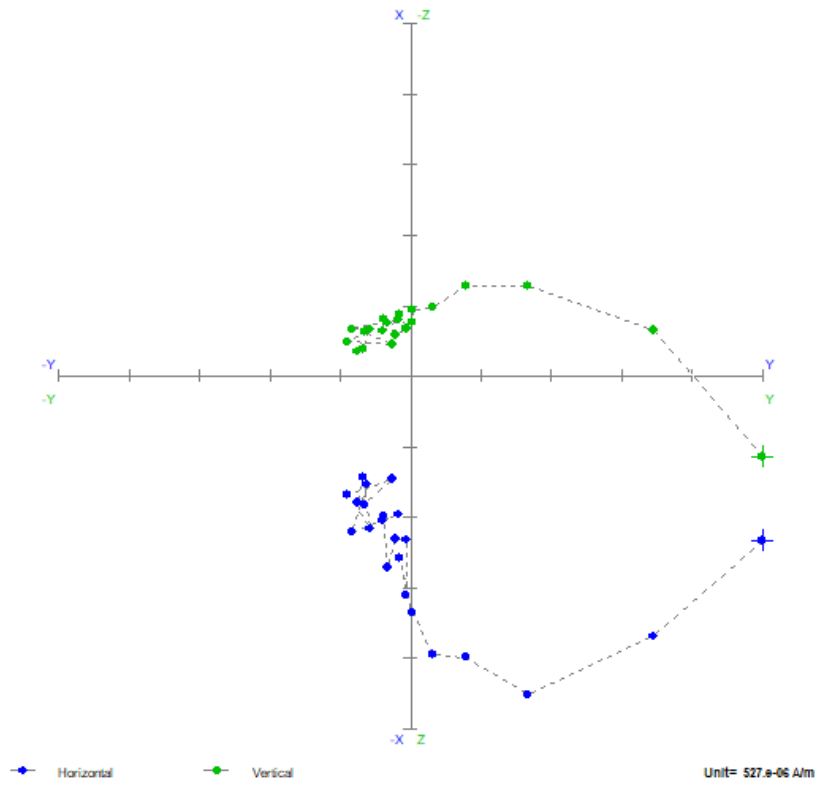
Figure 12) 4RS2-4 Zijderveld plot displaying a reversed polarity sample, B quality data. Representative of a sample with multiple magnetic components. Blue (green) circles represent the declination (inclination).
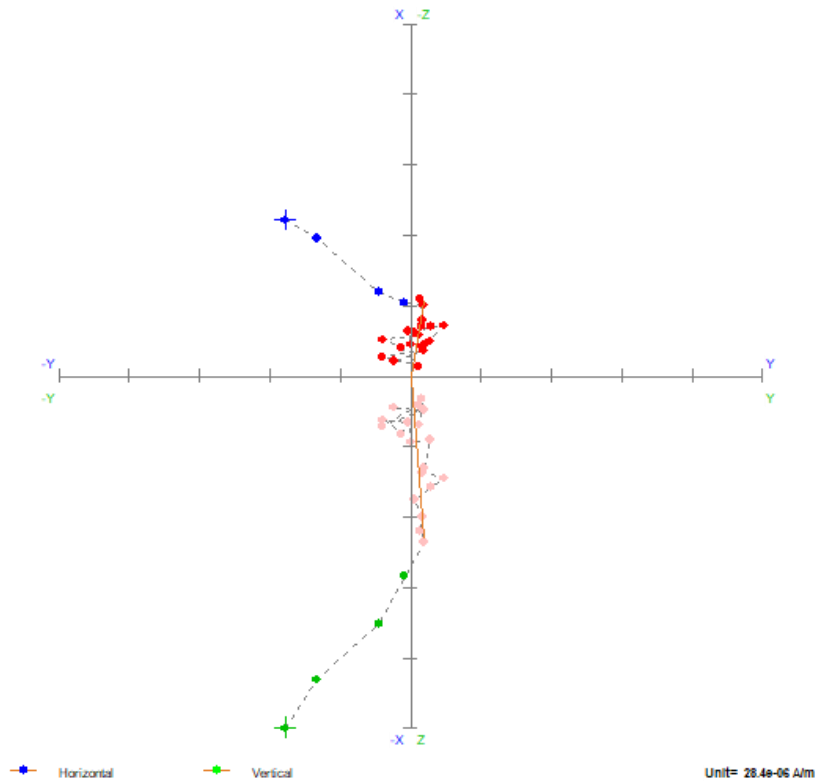
Figure 13) MV2-4 Zijderveld plot showing a normal polarity sample, C quality data. Data points stack and cluster near the origin, representative of a relatively unstable magnetic remanence. Blue (green) circles represent the declination (inclination). The red and pink (declination and inclination, respectively) circles represent the characteristic remanent magnetization identified by the author.
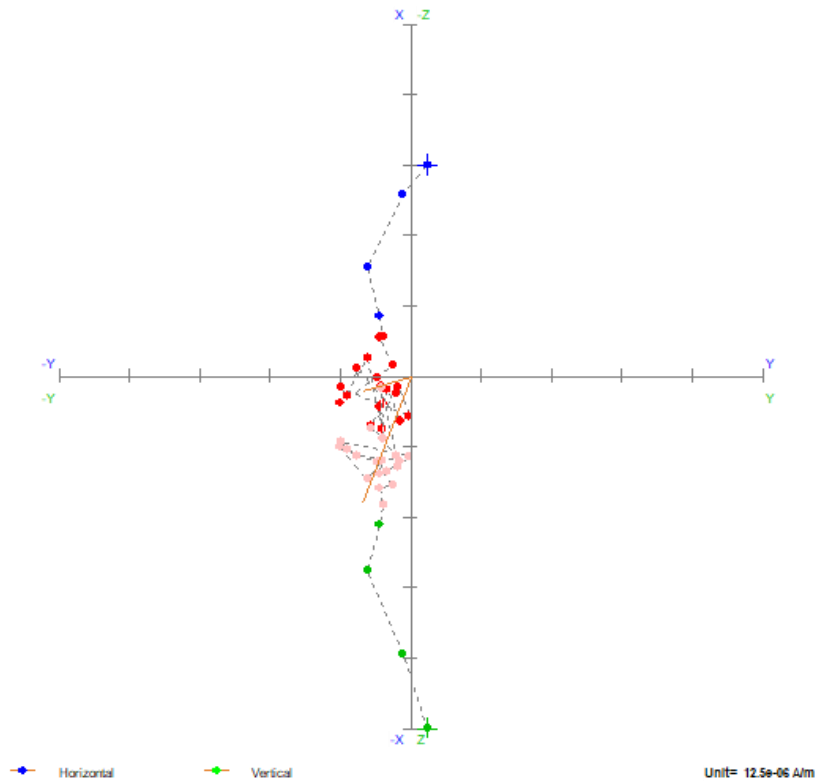
Figure 14) MV4-2 Zijderveld plot showing a normal polarity sample, D quality data.
Data points cluster near the origin and do not provide a clear direction. Blue (green)
circles represent the declination (inclination). The red and pink (declination and
inclination, respectively) circles represent the characteristic remanent magnetization
identified by the author.
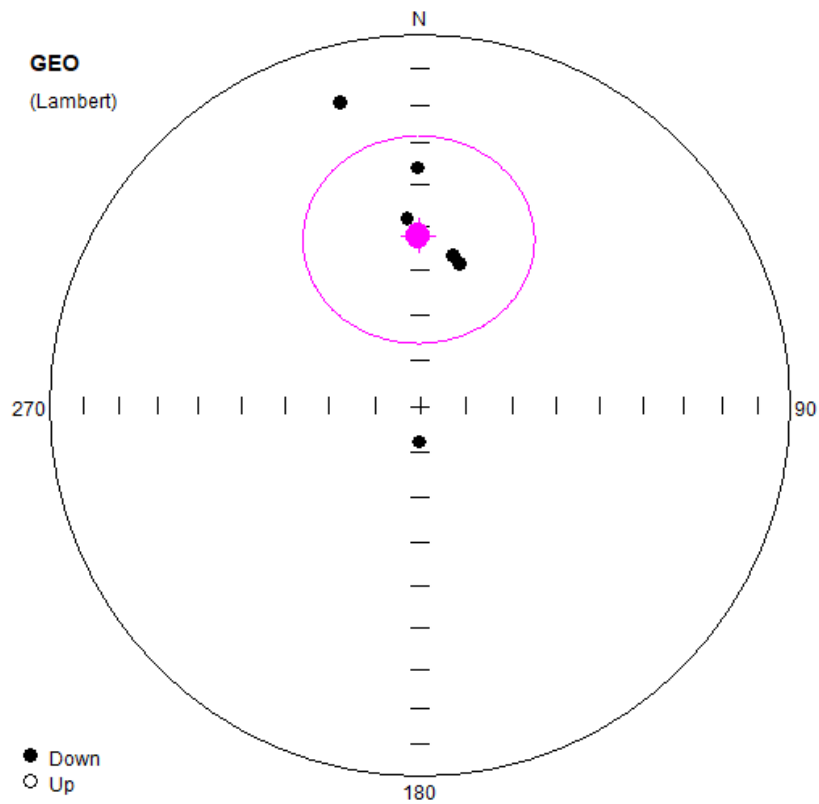
Figure 15) HMW Site Direction (AF) displayed on an equal area projection. Each dot represents a site's mean direction, which consists of 3-7 samples. The pink dot represents the mean of means and the associate error ellipse. Closed (open) circles represent positive (negative) inclinations.
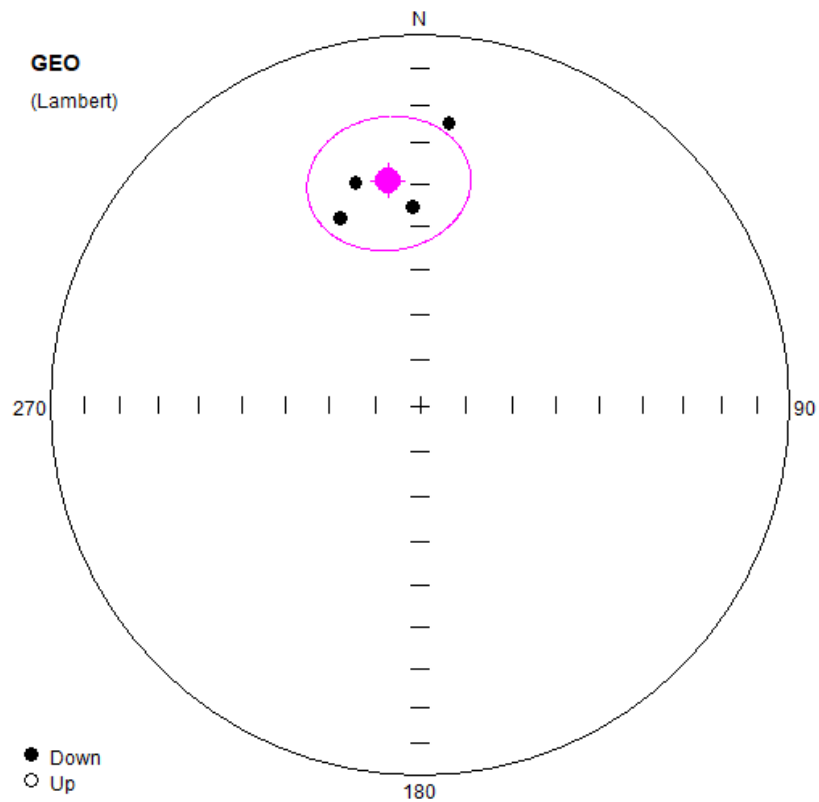
Figure 16) 1RS Site Means displayed on an equal area projection. Each dot represents a site's mean direction, which consists of 3-7 samples. The pink dot represents the mean of means and the associate error ellipse. Closed (open) circles represent positive (negative) inclinations.
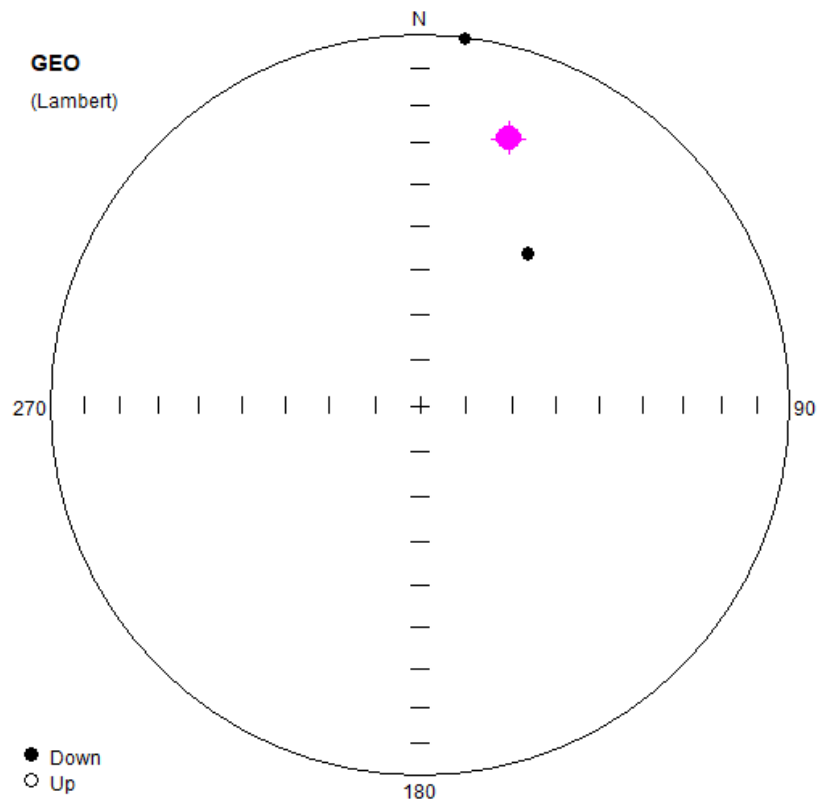
Figure 17) 4RS Site Means (normal) displayed on an equal area plot. Each dot represents a site's mean direction, which consists of 3-7 samples. The pink dot represents the mean of means and the associate error ellipse. Closed (open) circles represent positive (negative) inclinations.
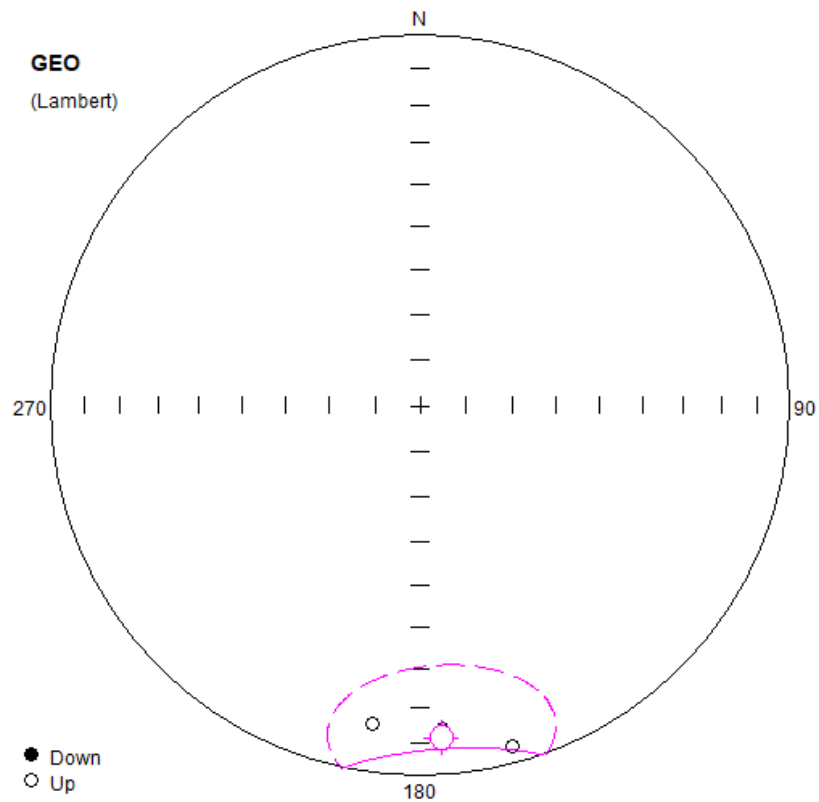
Figure 18) 4RS Site Means (Reversed) displayed on an equal area plot. Each dot represents a site's mean direction, which consists of 3-7 samples. The pink dot represents the mean of means and the associate error ellipse. Closed (open) circles represent positive (negative) inclinations.
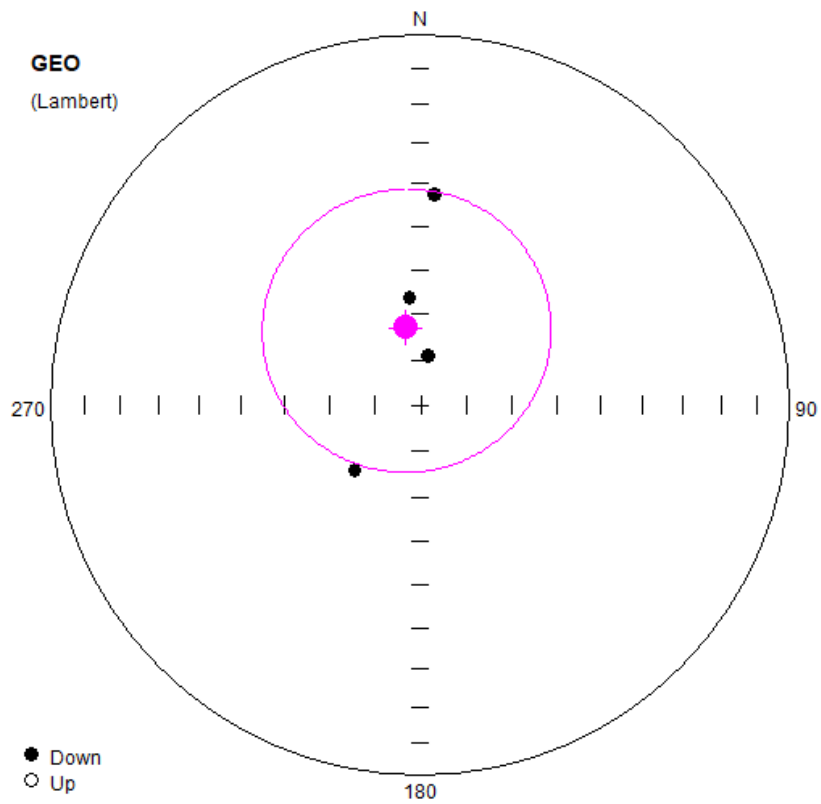
Figure 19) MV Site Means (Normal) displayed on an equal area plot. Each dot represents a site's mean direction, which consists of 3-7 samples. The pink dot represents the mean of means and the associate error ellipse. Closed (open) circles represent positive (negative) inclinations.
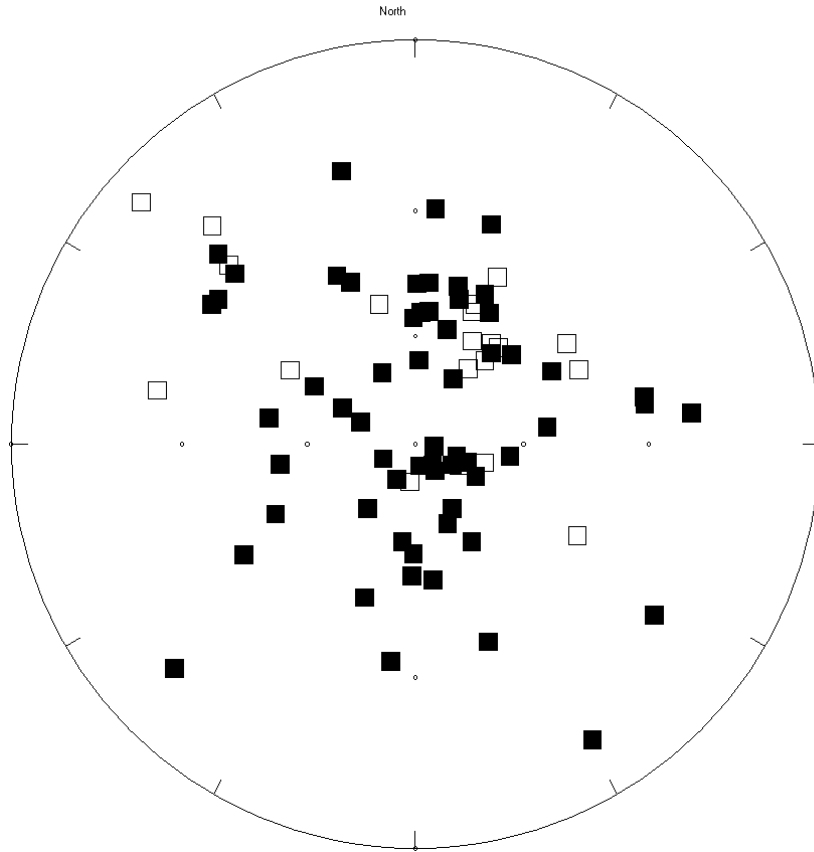
Figure 20) HMW Sites. All Data Used for Reversal Test. Each square represents an individual sample, rather than a site mean. Closed (open) squares represent positive (negative) inclinations. Although the data are scattered, this is likely due to the steep inclinations displaying "wobbling" declinations.
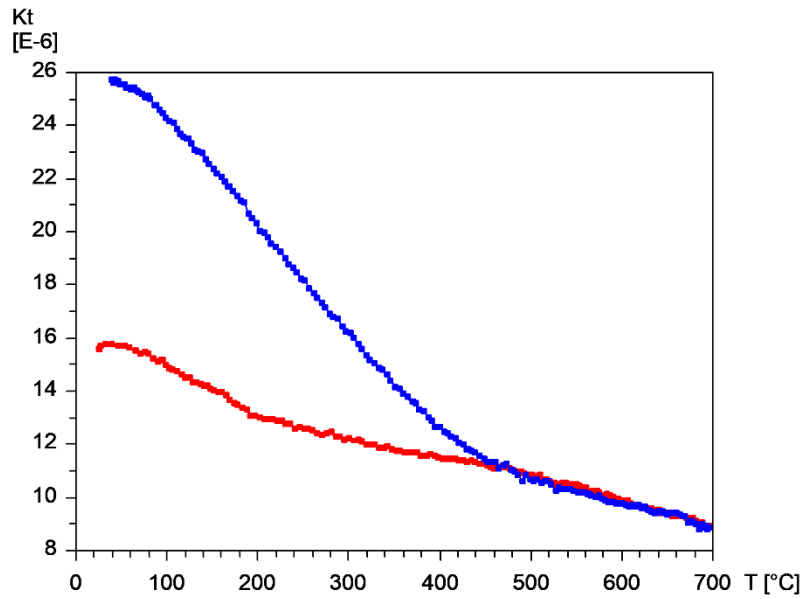
Figure 21) Thermomagnetic curve 1RS1, displaying a Curie temperature of ~450°C. The y-axis represents the magnetic moment of the sample in kilo Tesla, the x-axis represents the overall temperature of the sample in degrees Celsius.
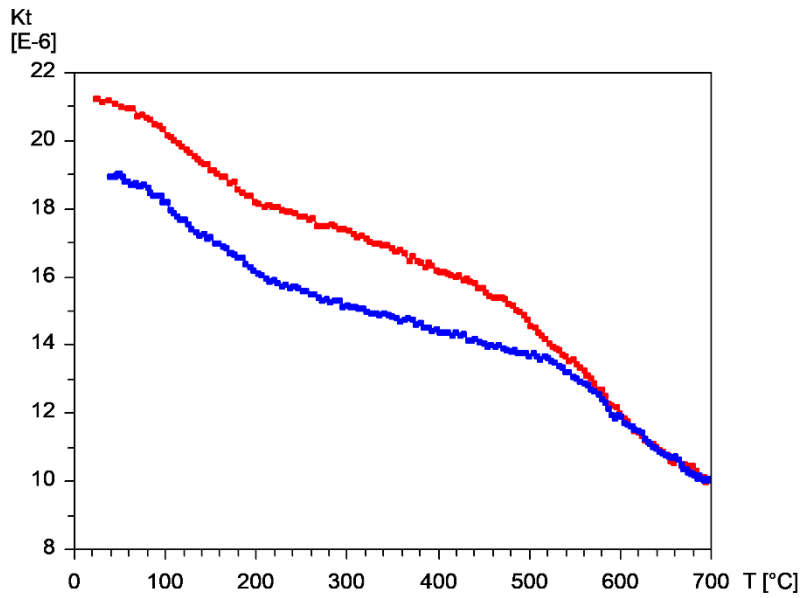
Figure 22) Thermomagnetic curve 4RS2 displaying a Curie temperature of ~600°C. The y-axis represents the magnetic moment of the sample in kilo Tesla, the x-axis represents the overall temperature of the sample in degrees Celsius.
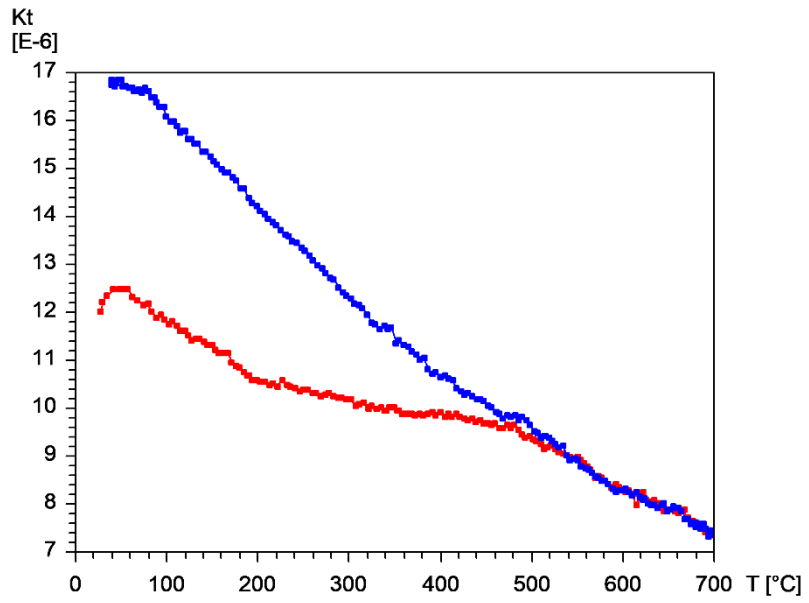
Figure 23) Thermomagnetic curve HMW1 displaying a Curie temperature of 550°C. The y-axis represents the magnetic moment of the sample in kilo Tesla, the x-axis represents the overall temperature of the sample in degrees Celsius.
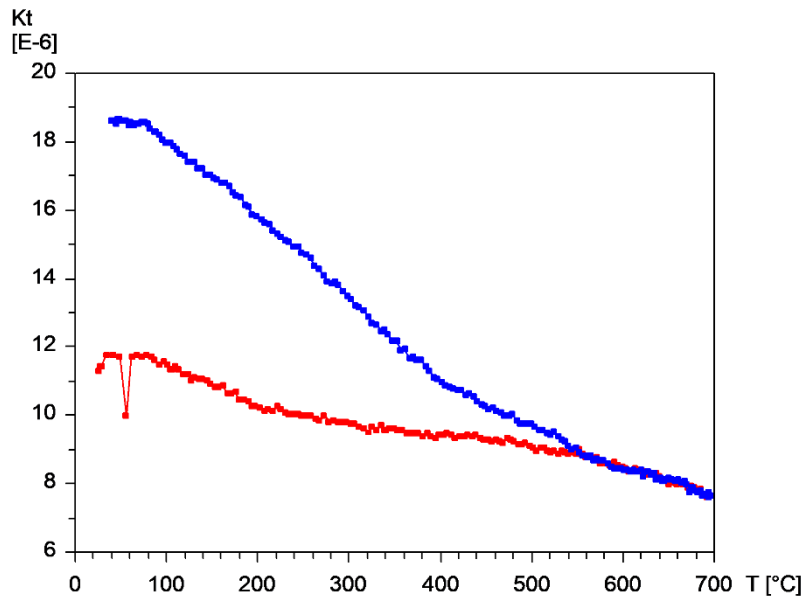
Figure 24) Thermomagnetic curve HMW8 displaying a Curie temperature of ~550°C. The y-axis represents the magnetic moment of the sample in kilo Tesla, the x-axis represents the overall temperature of the sample in degrees Celsius.
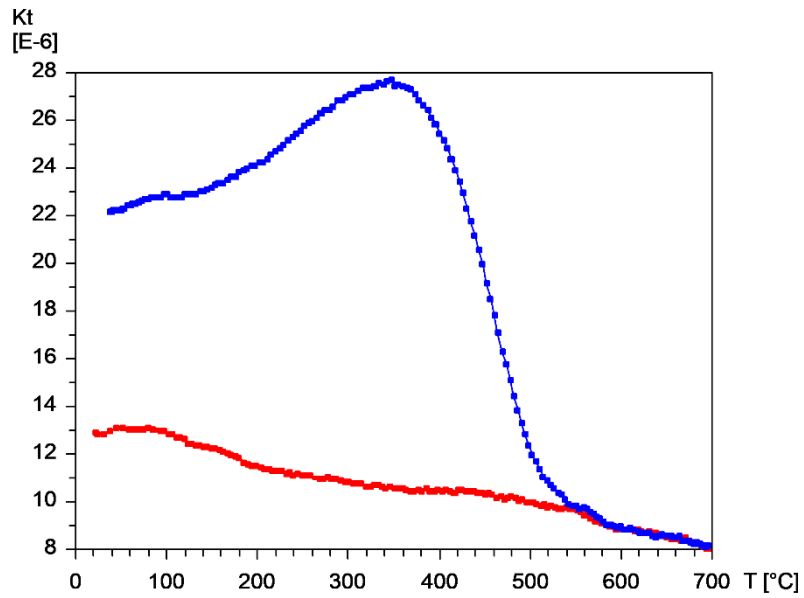
Figure 25) Curie Temperature data for MV1 displaying a Curie temperature of
~550°C. The y-axis represents the magnetic moment of the sample in kilo Tesla, the
x-axis represents the overall temperature of the sample in degrees Celsius.
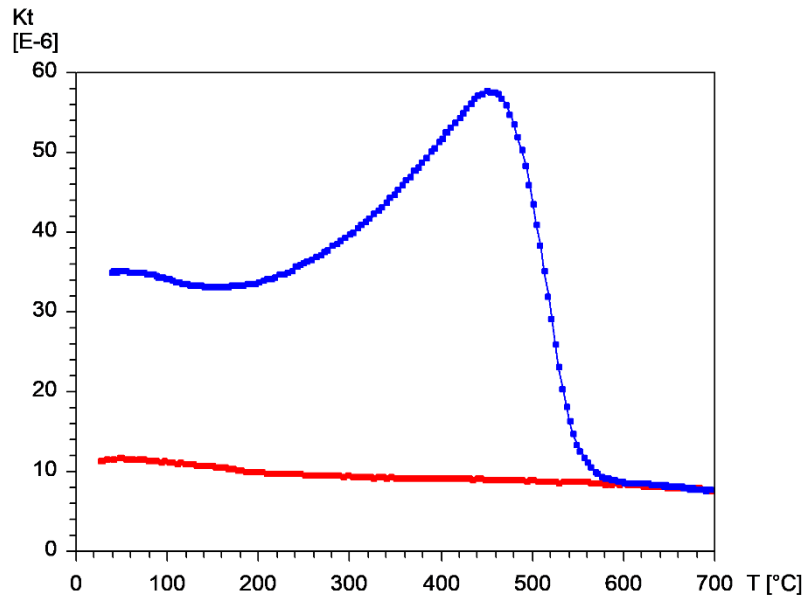
Figure 26) Curie Temperature data for MV4 displaying a Curie temperature of ~550°C. The y-axis represents the magnetic moment of the sample in kilo Tesla, the x-axis represents the overall temperature of the sample in degrees Celsius.
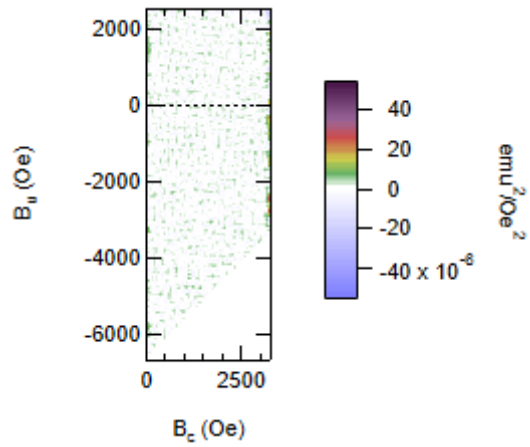
Figure 27) FORC Contour plot for 1RS1 displaying a null result. $B_C = (B_B - B_A)/2$ and $B_U = (B_B + B_A)/2$, where B= magnetic field. Subscripts A and B refer to X and Y components of the magnetic field curve.
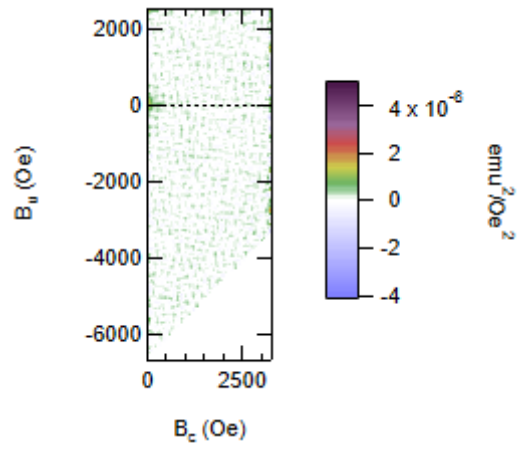
Figure 28) FORC Contour plot for 4RS2 displaying a multi domain magnetic domain. $B_C = (B_B - B_A)/2$ and $B_U = (B_B + B_A)/2$, where B= magnetic field. Subscripts A and B refer to X and Y components of the magnetic field curve.
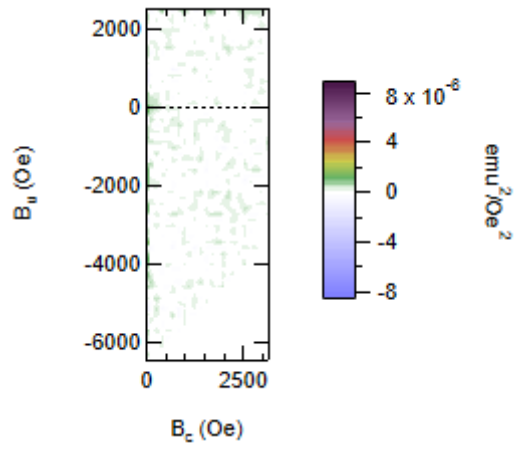
Figure 29) FORC Contour Plot for 4RS5 displaying a multi domain magnetic domain. $B_C = (B_B - B_A)/2$ and $B_U = (B_B + B_A)/2$, where B= magnetic field. Subscripts A and B refer to X and Y components of the magnetic field curve.
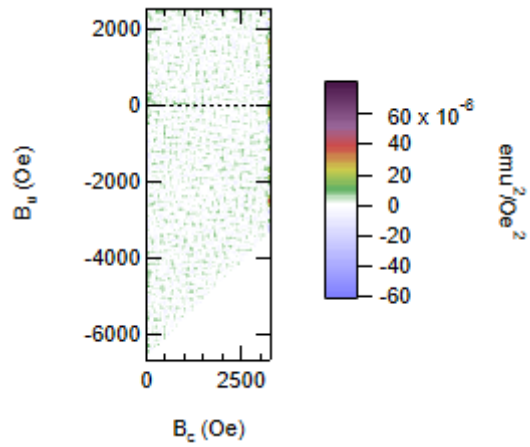
Figure 30) FORC Contour Plot for HMW1 displaying a null result. $B_C = (B_B - B_A)/2$ and $B_U = (B_B + B_A)/2$, where B= magnetic field. Subscripts A and B refer to X and Y components of the magnetic field curve.
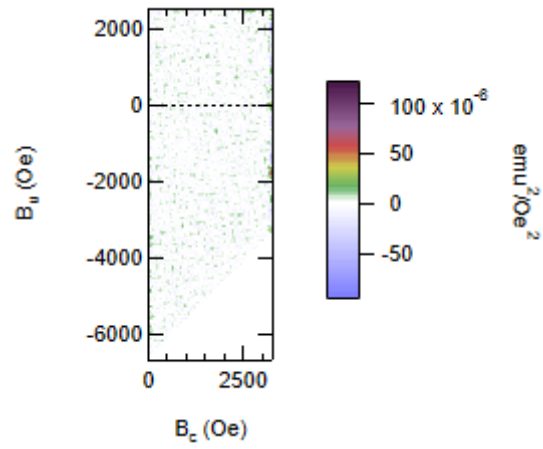
Figure 31) FORC Contour Plot for MV1 displaying a null result. $B_C = (B_B - B_A)/2$ and $B_U = (B_B + B_A)/2$, where B= magnetic field. Subscripts A and B refer to X and Y components of the magnetic field curve.
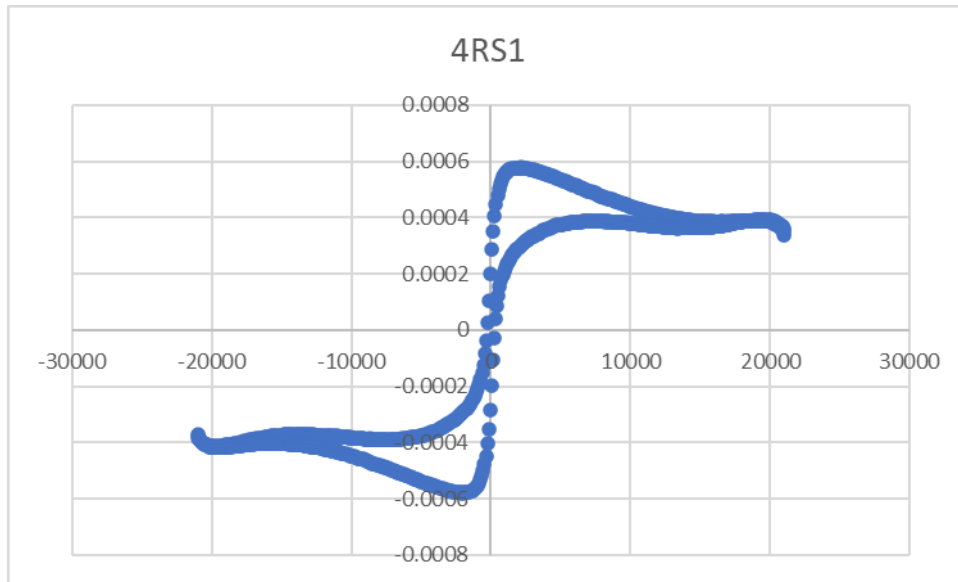
Figure 32) Hysteresis Curve for 4RS1, displaying a "wasp wasted" curve. The y-axis = electromagnetic moment in EMU (electromagnetic units) and the x-axis = magnetic field in Oe (Oersted's).
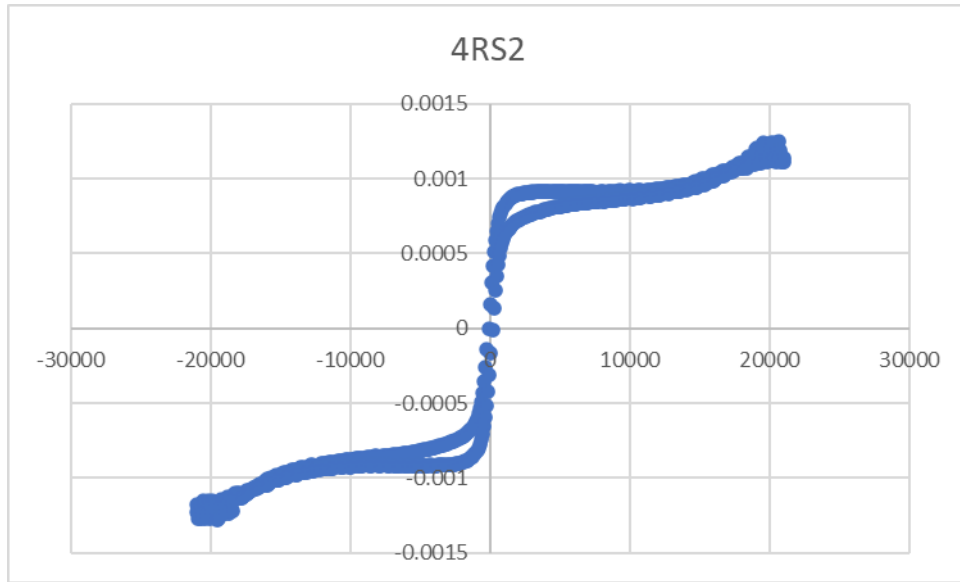
Figure 33) Hysteresis Curve for 4RS2 displaying a near "wasp wasted" curve. The y-axis = electromagnetic moment in EMU (electromagnetic units) and the x-axis = magnetic field in Oe (Oersted's).
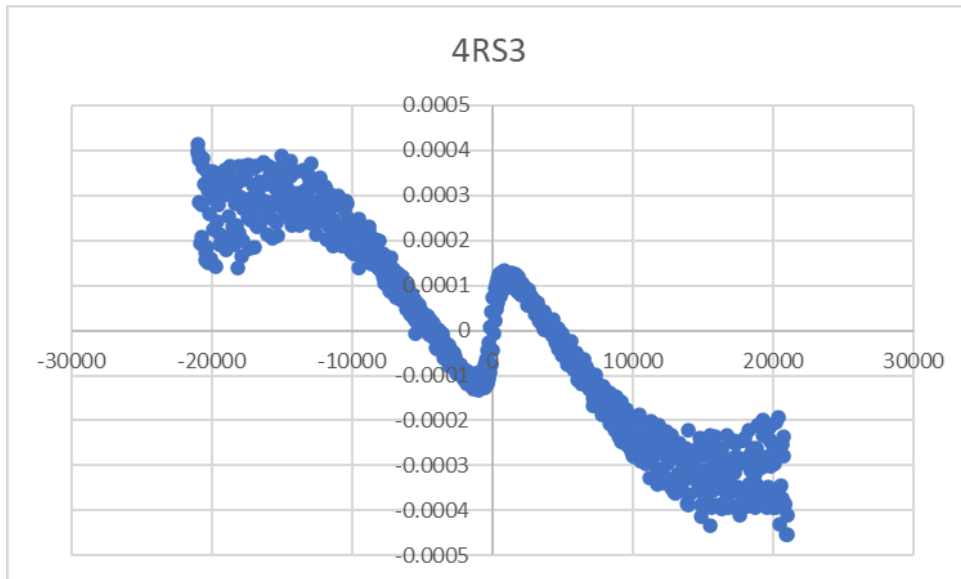
Figure 34) Hysteresis Curve for 4RS3 displaying a noisy and null result. The y-axis = electromagnetic moment in EMU (electromagnetic units) and the x-axis = magnetic field in Oe (Oersted's).
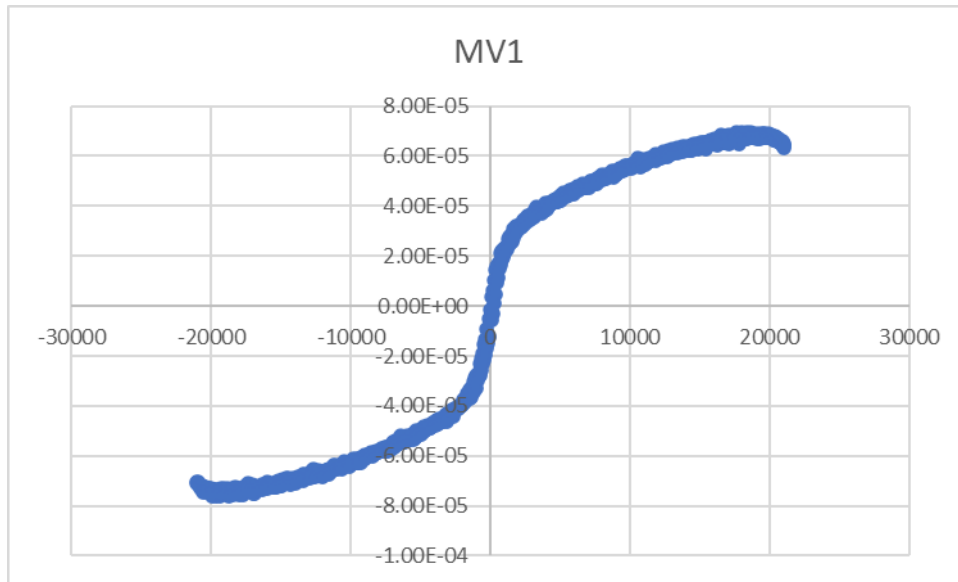
Figure 35) Hysteresis Curve for MV1 displaying a null result. The y-axis = electromagnetic moment in EMU (electromagnetic units) and the x-axis = magnetic field in Oe (Oersted's).
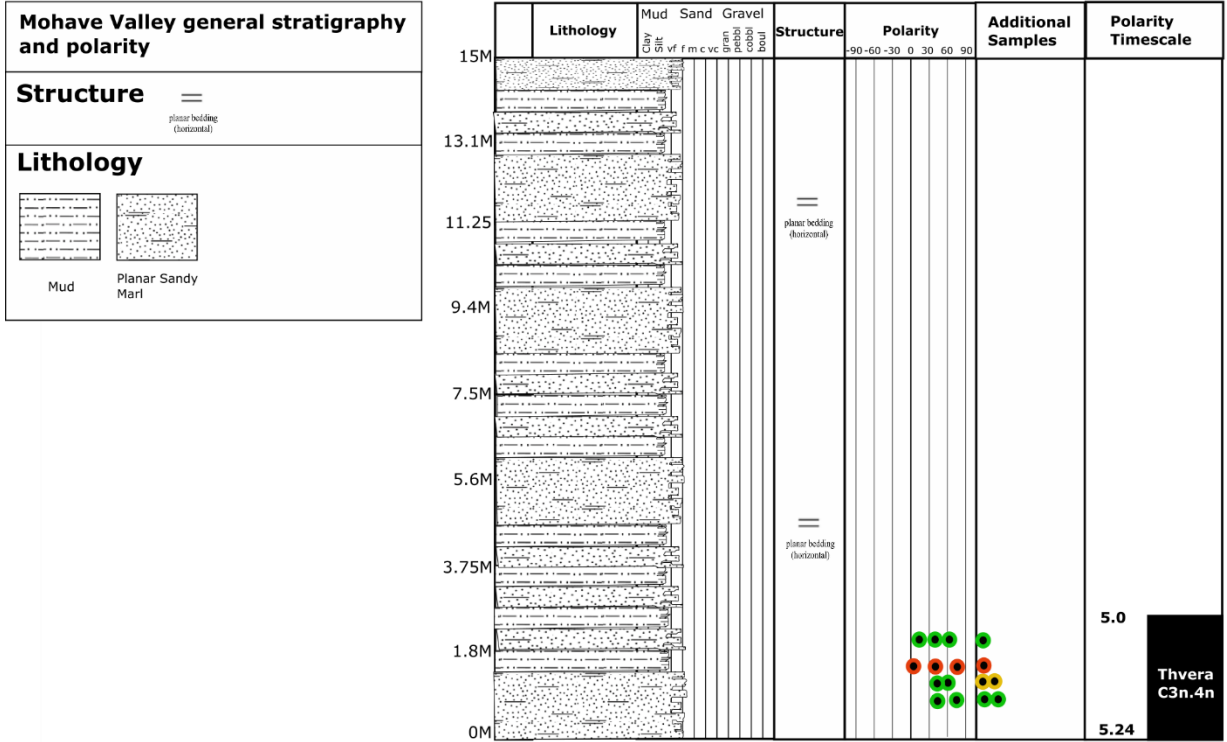
Figure 36) Stratigraphy and Polarity of samples associated with the Mohave Valley Site (MV). Filled in circles represent normal polarity samples. Solid (open) circles represent normal (reversed) polarity samples. The colors code with site "grades" as described in the text. Green = good, yellow = acceptable, red = poor.
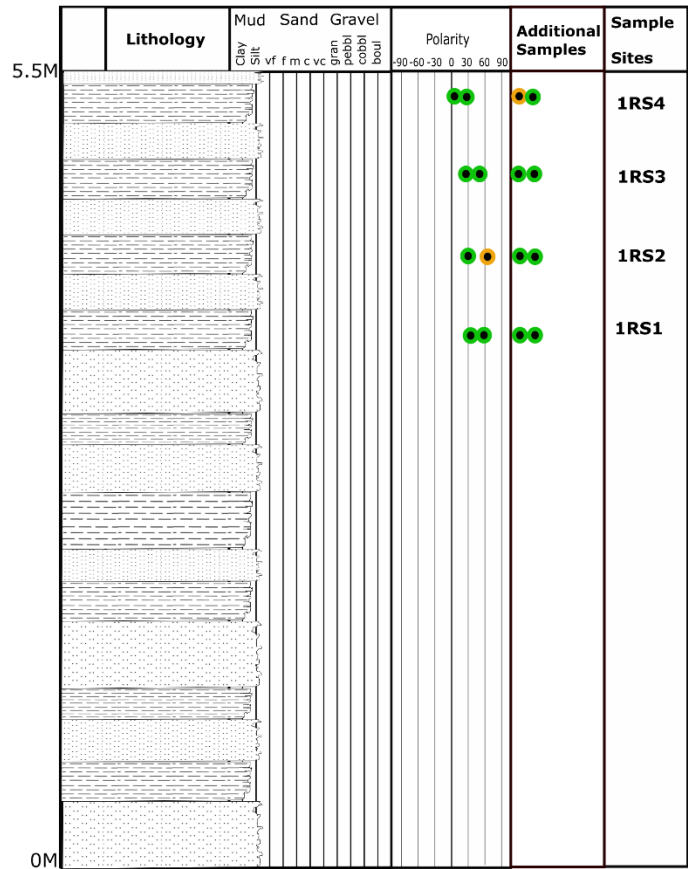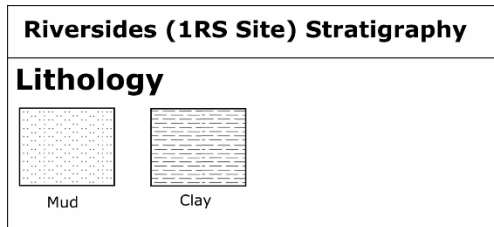
Figure 37) Stratigraphy and associated polarity of samples in the Riversides site (1RS). Solid (open) circles represent normal (reversed) polarity samples. The colors code with site "grades" as described in the text. Green = good, yellow = acceptable, red = poor.

Figure 38) Stratigraphy and associated polarity of samples in the Riversides site (4RS). Filled in circles represent normal polarity samples. Solid (open) circles represent normal (reversed) polarity samples. The colors code with site "grades" as described in the text. Green = good, yellow = acceptable, red = poor.
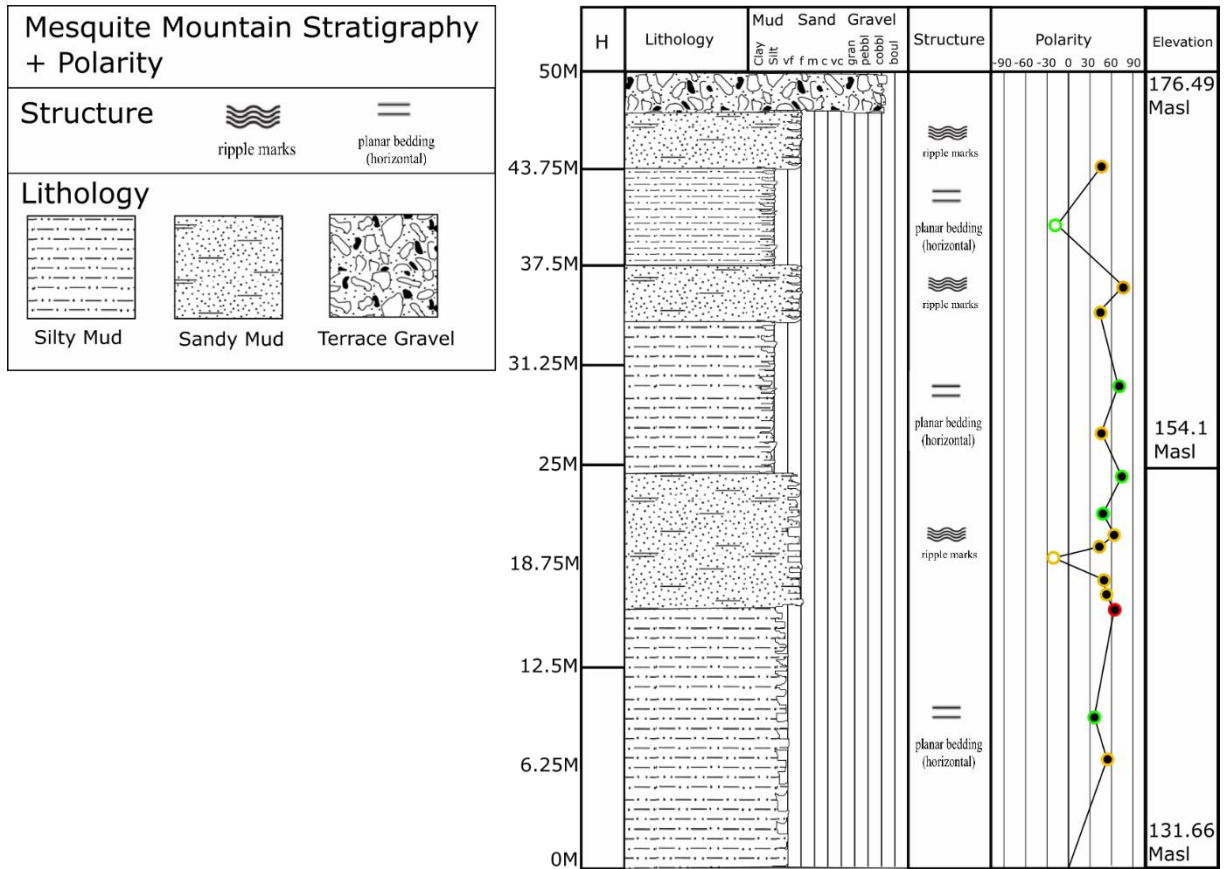
Figure 39) Stratigraphy and associated polarity with Mesquite Mountain Samples (MM). Filled in circles represent normal polarity samples. Solid (open) circles represent normal (reversed) polarity samples. The colors code with site "grades" as described in the text. Green = good, yellow = acceptable, red = poor.
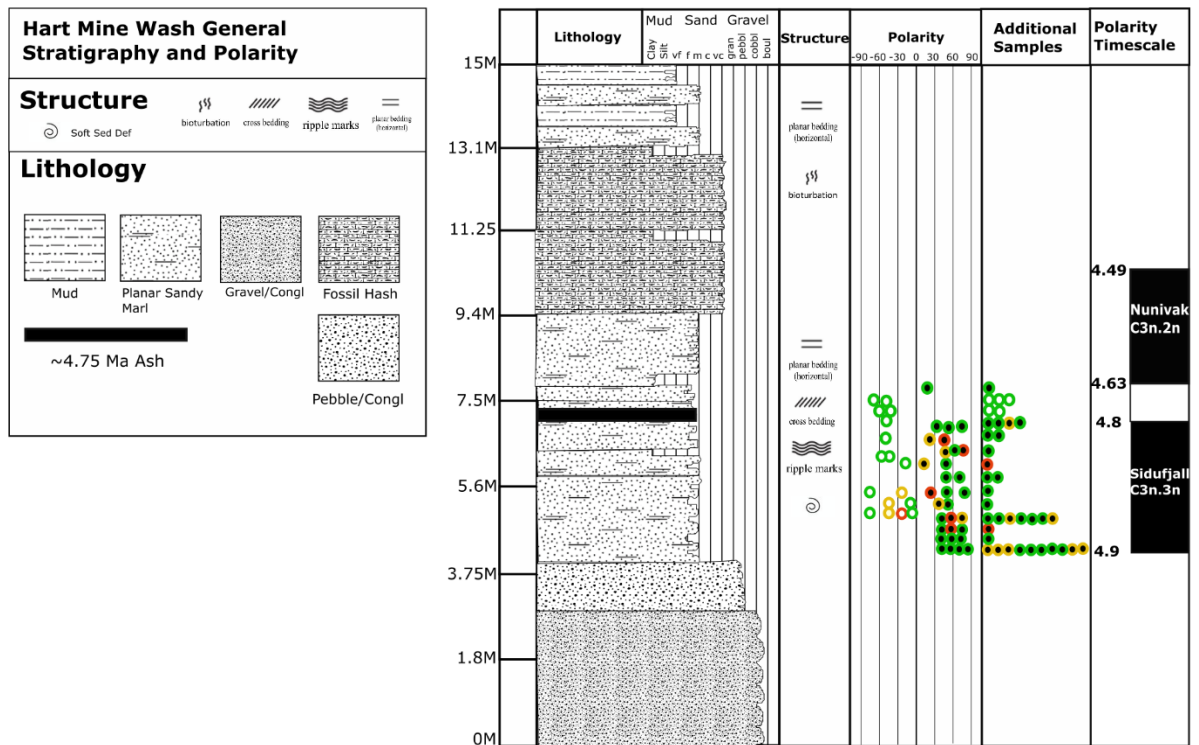
Figure 40) Stratigraphy and associated polarity with HMW samples. Solid (open) circles represent normal (reversed) polarity samples. The colors code with site "grades" as described in the text. Green = good, yellow = acceptable, red = poor.
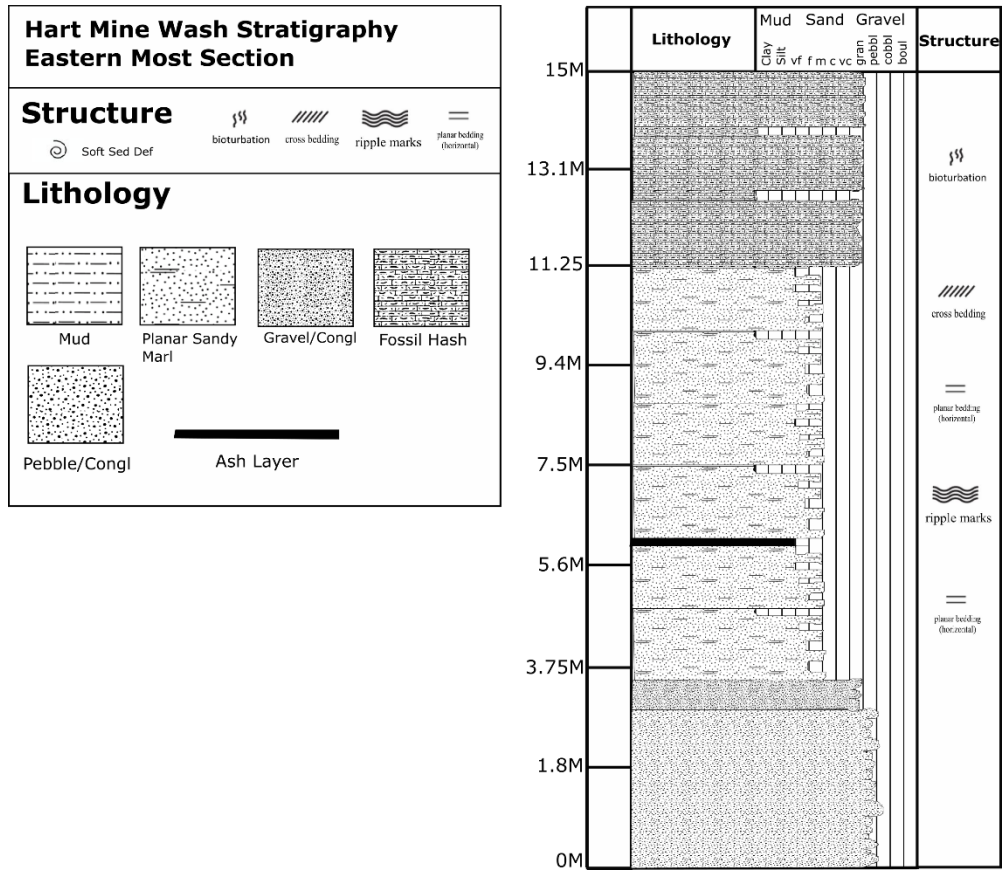
Figure 41) Stratigraphic representation of the eastern section of Hart Mine Wash
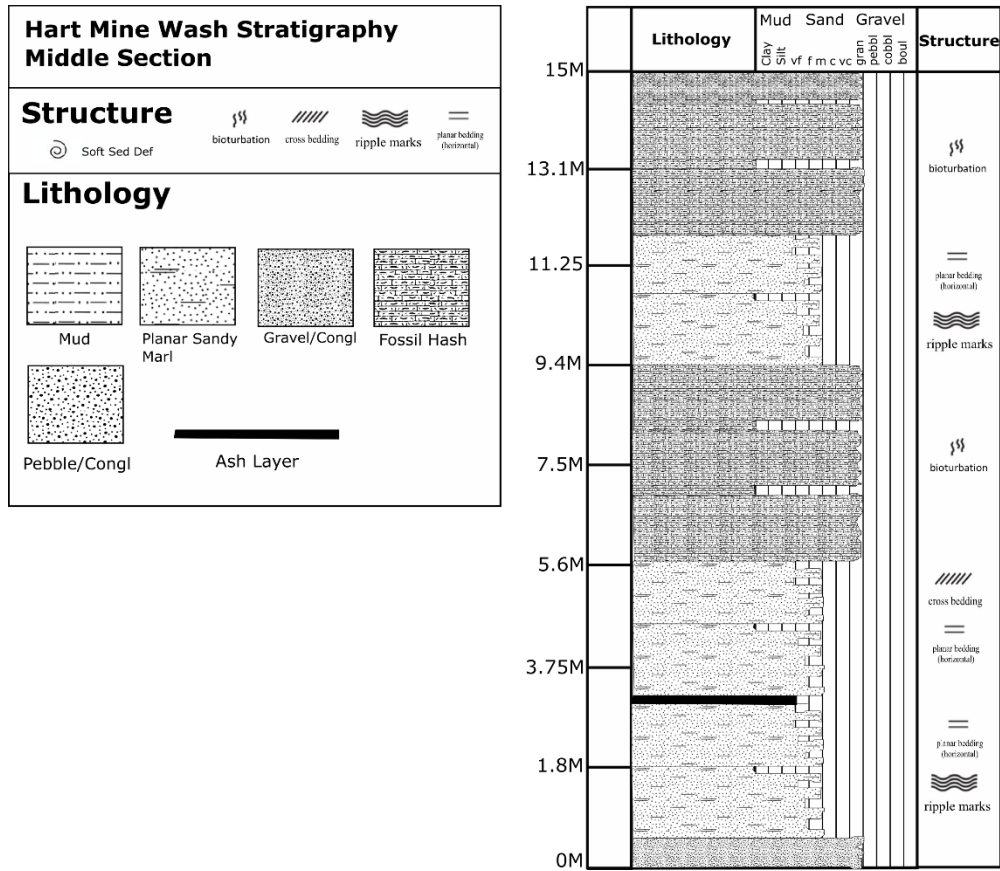
Figure 42) Stratigraphic representation of the Middle section of Hart Mine Wash
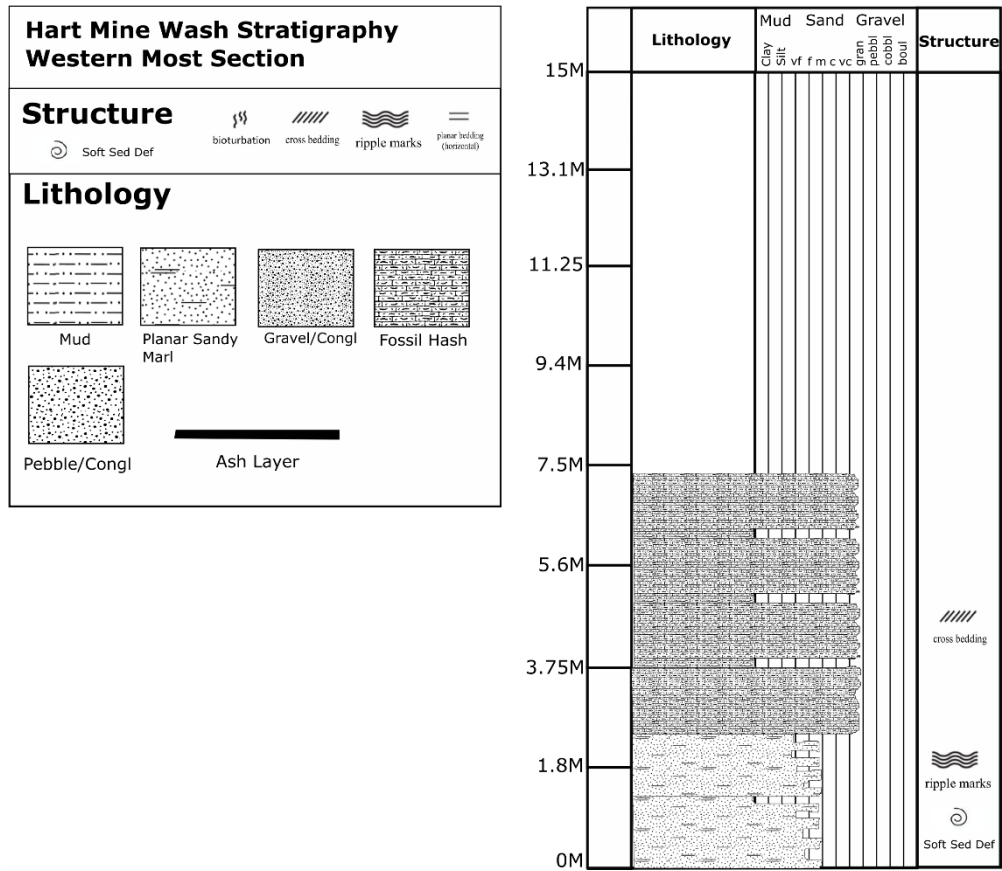
Figure 43) Stratigraphic representation of the Western most end of Hart Mine Wash
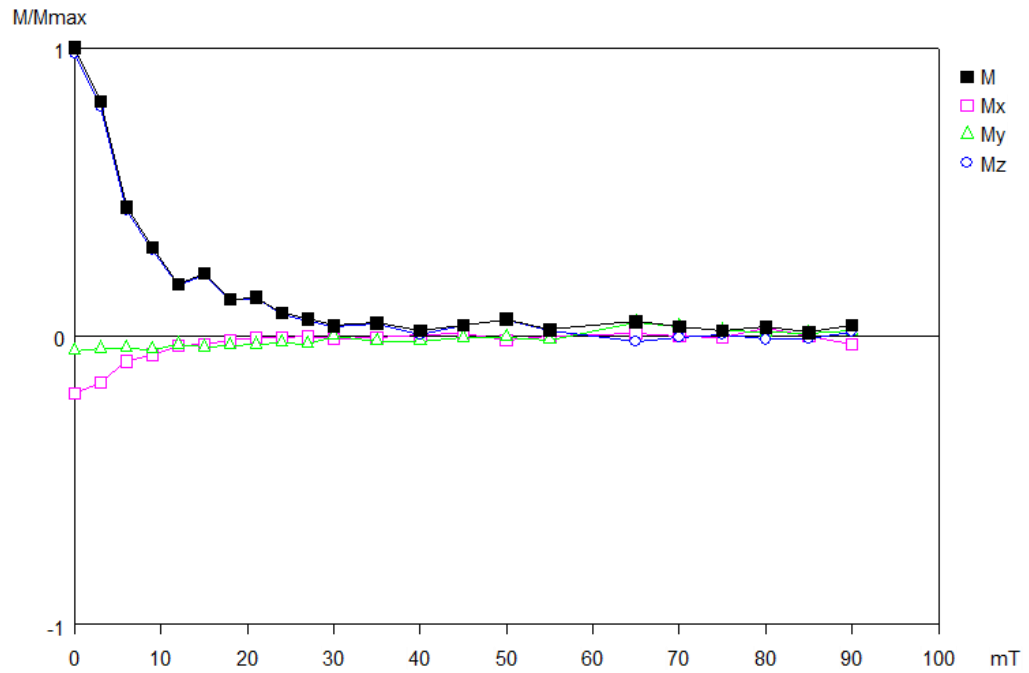
Figure 44) HMW8-1 Module Plot displaying rapid decay within a sample. The y-axis displays the maximum magnetic moment, and the x-axis displays the step in AF demagnetization, or Mili Tesla associated with that step.
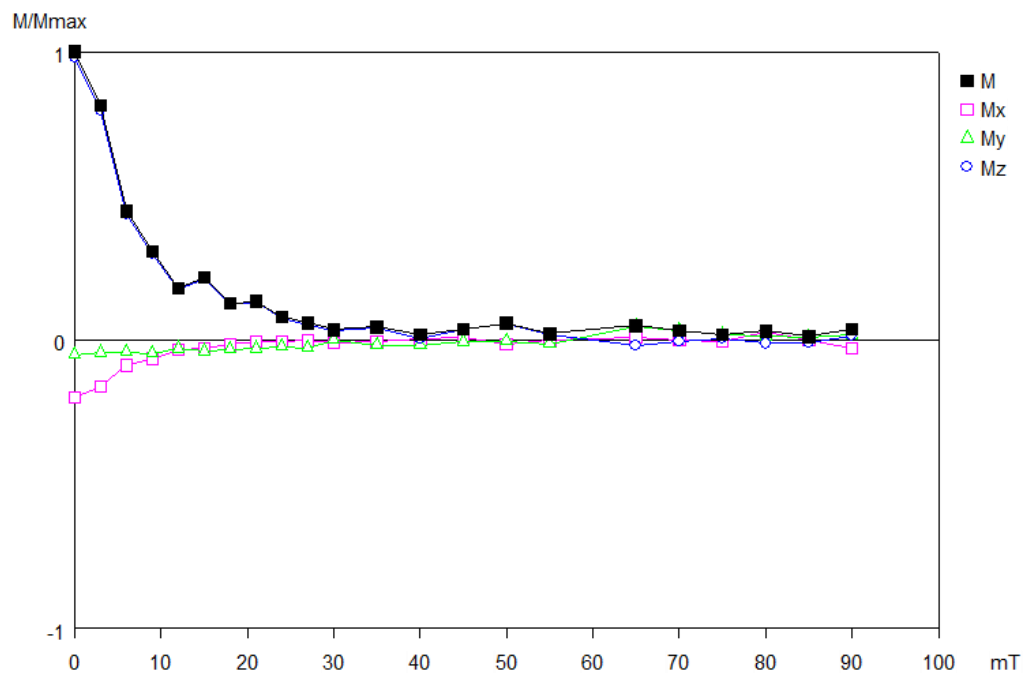
Figure 45) HMW14-2 Module Plot displaying rapid decay within a sample. The y-axis displays the maximum magnetic moment, and the x-axis displays the step in AF demagnetization, or Mili Tesla associated with that step.
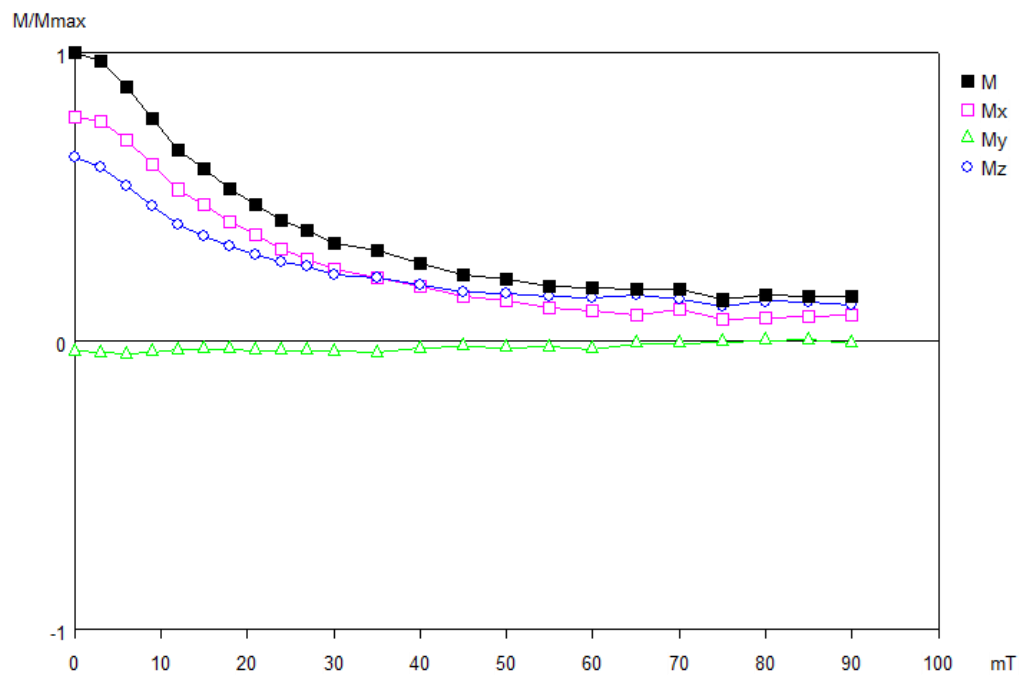
Figure 46) 1RS1-2 Module Plot displaying more resistant decay curve. The y-axis displays the maximum magnetic moment, and the x-axis displays the step in AF demagnetization, or Mili Tesla associated with that step.
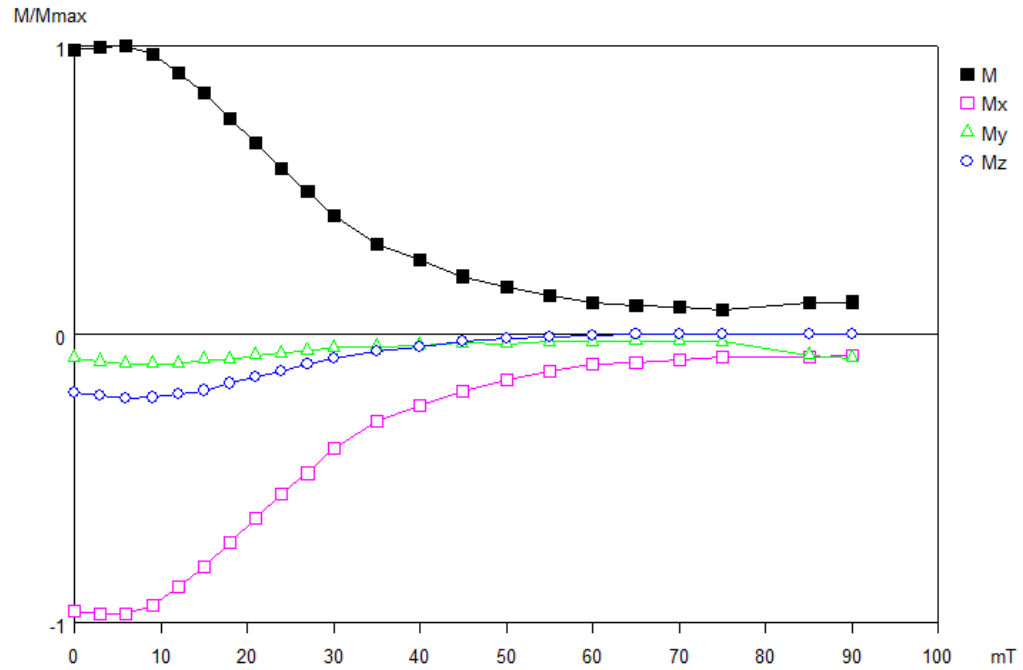
Figure 47) 4RS2-1 Module Plot displaying a more resistant decay curve, and a reversed polarity component in the x, y, and z axes. The y-axis displays the maximum magnetic moment, and the x-axis displays the step in AF demagnetization, or Mili Tesla associated with that step.
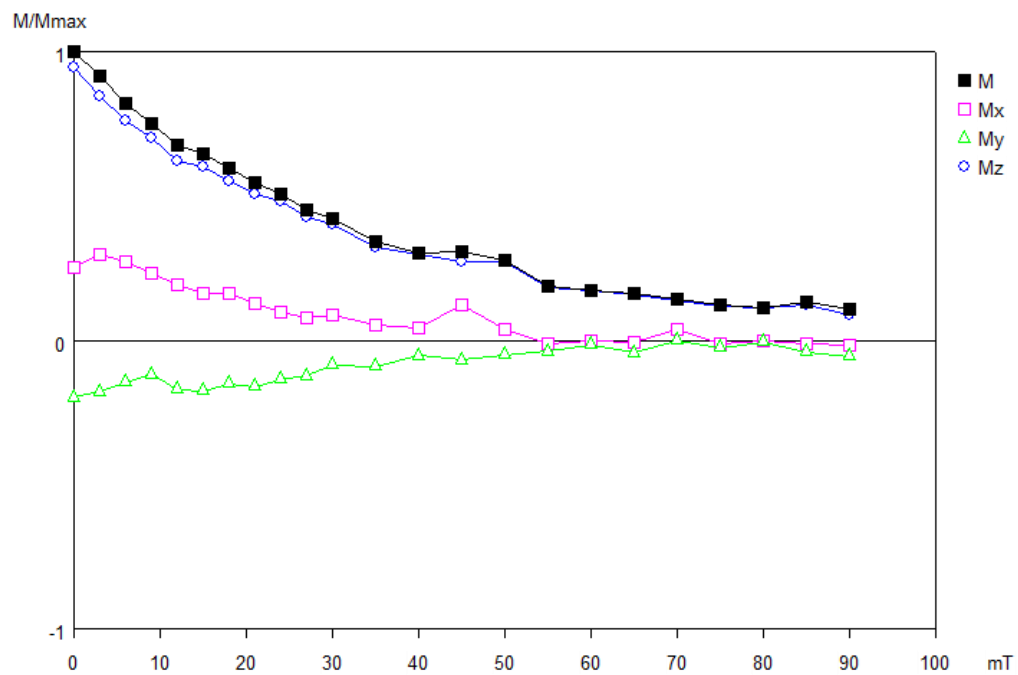
Figure 48) MV1-2 Module Plot displaying more resistant decay and a reversed y component. The y-axis displays the maximum magnetic moment, and the x-axis displays the step in AF demagnetization, or Mili Tesla associated with that step.
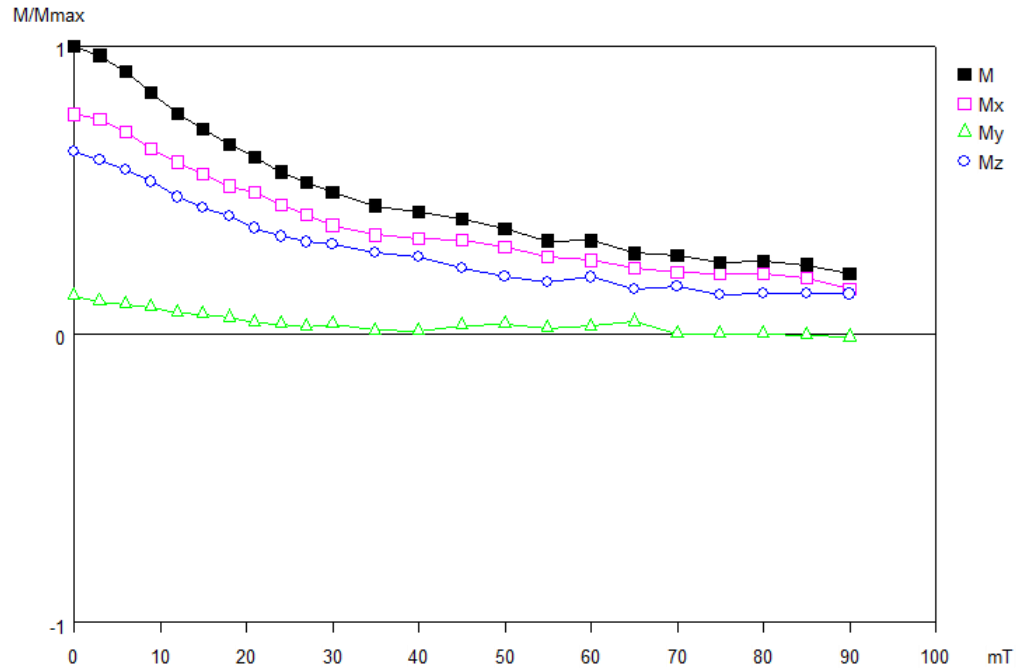
Figure 49) MV5-2 Module Plot displaying more resistant decay curve. The y-axis displays the maximum magnetic moment, and the x-axis displays the step in AF demagnetization, or Mili Tesla associated with that step.
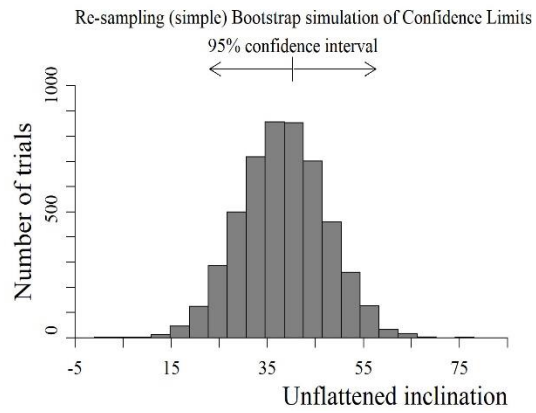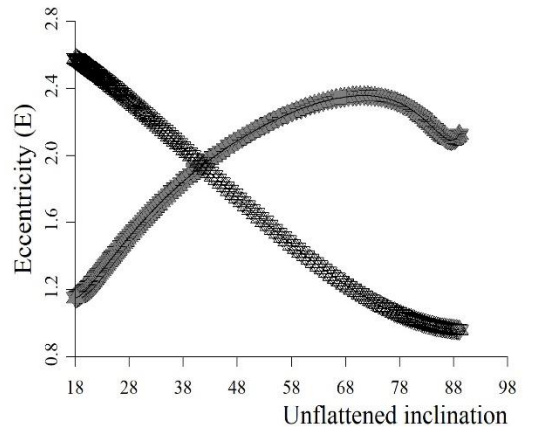
Figure 50) Elongation vs inclination plot (top) and bootstrap simulation histogram (bottom). Elongation plots the curve of the HMW data set and the field model data set. The y-axis represents the expected eccentricity, and the x-axis represents the expected inclination at that point.
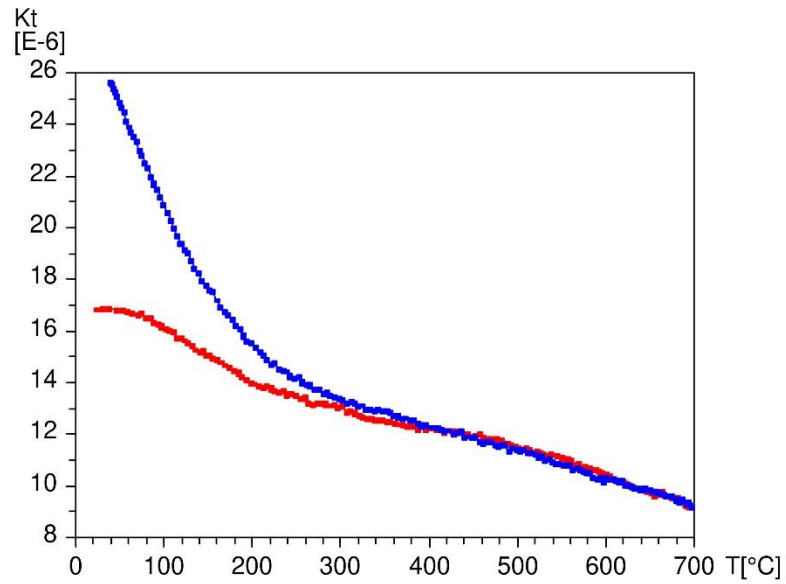
Thermomagnetic curve 1RS4 displaying a Curie temperature of ~420°C. The y-axis represents the magnetic moment of the sample in kilo Tesla, the x-axis represents the overall temperature of the sample in degrees Celsius.
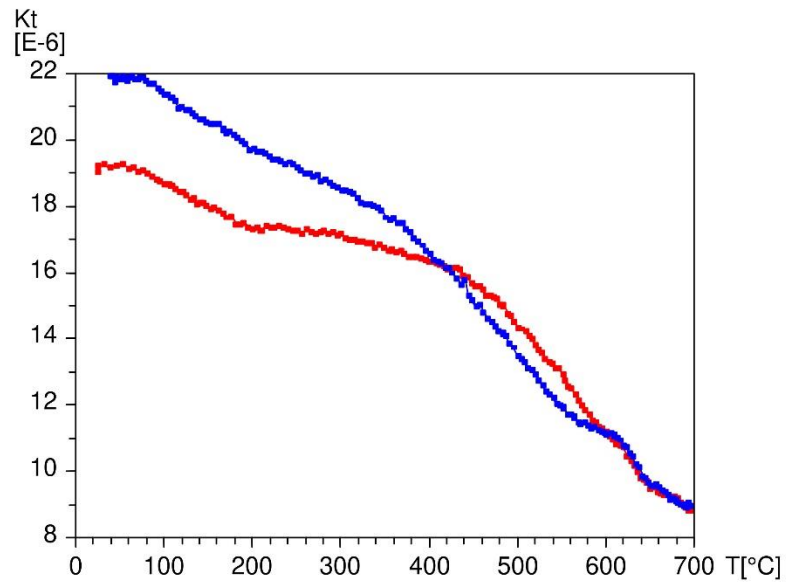
Thermomagnetic curve 4RS1 displaying an ambiguous Curie temperature of ~650°C. The y-axis represents the magnetic moment of the sample in kilo Tesla, the x-axis represents the overall temperature of the sample in degrees Celsius.
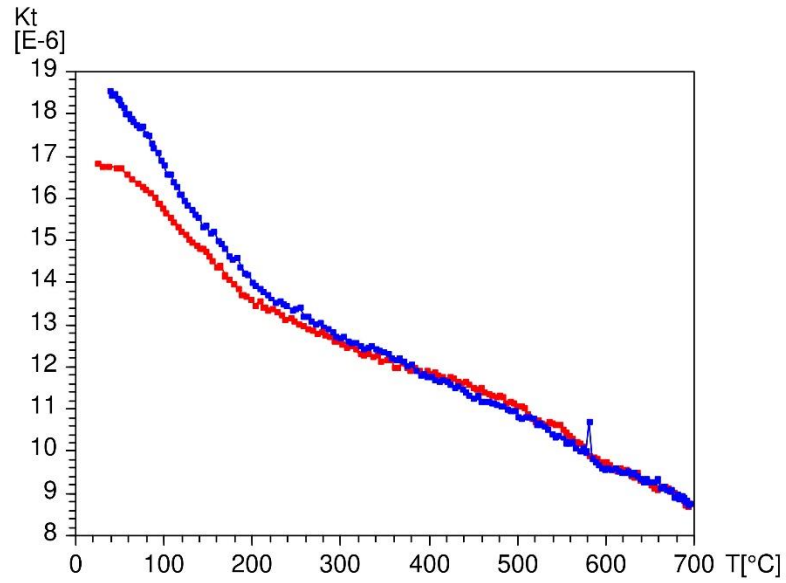
Thermomagnetic curve 4RS3 displaying an ambiguous Curie temperature of 600°C. The y-axis represents the magnetic moment of the sample in kilo Tesla, the x-axis represents the overall temperature of the sample in degrees Celsius.
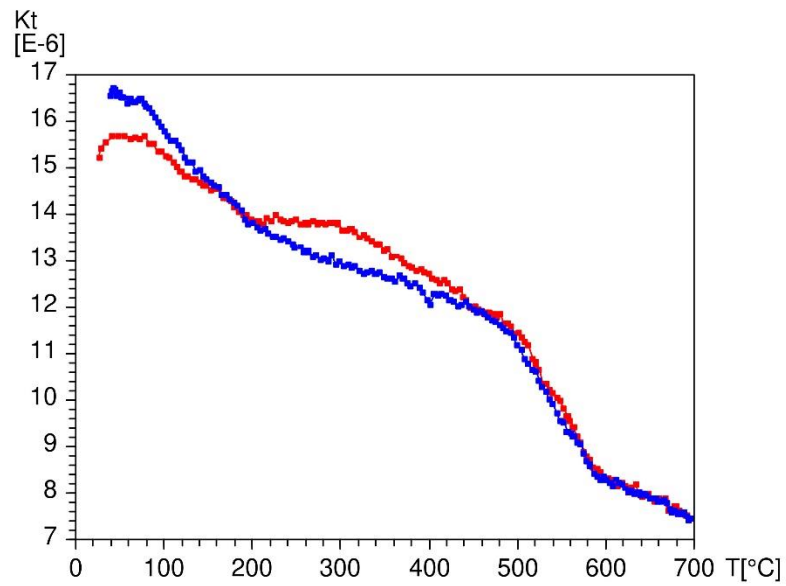
Thermomagnetic curve 4RS5 displaying an ambiguous Curie temperature of ~600°C. The y-axis represents the magnetic moment of the sample in kilo Tesla, the x-axis represents the overall temperature of the sample in degrees Celsius.
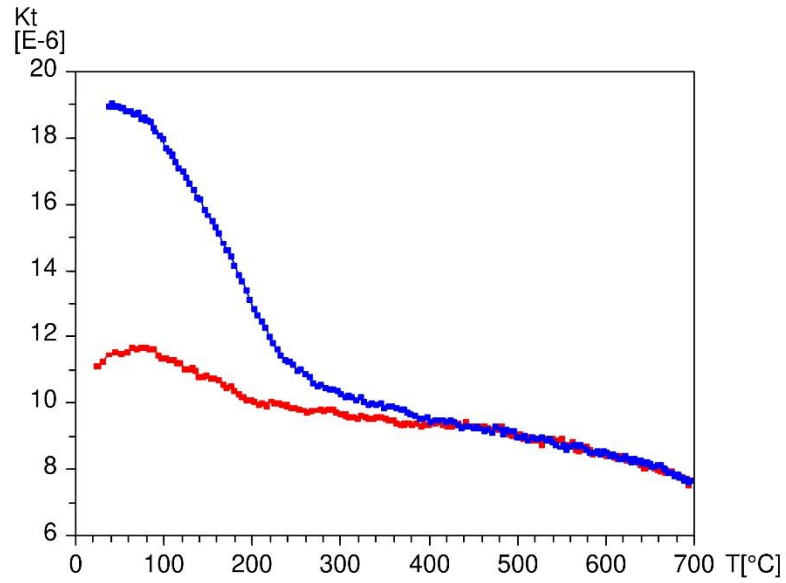
Thermomagnetic curve HMW5 displaying a Curie temperature of 450°C. The y-axis represents the magnetic moment of the sample in kilo Tesla, the x-axis represents the overall temperature of the sample in degrees Celsius.
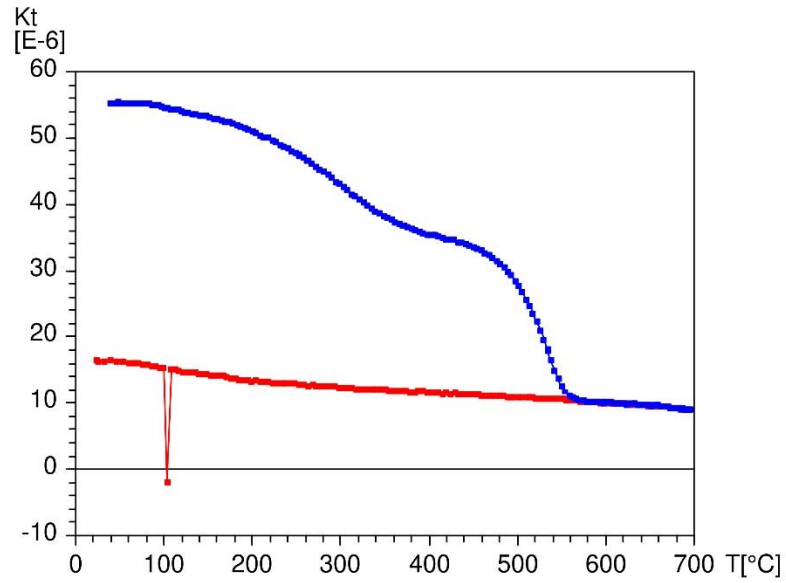
Thermomagnetic curve MV5 displays a Curie temperature of ~550°C. The y-axis represents the magnetic moment of the sample in kilo Tesla, the x-axis represents the overall temperature of the sample in degrees Celsius.
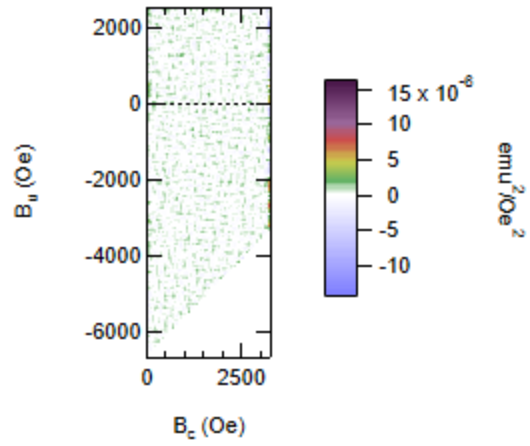
FORC contour plot 1RS4 displaying a null result. $B_C = (B_B - B_A)/2$ and $B_U = (B_B + B_A)/2$, where B= magnetic field. Subscripts A and B refer to X and Y components of the magnetic field curve.
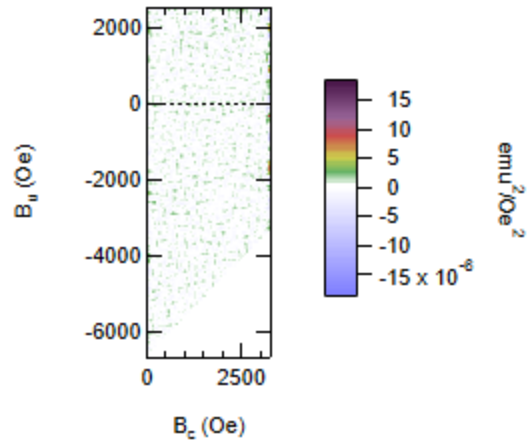
FORC contour plot 4RS3 displaying a null result. $B_C = (B_B - B_A)/2$ and $B_U = (B_B + B_A)/2$, where B= magnetic field. Subscripts A and B refer to X and Y components of the magnetic field curve.
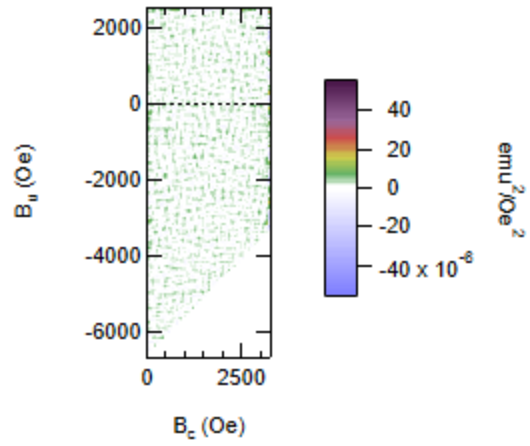
FORC contour plot Fold Test displaying a null result. $B_C = (B_B - B_A)/2$ and $B_U = (B_B + B_A)/2$, where B= magnetic field. Subscripts A and B refer to X and Y components of the magnetic field curve.
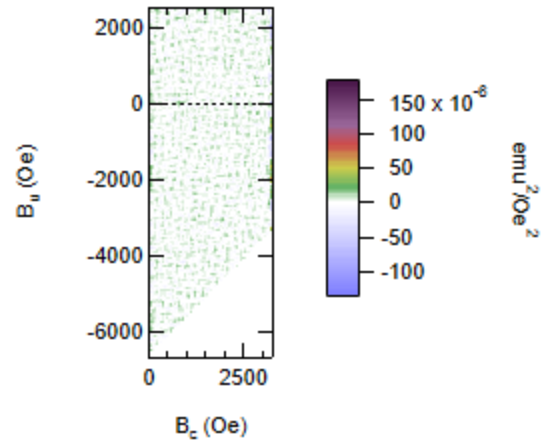
FORC contour plot HMW5 displaying a null result. $B_C = (B_B - B_A)/2$ and $B_U = (B_B + B_A)/2$, where B= magnetic field. Subscripts A and B refer to X and Y components of the magnetic field curve.
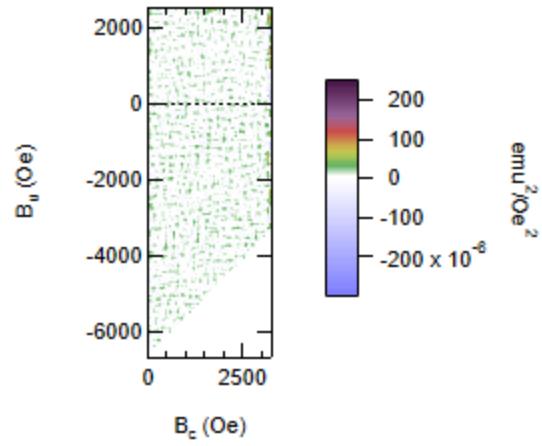
FORC contour plot HMW8 displaying a null result. $B_C = (B_B - B_A)/2$ and $B_U = (B_B + B_A)/2$, where B= magnetic field. Subscripts A and B refer to X and Y components of the magnetic field curve.
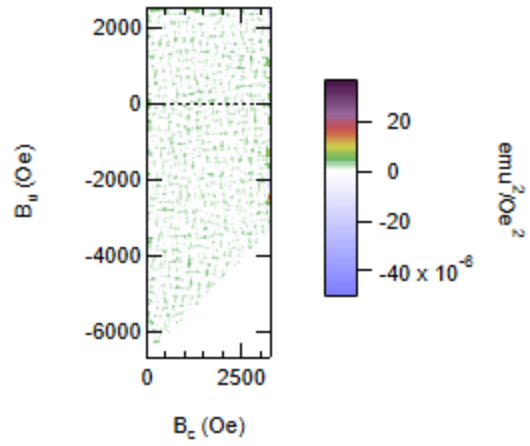
FORC contour plot MV4 displaying a null result. $B_C = (B_B - B_A)/2$ and $B_U = (B_B + B_A)/2$, where B= magnetic field. Subscripts A and B refer to X and Y components of the magnetic field curve.
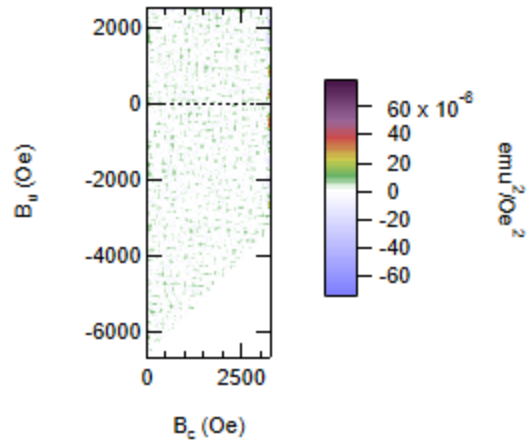
FORC contour plot MV5 displaying a null result. $B_C = (B_B - B_A)/2$ and $B_U = (B_B + B_A)/2$, where B= magnetic field. Subscripts A and B refer to X and Y components of the magnetic field curve.

MV5
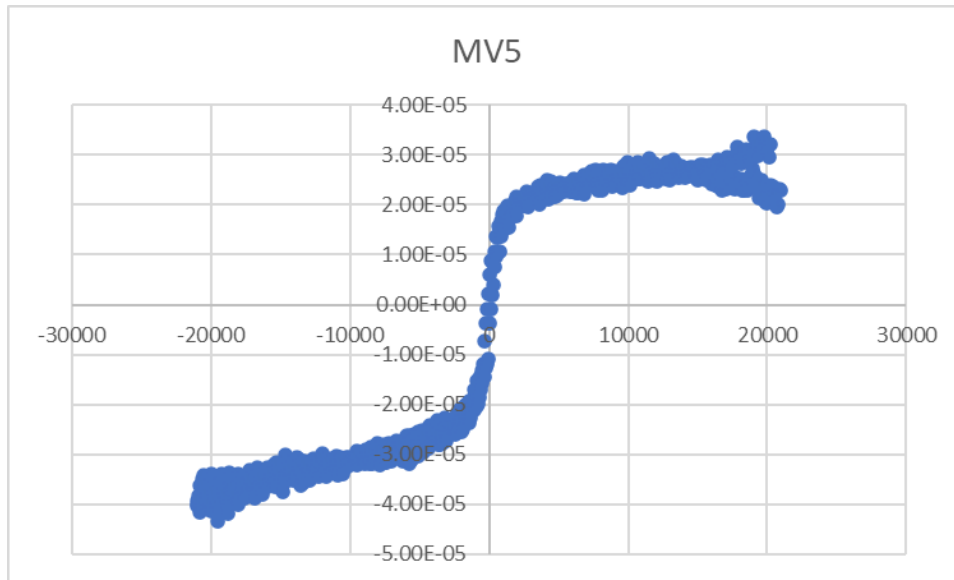
Hysteresis Curve for MV5 displays a noisy and unclear result. The y-axis = electromagnetic moment in EMU (electromagnetic units) and the x-axis = magnetic field in Oe (Oersted's).
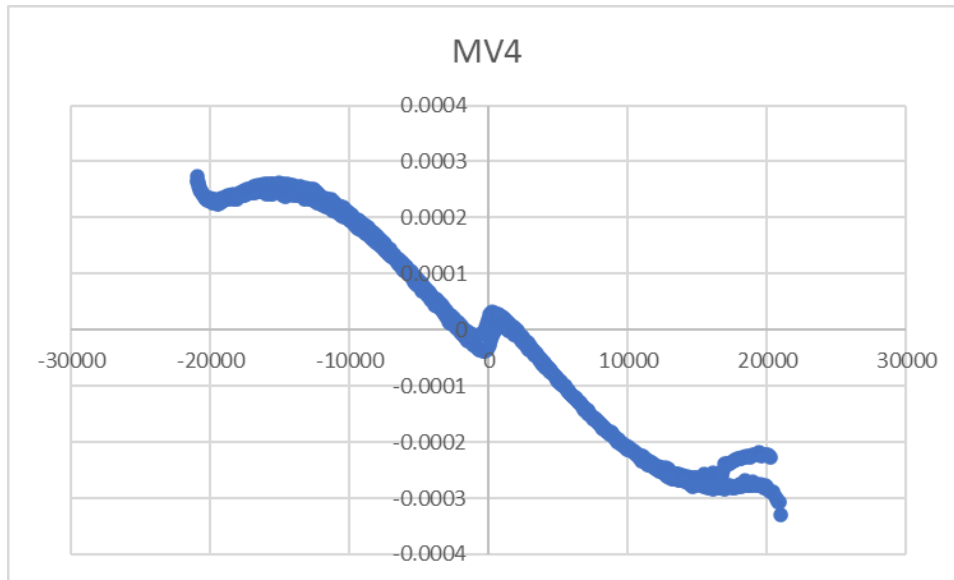
Hysteresis Curve for MV4 displaying an unclear result. The y-axis = electromagnetic moment in EMU (electromagnetic units) and the x-axis = magnetic field in Oe (Oersted's).
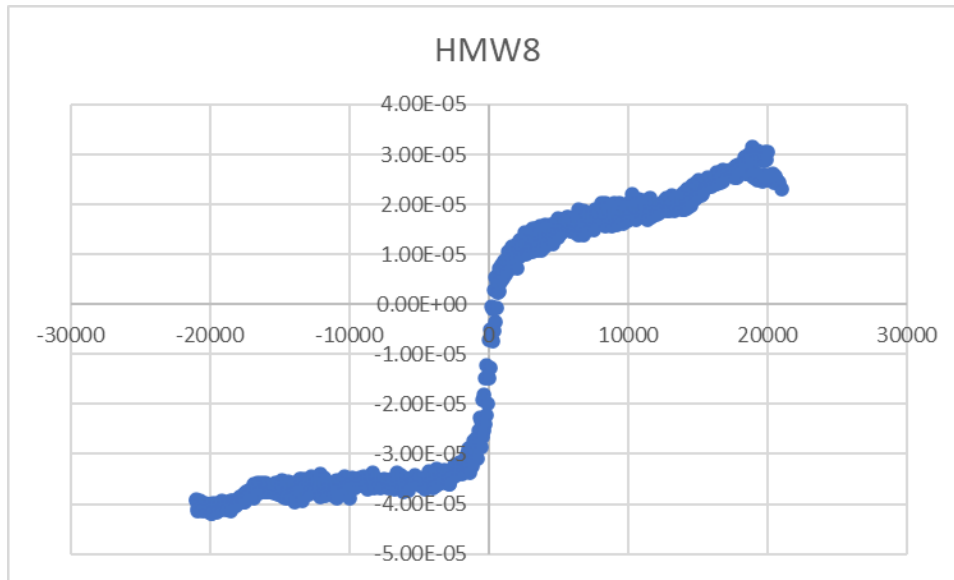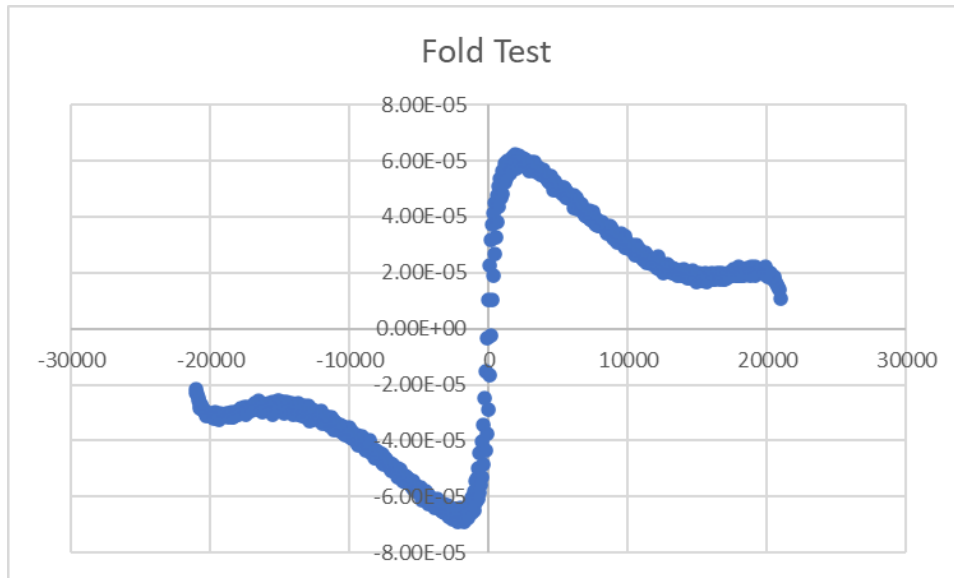
Hysteresis Curve for HMW8 displaying an unclear result. The y-axis = electromagnetic moment in EMU (electromagnetic units) and the x-axis = magnetic field in Oe (Oersted's).
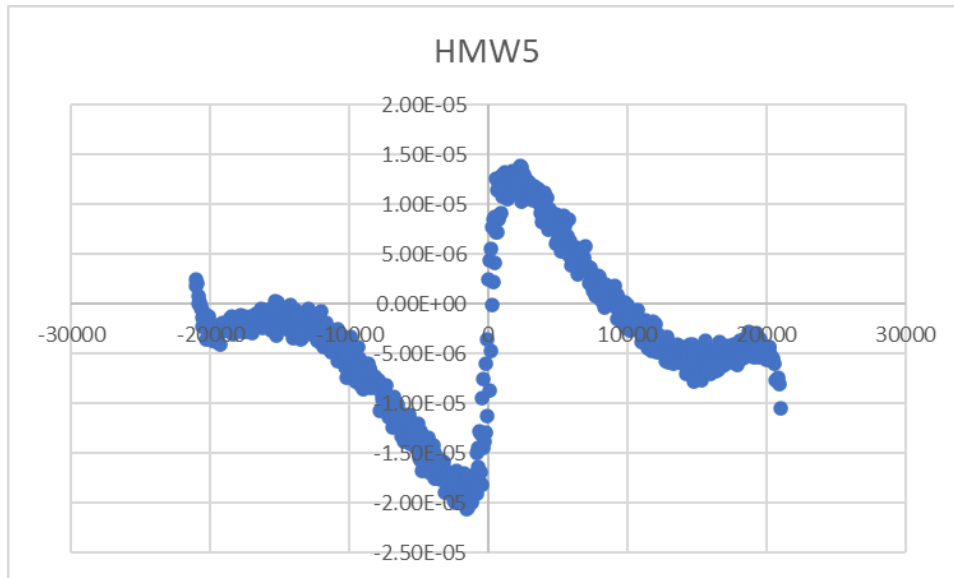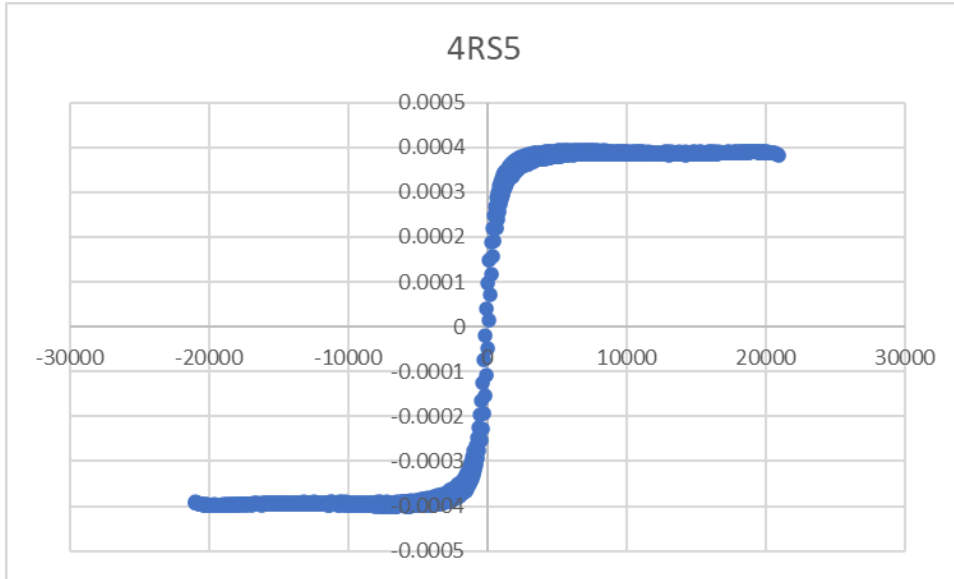
Hysteresis Curve for HMW5 displaying a noisy and unclear result. The y-axis = electromagnetic moment in EMU (electromagnetic units) and the x-axis = magnetic field in Oe (Oersted's).
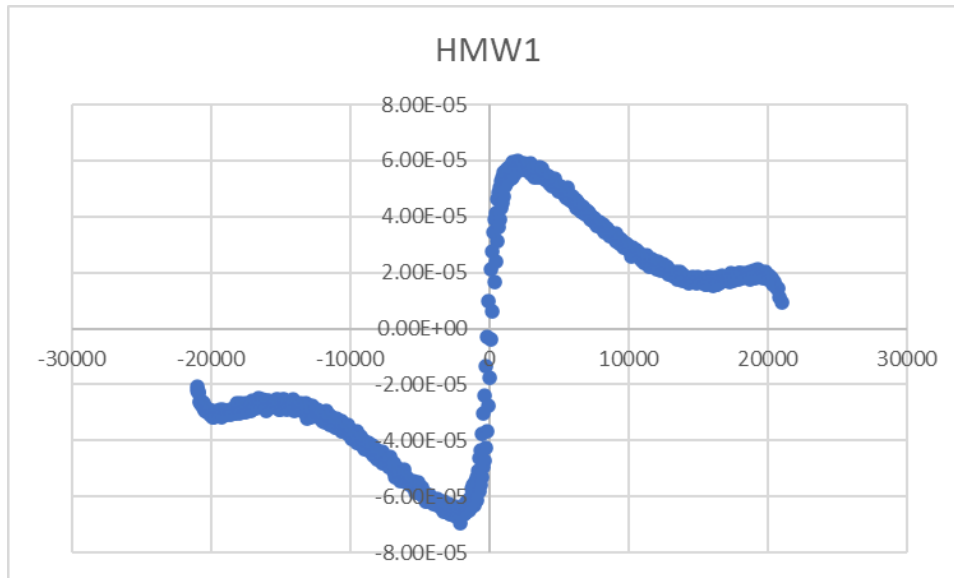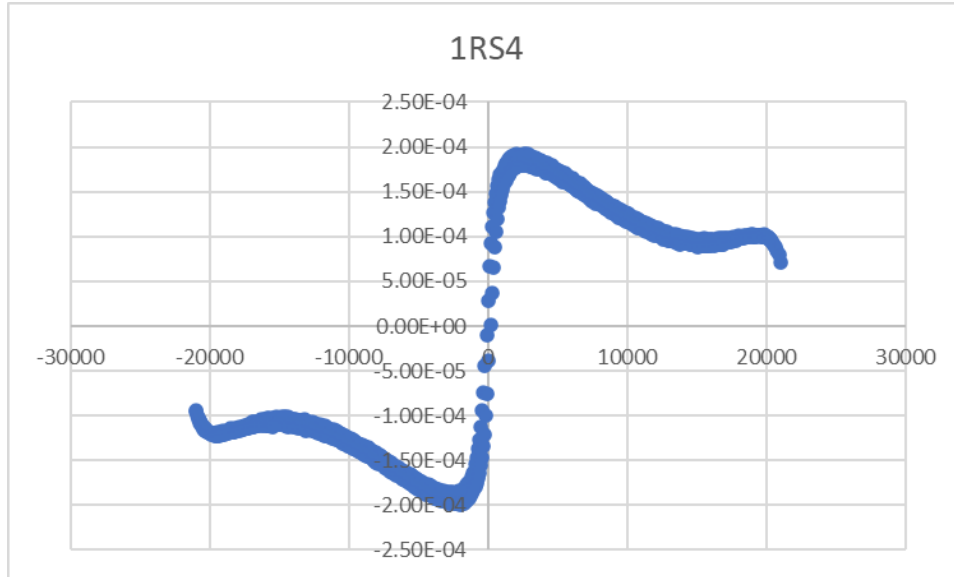
Hysteresis Curve for HMW1 displaying an unclear result. The y-axis = electromagnetic moment in EMU (electromagnetic units) and the x-axis = magnetic field in Oe (Oersted's).
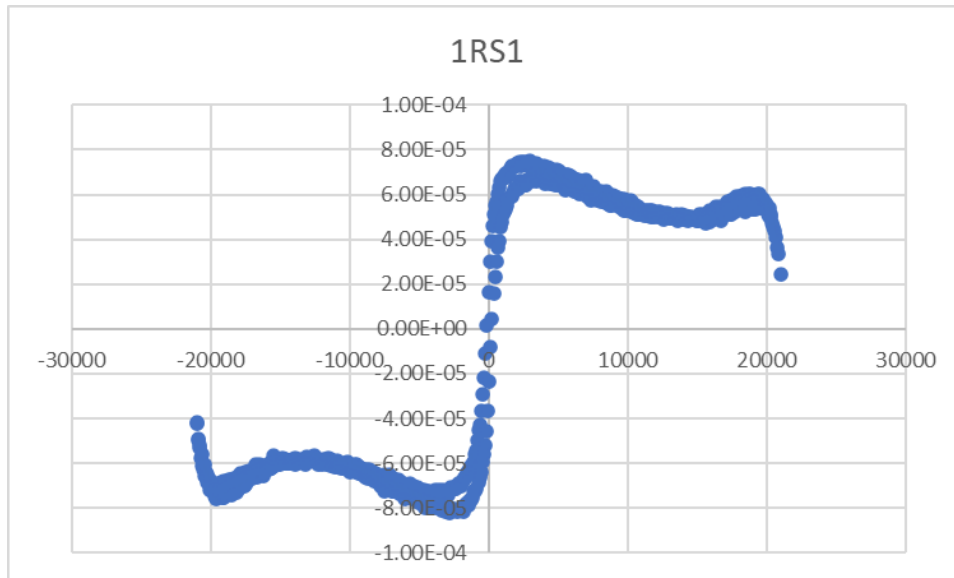
Hysteresis Curve for the Fold Test site displaying an unclear result. The y-axis = electromagnetic moment in EMU (electromagnetic units) and the x-axis = magnetic field in Oe (Oersted's).

Hysteresis Curve for 4RS5 displaying an unclear result. The y-axis = electromagnetic moment in EMU (electromagnetic units) and the x-axis = magnetic field in Oe (Oersted's).

Hysteresis Curve for 1RS4 displaying an unclear result. The y-axis = electromagnetic moment in EMU (electromagnetic units) and the x-axis = magnetic field in Oe (Oersted's).

Hysteresis Curve for 1RS1 displaying a result most consistent with a wasp wasted hysteresis loop. The y-axis = electromagnetic moment in EMU (electromagnetic units) and the x-axis = magnetic field in Oe (Oersted's).